UNIVERSITY OF LONDON THESIS

Degree PhD Year 2007 Name of Author BLANCO GONZALEZ DE LA PENA, Esperanza Macarena

Patterning Biomolecules Using AFM Charge-Writing on Polymeric and Silicon Dioxide Substrates

by

Esperanza Macarena Blanco González de la Peña

Department of Medicine

University College London

Thesis submitted for the degree of Doctor in Philosophy (Ph.D.)

at the University of London

Prof. M. Horton and Dr. P. Mesquida

University Supervisors

University College London

May 2007

ProQuest LLC
789 East Eisenhower Parkway
P.O. Box 1346
Ann Arbor, MI 48106-1346

Acknowledgements

The research leading to this doctoral thesis was carried out in the London Centre for Nanotechnology (LCN) group at the Bone and Mineral Centre in the Division of Medicine of University College London from 2003 to 2007 with financial support from the Interdisciplinary Research Collaboration (IRC) in Nanotechnology.

Firstly I would like to thank Professor Mike Horton for giving me the opportunity to be part of his group and allowing me great freedom to conduct research at his lab. I also owe a special thanks to Dr Rachel McKendry for her help and support on the first days of my venture at the Bone and Mineral Centre.

I would like to highlight my gratitude to Dr Patrick Mesquida for his supervision and all the fruitful discussions that helped me keep a clear focus. My special thanks to Steve Nesbitt and Brian Nicholls for their kind and patient advice in the biology-related aspects of my research.

In addition I must thank all members of the group for creating such a good atmosphere. In order of appearance: Dr. Laurent Bozec, Dr. Christian Riener, Dr. Monica Ritco-Vonsovici, Dr. Gudrun Stenbeck, Dr. Birgit Leitinger, Dr. Nafessa Noordeen, Dr. Jaco de Groot, Moyu Watari, Marco Wenger, Dr. Belinda Haupt, Dr. Andrew Pelling, Yaron Silverberg, Ben Dueck, Dr. Joseph Wafula, Alejandra Donoso and Deepa Visavadia: It has been a pleasure to work with all of you.

Finally I would like to thank my parents and Daniel Hall for their support and encouragement through the ups and downs of writing this thesis.

Declaration

Contents

Abstract

Electrostatic interactions are common-place in biological processes with biomolecules typically charged in solution. In this thesis electrostatic forces were used for the spatial manipulation of biomolecules by driving their attachment to surfaces patterned with localised charges. Charge-patterns can be created on dielectric materials using Atomic Force Microscope Charge-Writing and imaged by Kelvin-probe Force Microscopy with a resolution of one hundred nanometres.

There are a wide variety of materials that can be used for charge-patterning including polymers such as poly(methyl methacrylate) (PMMA) and polystyrene (PS), which are also commonly used in nanofabrication and in biological environments. Silicon dioxide is also well known for its charge storage capabilities. Since it is a key material for microfabrication and electronic devices, achieving controlled attachment of biomolecules on its surface would have far-reaching applications for the development of novel biosensors. The charge-pattern stability on PMMA, PS and SiO_2 was investigated regarding their preparation and the surrounding media.

The charge-patterns were subsequently used to localise biomolecular attachment. The biomolecules were enclosed in water droplets dispersed in a dielectric oil to pre-

vent the rapid decay of charge-patterns in an aqueous environment. The droplets were attracted electrostatically to the charge-patterns. After removing the liquid, the contents of the droplets remained localised on the surface and a resolution of approximately 1 μm was achieved. To illustrate the repeatability of the process, different types of biomolecules commonly used in immunoassays were patterned on silicon dioxide: mouse immunoglobulin G, rabbit immunoglobulin G and biotinylated bovine serum albumin. The multiprotein array thus produced was tested by immersing it in a solution containing three different fluorescently labelled biomolecules. each exhibiting specific, biomolecular interaction to the deposited ones. The discrimination from the mixture of these secondary biomolecules by antibody-antibody or biotin-avidin interactions confirmed the functionality and high selectivity of the patterned array.

Chapter 1

Introduction and Motivation

1.1 Nanostructuring techniques

The success of nanotechnology relies on the ability to manipulate and control the formation of structures in the nanoscale. For the constant trend of miniaturisation to be maintained, new approaches to fabrication are continuously being developed. Nanostructures are created using two main approaches: top-down and bottom-up structuring. Top-down fabrication techniques downscale the existing microstructuring techniques based in lithography to create sub-micrometre structures. The bottom-up approach involves the use of particles or molecules of nanometre dimension as building blocks to fabricate structures. Both approaches can be combined offering a great range of possibilities for the development of novel nanoscale devices ([Kohler 2004], p.1).

Different methods are used for patterning depending on the intended application, the material to be patterned and the minimum feature size to be achieved. Physical

or chemical changes can be induced on a substrate, directly forming the desired structure or producing a latent pattern to be developed in subsequent steps.

Self-assembly techniques form part of the bottom-up patterning approach. The size of the building blocks used, range from molecular size to objects of meso- and macroscale. The building blocks will self-assemble if their interactions allow them to aggregate into stable, well defined periodic structures. The final stable structure is obtained by balancing the attraction and repulsion between building blocks to achieve the lowest free-energy state. The characteristics of the resulting structures are controlled by varying the interactions between the building blocks, tailoring properties such as their topography, shape, surface functionality or electrical potentials [Isaacs 1999]. The size of the structures vary from several nanometres to millimetres. An example of self-assembled structures is phase-separated block co-polymers. At equilibrium, these polymer fragments can arrange in regular domain patterns. Their molecular structure consists of two or more polymer fragments chemically different and immiscible joined by a covalent bond [Forster 1998]. Because of the differences in their chemical or physical nature, it is often possible to remove one of the fragments to obtain an ordered pattern that can be used as a mask for lithographic applications [Park 1997]. The phase-separated block copolymers can also be used as templates to order particles that would adsorb preferentially to one of their components [Lopes 2001]. The main problem of self-assembly techniques is to achieve one single highly ordered domain over a large area. Long-range order can be obtained in self-assembled structures using templates to direct the assembly. Different approaches can be used to guide the assembly such as patterning chemi-

cal modifications [Fan 2004], writing electrical charges [Mesquida 2001] or creating topographical features [Yin 2001] on the substrate.

Photolithography is a well established top-down method for patterning photoresists with nanoscale resolution. Photosensitive films are usually patterned under exposure to a spatially modulated UV-light. Stable structures are obtained by creating or breaking bonds between the atoms of the exposed resist layer. Photons can be used to change these bonds either through chemical amplification or by each of the photons providing enough energy to change the bonds. In chemical amplification systems, the incident photons change molecules within the film into catalysts; photoacids that trigger a chemical cascade as they diffuse through the film [Ito 1984]. Thus, the lateral diffusion of the catalyst ultimately determines the resolution of the pattern, not the wavelength of the incident photon.

To overcome this problem, the energy needed to change the bonds in the resist can be introduced with photons, each of them providing enough energy for the bond activation rather than using a catalytic cycle. The typical bond energy for materials stable at room temperature is 1 eV per bond. To achieve this energy, the wavelength of the photons used must be below 1.2 μm. To downscale the structures to dimensions below 100 nm, vacuum UV, soft X-ray or extreme UV are required ([Kohler 2004], p.105). At these wavelengths technical problems arise for the realization of high resolution optical projection systems. Another difficulty is that materials in the soft X-ray region do not present differences of more than two orders of magnitude in their absorption coefficients. This makes the creation of transmissive and mechanically stable masks very difficult.

Other energetic particles, such as electrons, protons or ions, are also used for the generation of nanostructures. Focused beams of these particles can be scanned over a susceptible material. The beam energy can induce various types of chemical or physical modifications depending on the materials involved and the energies applied. An advantage of this method is that the associated de-Broglie wavelengths of these particles can be in the lower nm range or less depending on their velocity. Particle beams can be focused below 1 nm. The size of the focused beam is therefore not the main limitation for the resolution of this method; the main limitation arises with the further interaction of the energetic particles within the material ([Kohler 2004], p.110). Although high throughput is still a challenge for scanning techniques, e-beam lithography has been extensively used for patterning organic polymers [Haghiri-Gosnet 1995]. It is also used for patterning inorganic materials such us metal fluorides [Kratschmer 1987] or to pattern self-assembled monolayers [Lercel 1993]. Focused Ion Beam (FIB) patterning can be used for the local implantation of ions [Hanley 2002] or for the creation of patterns by ion beam erosion [Frost 2003]. Because of their higher mass, ions are less prone to produce distortion in the pattern due to back-scattering in the substrate.

Bombarding the surface of a dielectric with charged particles can produce a trapped charge distribution [Sessler 1999]. The trapped charge creates an electrical field that can be used for electrostatic attachment of charged particles or biomolecules. E-beams [Wybourne 1996], patterned electrodes [Jacobs 2001] or scanning probe techniques [Mesquida 2001] have been used to generate charge-patterns in dielectric materials to be used as electrostatic templates. Charge-

patterns can also be created by injecting ions locally on a substrate and subsequent electrostatic attachment of microsize particles dispersed in non-polar solvents has been achieved [Fudouzi 2002].

Microcontact printing (soft lithography) uses a patterned polymer stamp to achieve parallel patterning. The stamp, usually made of poly-(dimethylsiloxane) (PDMS), is fabricated using photolithographic techniques and silicon etching. In the printing process, the patterned stamp is covered with a solution of ink, dried and brought into contact with the substrate. No expensive equipment is required and it can be used to pattern curved surfaces but precise alignment of prefabricated structures can present problems. The typical feature size ranges from 200 nm to several millimetres [Xia 1995]. Patterned stamps have also been used in nanoxerographic applications. A flexible stamp can be used as a patterned electrode by coating it with a conductive layer. Dielectric films can be patterned with charges by biasing the patterned electrode when it is in contact with the film [Barry 2003]. Charged particles attach to the charged patterns by electrostatic forces achieving features of 100 nm from gas phase and 200 nm from liquid phase [Barry 2003]. Using this method for the creation of submicrometer structures presents difficulties related to the fabrication of the stamps and the results are prone to distortion effects. PDMS is the most commonly used material but presents geometrical limitations due to its softness [Csucs 2003]. The resolution is limited by the feature size of the PDMS stamp but, for nanoxerographic applications, Si-based patterned electrodes can be a solution for down-scaling this method to the lower nm range as the patterned electrode does not need to be flexible.

Several techniques have been developed to generate patterns of functional biomolecules directly. Ink-jet printing consists in the delivery of drops on a surface through micrometre-size nozzles. This technique has been applied to the development of biosensors [Okamoto 2000] and for polymeric patterning [Wang 2004]. The resolution of this method is 20-50 μm. The diameter of the dot can be decreased to 100 nm by delivering the ink with a scanning probe in dip-pen nanolithography (DPN). However, the limited capacity of ink that can be carried on the tip and the preparation of the pen-tip makes it difficult to incorporate this method in a production line. Another drawback is the lack of speed inherent of serial techniques. The current approach to increase patterning speed relies in parallelisation. Single-feedback, multiple-tips devices are currently being developed [Salaita 2006].

The application of scanning probe techniques as nanopatterning tools provides a range of different methods to achieve nanometre scale feature sizes. Their precise positioning system and the use of ultrasharp probes allow accurate local manipulation at that scale and parallelisation can add speed to the patterning process [Vettiger 2000]. Thus, scanning probe techniques and their nanostructuring applications are discussed in detail in section 1.2.

1.2 Scanning-probe techniques

In Scanning Probe Microscopy (SPM) the images are obtained by mapping the local interactions between the substrate and an ultrasharp probe that is scanned over it. Depending on the interaction measured, different types of information can be ob-

tained. SPM techniques also allow the generation of controlled physical or chemical modifications on the surface of the material with very high resolution. Scanning probe techniques began with the development of the Scanning Tunnelling Microscope (STM) by Heinrich Rohrer and Gerd Binnig in the early 1980s [Binnig 1983]. Based on the same principle other techniques were soon developed. The scanning probe system was extended to non-conductive substrates and to biocompatible environments in the case of Atomic Force Microscopy (AFM) [Binnig 1986]. The development of near-field scanning-probe microscopy (SNOM) provided a way of overcoming the diffraction limitations in optical microscopy [Betzig 1991].

The STM monitors the tunnelling current between a conductive probe and a conductive substrate. Increasing the distance between probe and substrate, the tunnelling current decays exponentially. An atomic-size variation in the probe-substrate distance involves changes in the tunnelling current of one order of magnitude [Morris 1999]. Because of the exponential dependence of the tunnelling current, the spatial resolution of this technique is approximately 0.2 nm laterally and $< 10^{-3}$ nm vertically [Colton 2004]. The tunnelling current is proportional to the surface local density of states [Tersoff 1985]. Therefore, the STM can map the electronic structure of the sample surface with atomic resolution [Binnig 1983]. The images can be made using a feedback system to maintain the tunnelling current constant by changing the probe-sample distance or maintaining the probe-sample distance constant and recording the changes in the tunnelling current.

Spectroscopic information can be obtained making different constant-current STM images at different applied voltages or keeping the probe at a precise loca-

tion and measuring the voltage dependence of the current over a ± 4 V range. The images depend strongly on the bias applied to the tip. With a negatively-biased tip the electrons will tunnel from occupied electronic states in the tip to empty states on the surface and vice versa for a positively-biased tip. Therefore, the information obtained is a convolution of the electron density of states of the tip and sample surfaces. One of the applications of STM spectroscopy is the investigation of conduction mechanisms and electron tunnelling in single molecules and atomic and molecular wires [Colton 2004].

The STM is also used for the research and development of new nanostructuring techniques. Individual particles can be mechanically manipulated by being pushed over the surface with the probe. Controlling the movement of the probe the particles are placed on the desired locations [Junno 1995]. Manipulation of single atoms and small molecules can also be achieved by tuning the STM potential and the tip-sample distance to adjust the tip-molecule and surface-molecule interactions [Meyer 1998]. Nevertheless, this individual manipulation is a very slow process requiring low temperatures. Using electrical patterns, the electrostatic deposition of charged nanoparticles takes place in a few seconds in a parallel fashion. The charge-patterns can also be created in parallel using patterned electrodes instead of an SPM probe [Barry 2003].

Scanning near-field optical microscopy (SNOM) combines the high resolution of the scanning probe methods and the interaction mechanisms of optical microscopy. The limitation of optical microscopy due to diffraction can be overcome by scanning the light source or detector very close to the surface instead of many wavelengths

away. The resolution will then only depend on the probe size and the probe to sample distance [Betzig 1992]. The resolution is limited by the optical skin depth of the metals used for coating the sub-wavelength optical fibre used as light source and detector. Apertureless SNOM was developed to solve this problem using the light reflected from an AFM or STM tip as a light source and achieved nanometre resolution [Wickramasinghe 1994]. Near-field scanning probe methods can also be used to generate structures by photochemistry or ablation [Iwata 2002]. These methods are useful for generation of masks in a top-down approach. Resist materials can be used for the photochemical patterning but the whole resist layer must be in the near field (below 100 nm). The restrictions in the dimensions of the resist film leads to limitations in the resist viscosity and the topography of the substrate on which it is spin-coated.

Binnig, Quate and Gerber developed Atomic Force Microscopy combining the STM and the stylus profiler concept [Binnig 1986]. It provided a straightforward method to overcome the limitations of the STM for imaging non-conductive samples. AFM operates by measuring the vertical displacement of a low-spring-constant cantilever with an ultrasharp tip. During the tip-surface interaction, the tip can experience repulsive or attractive forces that vary differently with the tip-sample distance ([Morris 1999], p.44).

Forces such as electrostatic, magnetic, hydrophobic, capillary, adhesion or Van der Waals become the dominant interaction at different tip-surface distances. At small tip-surface separations Van der Waals attractive forces, adhesion and electrostatic interaction between electrical double layers in electrolyte solutions may be

dominant. In solution, steric repulsion can also occur if chain molecules are placed on a surface. Upon tip-sample contact, adhesion and Born repulsion dominate the interaction and sample deformation may occur under an applied load [Colton 2004].

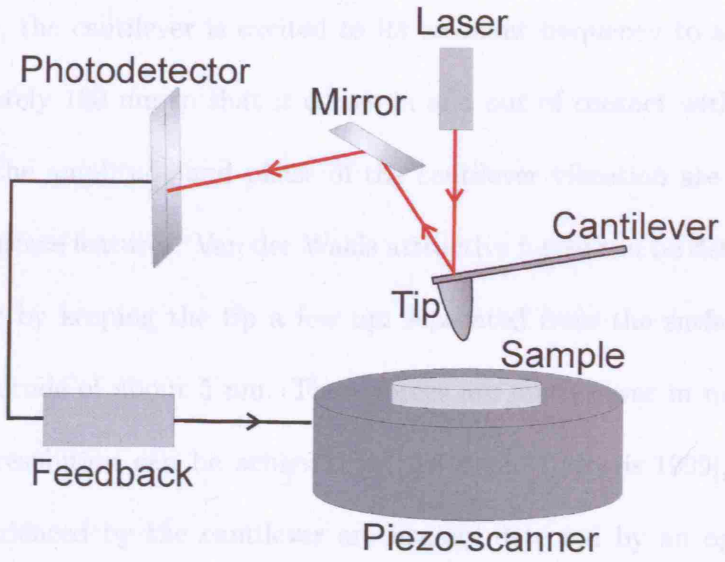

Figure 1.1: **AFM diagram.** The cantilever deflection is detected by measuring the deflection of a laser beam focused on and reflected from the back of the cantilever. A mirror is used to direct the deflected beam on to a set of photodiodes to increase the beam optical path. Thus, the small vertical movement of the cantilever results in an increased vertical displacement of the beam spot on the photodiode plane. The deflection of the beam is measured by comparing the incident light on the photodiodes. The difference between the top and bottom photodiodes measures the vertical movement of the cantilever and the difference between the left and right photodiodes measures the cantilever torsion. The cantilever deflection is compared to the deflection setpoint in contact mode or amplitude setpoint in tapping-mode. The feedback system will make the piezo-scanner move the sample in z-direction accordingly.

The main operational modes of the AFM are contact mode, non-contact mode and tapping-mode in an air or liquid environment. In contact mode, the tip is

scanned in close contact with the surface and the forces experienced by the tip are repulsive. The tapping mode was developed to prevent frictional forces and capillary forces as well as damage on soft samples or influence of electrostatic interactions. In this mode, the cantilever is excited to its resonant frequency to amplitudes up to approximately 100 nm so that it comes in and out of contact with the surface. Changes on the amplitude and phase of the cantilever vibration are correlated to the sample surface features. Van der Waals attractive forces can be detected in non-contact mode by keeping the tip a few nm separated from the surface oscillating with an amplitude of about 5 nm. These forces are much lower in magnitude but true atomic resolution can be achieved in this mode ([Morris 1999], p.44). The changes experienced by the cantilever are usually detected by an optical system consisting of a laser beam focused on, and reflected from, the back of the cantilever, and a mirror that deflects the reflected beam on to a set of detecting photodiodes (Fig. 1.1). A feedback system maintains constant the forces experienced by the tip for topographical imaging or the cantilever-surface distance for force mapping.

Apart from topographical images, normal and lateral force imaging can be performed [Mate 1987]. By introducing specific modifications, other types of information can be extracted from the sample surface such as the contact potential difference between tip and sample [Nonnenmacher 1991] or magnetic force mapping [Martin 1986]. Chemical contrast can also be obtained [Overney 2002] as the AFM tip is sensitive to changes in surface energy [Burnham 1990]. Measuring and comparing adhesion forces with a chemically-modified tip, nucleobases self-assembled in a monolayer can be mapped as the adhesion forces between complementary nu-

cleobases is larger than between non-complementary ones [Ijiro 2002]. The local interaction between tip and sample can also be tailored to generate local chemical or physical modifications on the substrate. Therefore, high-resolution patterned structures can be fabricated using the precise positioning system of the AFM. For example, a wide range of materials such as biomolecules, colloidal particles or polymers can be delivered directly to the surface by DPN. The liquid ink containing such materials is loaded on to the AFM tip and delivered during the directed scanning through the thin water meniscus formed between tip and sample [Demers 2002].

Deformable materials such as PMMA can be thermo-mechanically patterned by heating the tip [Vettiger 2000]. Joule heating resulting from biasing the tip can also be used to melt these polymers. Structures are raised by the electrical pressure that results in mass transport of the melted polymer [Lyuksyutov 2004]. Applying a voltage between a conductive AFM tip and the sample substrate can generate structures of different nature depending on the material and the mode of application. Using the water layer on the surface or the ambient oxygen as a reacting agent, Si substrates can be locally oxidised by biasing the tip [Kuramochi 2004]. The local electro-oxidation of self assembled monolayers provides a local chemical modification that can be used as a template for subsequent local covalent binding of molecules [Maoz 2000].

Furthermore, using dielectric thin layers as substrates, charges can be injected and trapped in the sample by biasing the AFM tip on the nanometre scale. Electrical patterns obtained by this method can be used for the attachment of nano-particles from the gas phase [Barry 2003] or suspended in non-polar liquids [Mesquida 2001].

1.3 Motivation for the thesis

The goal of this thesis is to investigate the use of electrical patterns written on dielectric materials to localise the attachment of biological molecules or nanoparticles on a surface. Manipulating biomolecules at the nanoscale is driven by the fundamental research of biological processes at molecular and sub-cellular length scales. Understanding these mechanisms could also lead to the development of novel nanodevices by manipulating biomolecules as mechanical elements. For example, biological and chemical sensors could be created by interfacing biomolecules with inorganic transducers [Lin 2004]. In the nanofabrication field, the bottom-up approach needs means to manipulate nanoparticles or biomolecules as building blocks, as they are usually not compatible with conventional micro-structuring techniques. Biomolecules and nanoparticles are typically charged in solution, therefore electrostatic forces can be used to drive rapid parallel deposition of large numbers of particles to specific locations on a substrate patterned with charges [Mesquida 2001].

AFM charge-writing allows the creation of high-resolution charge-patterns of either polarities. The patterns can be easily imaged immediately after charge-writing by Kelvin-probe Force Microscopy (KFM) using the same cantilever and cantilever holder. The KFM technique was the method chosen to characterise the charge-patterns as it gives a quantitative measure of the surface potential and the polarity of the patterned area with a resolution between 50 to 100 nm depending on the geometry of the tip [Jacobs 1998].

The creation of electrical patterns is not limited to AFM charge-writing. Charge-

patterns can be created on insulating films using a conductive stamp [Jacobs 2001] or irradiating selected areas of dielectric polymers with an e-beam [Wybourne 1996]. The substrates were subsequently patterned with nanoparticles by immersing the electrical-patterns in microparticle powder [Jacobs 2001] or exposing the charged areas to nanoparticles dispersed in gas phase or in non-polar solutions [Barry 2003]. The attachment of nanoparticles immersed in water droplets dispersed in non-polar liquids has also been achieved using electrical patterns written with an AFM-biased tip [Mesquida 2001]. The application of this charge-pattern driven attachment to biomolecules immersed in polar liquids needs to be investigated. Aqueous solutions are the adequate environment for biomolecules to be functional. Biomolecular functionality depends on the pH used, and in water-based solutions this can be easily selected using the appropriate buffer. On the other hand, nanoparticles are usually dispersed in water-based solutions. The use of charge-patterns in polar liquids is not straightforward as charge decay is faster than in air or in non-polar environments [MesquidaDiss 2002]. This limits the time available for the particles to attach to the pattern. The screening effect in electrolyte solutions also limits the volume of interaction between the charge-pattern and the charged particles in the solution. The interactions between the charge-pattern, the solvent and the nanoparticles needs to be investigated to understand how charge-written patterns influence particle deposition on substrates.

Water-in-oil emulsions can be used to deliver encapsulated biomolecules to the charge-patterns to prevent rapid charge-pattern decay and screening effects. Using this method, biotin-modified (biotinylated) antibodies were patterned on a polymer

substrate and the functionality of the biotin molecule was demonstrated using the well-known avidin-biotin interaction [Naujoks 2004]. Protein microarrays, however, often require different biomolecules to be immobilised on the same substrate especially for applications such as immunoassays. Thus, the sequential attachment of different biomolecules is the next logical step to be explored. Therefore, the implications of using this technique in biomolecule functionality, discrimination from solution and cross-contamination were investigated in this thesis.

Furthermore, combining this technique with materials such as silicon dioxide, may facilitate the integration of the patterned samples with electronic devices. This would be a clear advantage for the development of novel microdevices with biological applications.

Chapter 2

Charge-Patterning and Imaging

2.1 Electrets

In order to use charge-writing to aid nanotechnological manipulation, as suggested by Wright and Chetwynd in their review paper about scanning probe-based charge-writing [Wright 1998], the substrate must retain the electrical pattern at least during the time required for the attachment of the charged nano-objects to the charge-pattern. Electret materials, according to Sessler's definition, are dielectric materials that exhibit a quasi-permanent electrical charge, where the term quasi means that the charge-decay time constants are much longer than the period of time used for the studies performed with the electret ([Sessler 1987],p.1). The charge decay time constant depends on the material used, the thickness of the dielectric layer, the conductivity of the supporting substrate, the conductivity of the surrounding environment, the pre-treatment of the sample and the charging mechanism.

The electrical pattern can be formed by the arrangement of real charges or by

alignment of dipoles or a combination of both. The net charge in an electret metallized on one side is approximately zero due to the counter charges in the electrode. The electric field exhibited is due to the charge separation, not to the net charge ([Sessler 1987],p.1).

Injecting charge carriers into the material generates a charge-pattern formed by space or surface charges. These are localised in trapping states associated with impurities or defects in the bulk of the material, at the surface or at interfaces.

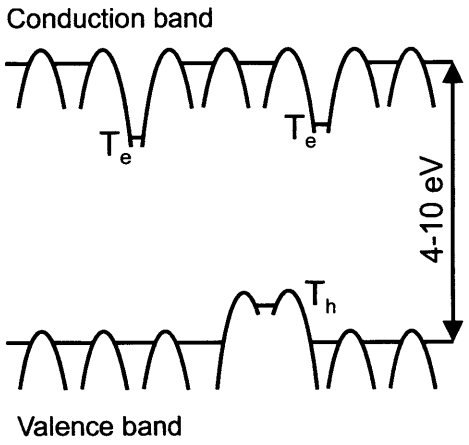

Figure 2.1: **Band-gap model**. [Sessler 1987], p.55. Trapping states exist in the volume and interfaces due to impurities and defects. These traps can be occupied by electrons if they are close to the conduction band (T_e) or by holes (T_h) if they are close to the valence band (T_h) exhibiting negative or positive surface potential.

In figure 2.1, the band gap model was applied to explain the charge trapping mechanism. Amorphous and microcrystalline dielectrics possess a short-range order. This allows the model to be applied over microscopic distances. The localised states in the gap are related to the lack of long range order and the presence of impurity centres and structural defects ([Sessler 1987], p.218).

There is a wide variety of electrets that can be used for charge-patterning [Wright 1998]. In this thesis, the charge-pattern decay on PMMA and PS thin films and a single layer of silicon dioxide on silicon substrate was studied in different environments.

2.2 Charge-patterning techniques

The generation of electrical patterns in electret materials can be achieved using different methods which usually involve the injection of charge carriers by electrical discharges, particle beams, or contact electrification using biased, patterned electrodes and scanning-probes.

Charge-patterns have been created on polymeric electrets with locally injected electrons by scanning a narrow e-beam over the surface [Feder 1976], [Wybourne 1996]. Charged Ga^{+} ions have also been locally injected on a $CaTiO_3$ substrate using a focused ion beam to create a 2-D charge-spots array with a few micrometre spot size[Fudouzi 2002]. Charge carriers can be injected by contact electrification when the materials brought into contact have different work functions. Nevertheless, charge-patterns written with the aid of an applied voltage proved to be more reliable [Saurenbach 1992].

Polymer thin-films are known to have good charge storage properties and are easily fabricated by vapour deposition or spin-coating techniques. Thus, PMMA, a polymeric electret, was one of the first materials to be explored for charge-writing using a scanning probe [Stern 1988]. Charge-spots of 2 μm in diameter were created

in a 1 mm PMMA layer using Ni wires as tips, biased with voltages above 100 V. However, using thinner PMMA films and applying voltages of 10 V with a W tip. spot sizes of 70 nm could be obtained [Schonenberger 1992]. Thus, one of the potential applications that first motivated the creation of charge-patterns was their use as data storage. The small size of the charge-spots generated by scanning probe techniques would allow a promising high-density of data storage using charge-spots as data bits.

Charge-patterns have also been proposed as electrostatic templates for the attachment of nanoparticles or biomolecules using PMMA or polytetrafluoroethylene (PTFE) films as substrates [Mesquida 2001], [Naujoks 2003]. Charge-writing in PTFE films has been systematically investigated using highly-doped commercial Si-AFM tips [MesquidaDiss 2002]. Both positive and negative charge-patterns could be written with charge decay times over one week under ambient conditions. A resolution lower than 200 nm could also be achieved. Furthermore, PTFE films do not dissolve in hydrocarbon-based solvents nor in polar solvents which represent an advantage for nanoxerographic applications.

The charge-trapping capabilities of SiO_2 have also been widely investigated as it is a key dielectric material for microelectronics. Using Atomic Force Microscope Charge-Writing (AFM-CW), a charge-pattern resolution of 320 nm with a charge decay time of 4 h has been reported [Jacobs 1999,a]. In principle, the polar silanol groups that are formed at the SiO_2 surface lead to the physisorption of water molecules increasing surface conductivity and thus, hampering the charge-pattern stability [Olthuis 1992]. However, several approaches to reduce charge decay have

been reported such as the removal of the absorbed water layer by heating treatments [Uchihashi 1994] or the reduction of surface hydrophilicity with surface coatings such as hexamethyldisilazane [Olthuis 1992], [Enikov 2004].

Diffusion and recombination of the injected charge carriers could lead to the lateral spread and overall decay of the charge-pattern and need to be taken into account in all cases. Using AFM-CW, the charge-pattern can be imaged, immediately after being written, in the specific location using KFM. This is a clear advantage for the study of charge-pattern dynamics. Thus, AFM-CW was the method chosen for electrostatic pattern generation and imaging in this thesis.

Regarding process speed, the creation of charge-patterns by AFM-CW is a serial technique and thus relatively slow. However, this is not a fundamental problem as high-speed scanning-probe systems and multiple-tip arrays are under development [Schitter 2001], [Humphris 2005], [Vettiger 2000] and could be employed in the future. An alternative would be to create charge-patterns in parallel by a xerography-type process [Mort 1989], where substrates would be limited to photoelectret materials, or by electrical microcontact-printing [Jacobs 2001].

2.3 Kelvin-probe force microscopy

A powerful application of scanning probe microscopy is to use the local electrostatic interaction between an AFM probe and the sample to generate an electric potential map of the surface. This is particularly interesting as the electric potential carries information about the surface composition, charge distribution or adsorbed layers.

High sensitivity measurements have been achieved by using modulating techniques, combining the vibrating capacitor or Kelvin method [Kelvin 1898] with an AFM and surface potential mapping has been performed with sub-micrometre resolution [Nonnenmacher 1991]. The KMF technique has been used for the detection of material contrasts [Jacobs 1997], for imaging potential differences of cell membranes [Knapp 1999] or for dopant profiling in p-n junctions [Kikukawa 1995]. A review of the method can be found in the article of Fujihira [Fujihira 1999]. Charges trapped in the dielectric thin-film contribute to the surface potential. Therefore, the distribution of localised charges in dielectric materials can be imaged by KFM [Jacobs 1999,a]. Thus, in this thesis, charge-patterns were imaged mapping the surface potential distribution using the KFM technique.

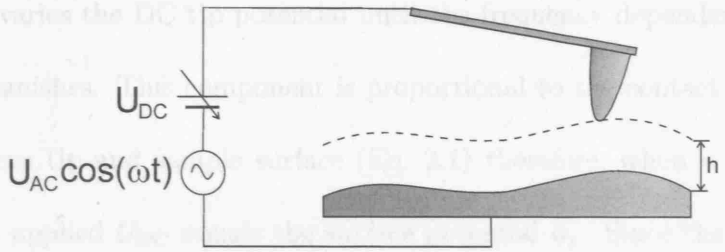

Figure 2.2: **Lift mode diagram**. First trace: topography measurement; Second lifted trace: electrostatic measurement: an AC voltage with an DC offset is applied to the cantilever at a lifted height h. U_{DC} equals the surface potential ϕ_s when the ω-component of the electrostatic force vanishes (Eq 2.1).

The principle used by the KFM technique to measure the surface potential distribution consists in sequentially recording the topography and the surface potential of each scanned line (Fig. 2.2). The topography is measured in tapping mode and the

surface potential in lift mode. This minimizes any contribution from the topography and short-range forces to the surface potential image.

During the lifted retrace of each imaged line, the tip is excited electrically by applying a voltage U between the AFM tip and the sample back electrode consisting of an AC voltage $U_{AC} \cdot \cos(\omega t)$ and an adjustable DC offset U_{DC} where ω is the resonance frequency of the cantilever. Also taking into account the surface potential $\phi_s(x)$ and the tip-sample capacitance C, the ω-component of the electrostatic force applied to the tip due to the tip-sample capacitance is:

$$F_C^{\omega} = \frac{\partial C}{\partial z}(U_{DC} - \phi_s(x)) \cdot U_{AC} \cdot \cos(\omega t) \tag{2.1}$$

The ω-component of the force is detected by a lock-in amplifier, and the feedback control varies the DC tip potential until the frequency dependent component of the force vanishes. This component is proportional to the contact potential difference between tip and sample surface (Eq. 2.1) therefore, when it vanishes, the voltage offset applied U_{DC} equals the surface potential ϕ_s. Since the amplitude of the cantilever oscillation is the same for a given potential difference $U_{DC} - \phi_s$ independently of its polarity, extra information is needed to adjust the voltage U_{DC} of the tip. Thus, the phase between the AC driving voltage and the cantilever oscillation is also monitored during KFM imaging since they are in phase when the potential difference is positive and 180° out of phase when it is negative.

The contribution of a fixed charge q to the overall force experienced by the AFM-tip, can be calculated as a Coulombic interaction between the fixed charge and the charge induced on the tip during the application of the voltage U in the

lifted trace [MesquidaDiss 2002]. Thus, the total ω-component of the force becomes the additive combination of such components of the forces due to the tip-sample capacitance and due to the fixed charge.

$$F^{\omega} = F_q^{\omega} + F_C^{\omega} \tag{2.2}$$

where F_q^{ω} can be expressed as,

$$F_q^{\omega} = \frac{C_t U_{AC} q}{4\pi\epsilon_0 (h+a)^2} cos(\omega t) \tag{2.3}$$

where C_t is the tip self-capacitance, a is the distance where the induced charge is located in the tip measured from the tip apex and h is the distance from the fixed charge to the tip apex.

Combining equations 2.3 and 2.1, the KFM potential U_{DC} that cancels F^{ω} is,

$$U_{DC} = -\frac{C_t}{4\pi\epsilon_0 (h+a)^2 \frac{\partial C}{\partial h}} q + \phi_s \tag{2.4}$$

Variations of ϕ_s along the sample are usually negligible when considering the clean homogeneous samples used for charge-writing. Therefore, setting the ϕ_s offset to zero, the KFM potential is proportional to the fixed charge. It is important to notice that $\frac{\partial C}{\partial h}$ is negative, thus, positive charges lead to positive KFM potentials and vice versa (Fig. 2.3).

Electrostatic forces are long range forces, therefore the surface potential of the area situated directly below the tip is not the only one contributing to the tip-sample interaction. One should expect that the measured data will include the interactions

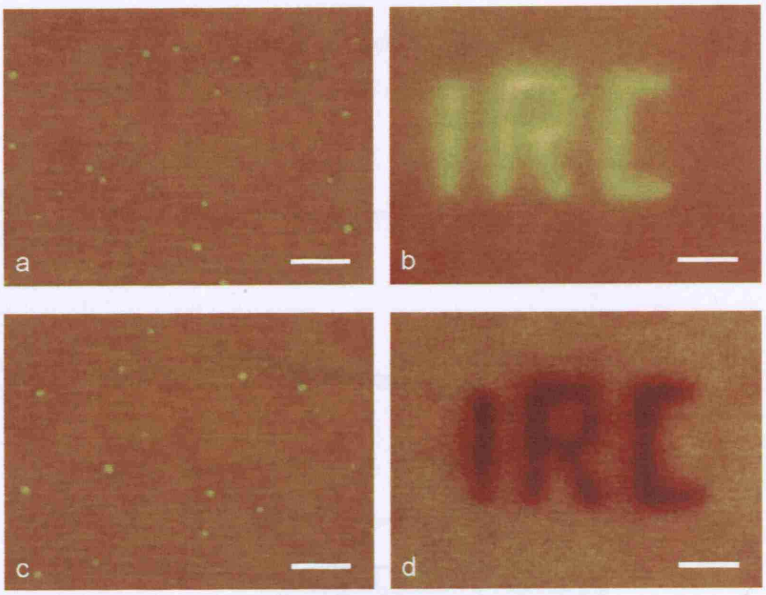

Figure 2.3: **Letters IRC written with positive and negative charges.** Voltage pulses of +30 V and −30 V magnitude and 0.5 ms length were applied between a plain Si tip and the sample substrate. The sample was a 70 nm thick PMMA thin-film on a Si substrate. (a) Topography image of the area charge-written with positive charges, z – scale range = 30 nm. (b) KFM surface potential image of the charge-pattern written applying positive voltage pulses, scale range = 250 mV. (c) Topography image of the area charge-written with negative charges, z – scale range = 30 nm. (d) KFM surface potential image of the charge-pattern written applying negative voltage pulses, scale range = 250 mV. Scale bars = 0.5 μm.

between different areas of the surface holding different potentials and the tip. This can be explained using a simple model in which the sample surface is considered as n electrodes of constant potential ϕ_i (Fig. 2.3). Being ϕ_t the tip potential, the electrostatic forces experimented by the tip in the vertical direction can be expressed in terms of the mutual capacitance between the different electrodes C_{ij}, and between each electrode and the tip C_{it} [Jacobs 1998].

Thus, the ω-component of the force can be expressed as:

$$F^{\omega} = \sum_{i=1}^{n} C'_{it}(\phi_i - U_{DC}) \cdot U_{AC} \tag{2.5}$$

where

$$C'_{it} = \frac{\partial C_{it}}{\partial z} \tag{2.6}$$

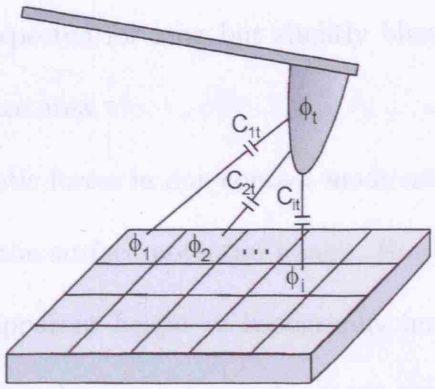

Figure 2.4: **Mutual capacitances model.** The sample is represented as a system of conductive electrodes. The electrostatic interactions are represented by mutual capacitances between electrodes C_{ij} and between each electrode and the tip C_{it}.

According to this model, U_{DC}, the measured KFM potential when the ω-component of the force vanishes, corresponds to a weighted average over all potentials ϕ_i of the surface. The weighting factor is the derivative of the mutual capacitance between the tip and the electrode at the actual tip location along the z-axis.

$$U_{DC} = \frac{\sum_{i=1}^{n}(C'_{it}\phi_i)}{\sum_{i=1}^{n} C'_{it}} \tag{2.7}$$

The resolution of the KFM technique depends on the geometry of the tip and cantilever as they contribute to changes in the mutual capacitances with the sample surface. Using numerical simulations applying the multiple multipole method and

performing experiments on surfaces of known surface potential features it has been estimated that the minimum resolution to be achieved by the KFM technique is between 50 nm - 100 nm depending on the tip and cantilever geometry [Jacobs 1998]. According to Jacobs' numerical simulations, if the tips used were too sharp the cantilever would dominate the electrostatic interactions with the sample which would also include an orientation-dependent contribution from the arm of the cantilevers. The best results were expected for long but slightly blunt tips with cantilever of minimal width and surface area.

Sensing the electrostatic forces in non-contact mode minimises any contribution of short-range forces to the surface potential image. However, strong electrostatic forces can produce an apparent height in topography images. The height values can be higher than the actual values when a strong attraction between the charged sample and the induced charge on the tip occurs. This effect is due to the feedback system retracting the tip as a response to the additional attracting force to maintain the amplitude set point. In AFM tapping mode topography images, this would be mistakenly interpreted as a height increase [Yan 2006]. Thus, topographical imaging when dealing with high surface potential distributions must be carefully interpreted.

Chapter 3

Charge-Writing

The goal of this thesis was to use electrostatic forces to attach charged nanoparticles or biomolecules to a surface previously patterned with charges on the nano- and microscale. The electrical patterns were written on polymeric and non-polymeric electrets using AFM charge-writing. In this chapter, the experimental method used to prepare and charge-pattern different electrets is described in detail followed by the analysis of the quality of such charge-patterns regarding pattern fidelity and stability.

3.1 Experimental method

3.1.1 Sample preparation

3.1.1.1 Polymeric electrets

There is a wide range of polymers, polymer blends and polymer ceramic composites that are electret materials [Goel 2003]. Their wide availability and charge storage properties make them the materials of choice for charge-writing applications [Wright 1998]. Polymer thin-films can be easily produced by spin-coating techniques; some are well established materials for nanofabrication. PMMA is a pho-

toresist material for e-beam lithography. It is also a material commonly used in biological environments. Synthetic bone scaffoldings or contact lenses are examples of medical applications of PMMA. The charge storage capabilities of this polymer together with its bio-compatibility, make it a promising material for the development of protein arrays using charge-pattern driven attachment [Naujoks 2004].

Another example of a polymeric electret is PS. Charge-patterns have been created on PS thin-films injecting electrons in the material by irradiating selected areas of the polymer with an e-beam [Wybourne 1996]. The charge-patterned film was incubated with a solution containing avidin-fluorescein which attached preferentially to the irradiated areas. This preferential attachment was attributed to electrostatic attraction between the charged protein and the charge-pattern created on the film [Wybourne 1996]. Therefore, PS was also investigated for AFM charge-writing and subsequent electrostatic attachment in this thesis.

The polymeric electrets used were PMMA (average M_w 996000) and PS (powder, typical M_w 200000) (Sigma-Aldrich Company Ltd., Poole, UK). They were solved in chlorobenzene (Sigma-Aldrich Company Ltd., Poole, UK) and xylene Analar® (BDH Ltd., Poole, UK) respectively in concentrations varying from 0.01 g/ml to 0.06 g/ml depending on the desired thin-film thickness.

Silicon pieces of approximately 0.25 cm^2 were used as conductive substrates. They were cut from a p-type $< 100 >$ Si wafer (ρ = 14.0 Ω·cm - 20.0 Ω·cm) manufactured by Scottish Microelectronics Centre (Edinburgh University, Edinburgh, UK). The substrates were cleaned by 10 min ultrasonication in ethanol Analar® (BDH Ltd., Poole, UK) and in UHQ-water ($\rho = 18.2 \cdot 10^6\ \Omega \cdot$ cm) consecutively

using a Fishebrand® FB11002 ultrasonic bath (Fisher Scientific UK Ltd., Loughborough, UK). After the ultrasonication they were dried under a stream of N_2.

The clean Si substrates were spin-coated with the polymeric solutions in a two step KW-4A precision spin-coater (Chemat Technology Inc., Wem, UK). After spin-coating, the samples were baked on a hot plate, a RCT basic magnetic stirrer with heating (Ika®-Werke GmbH & Co.KG, Staufen, Germany), to evaporate the remaining solvent. The spin-coating and baking parameters used for each polymer are shown in table 3.1. Fast-drying silver paint (Agar Scientific Ltd., Stansted, UK), was used to fix the Si substrates on to metallic specimen discs (Agar Scientific Ltd., Stansted, UK), to yield a conductive contact.

Polymer	**1_{st} Step speed (5 s)**	**2_{nd} Step speed (45 s)**	**Baking temperature**	**Baking time**
PMMA	400 rpm	4000 rpm	180°C	45 min
PS	400 rpm	2000 rpm	60°C	20 min

Table 3.1: **Spin-coating and baking parameters for PMMA and PS.**

It is known that the quality of the charge-pattern depends on the electret film thickness [MesquidaDiss 2002]. In the case of thick films, for a given voltage applied between the tip and the substrate, the field emerging from the tip might not be strong enough to inject electrons into the material. By decreasing the film thickness, the number of total trapping states in the bulk of the material also decreases affecting the amount of charge that can be injected. Thus, the thickness of the films produced was measured. A trench of polymer film was removed using steel tweezers without damaging the Si surface (Fig. 3.1). The depth of the trench was measured with an AFM by measuring the distance between the two main peaks in the raw data, height

histogram (Fig. 3.1, (e), (f)).

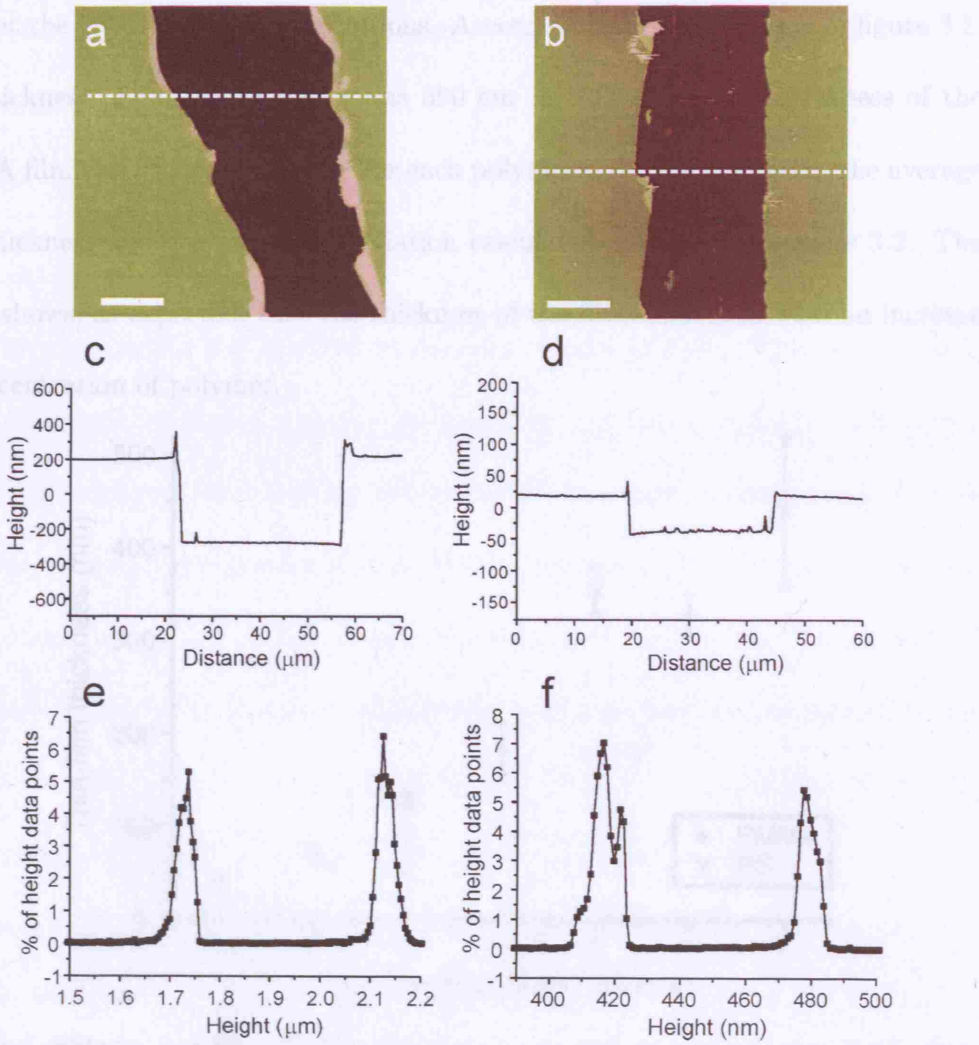

Figure 3.1: **Thickness of polymer thin-films.** a) AFM topography image of a trench made on a PS thin-film spin-coated using a 0.07 g/ml PS in xylene solution, z-scale range = 1000 nm, scale bar = 14 μm. (b) AFM topography image of a trench made on a PMMA thin-film spin-coated using 0.02 g/ml PMMA in chlorobenzene solution, z-scale range = 200 nm, scale bar = 12 μm. AFM topography images made in tapping mode with a plain Si-tip, cantilever A (Table 3.3). c-d) Cross-section of images (a) and (b) respectively. e-f) Height histograms of image (a) and (b) respectively.

The peak on the left of each histogram shows the distribution of height data in the trench. The peak on the right, at higher z-value, shows the distribution of height data of the film surface. The film thickness was measured by calculating the distance

between the two peaks and the error for each measurement was calculated taking into account the FWHM of the distributions. According to the histograms in figure 3.1, the thickness of the PS thin-film was 390 nm ± 30 nm and the thickness of the PMMA film was 61 nm ± 8 nm. For each polymer concentration used, the average film thickness and the standard deviation calculated are shown in figure 3.2. The figure shows, as expected, that the thickness of the films increased with an increase in concentration of polymer.

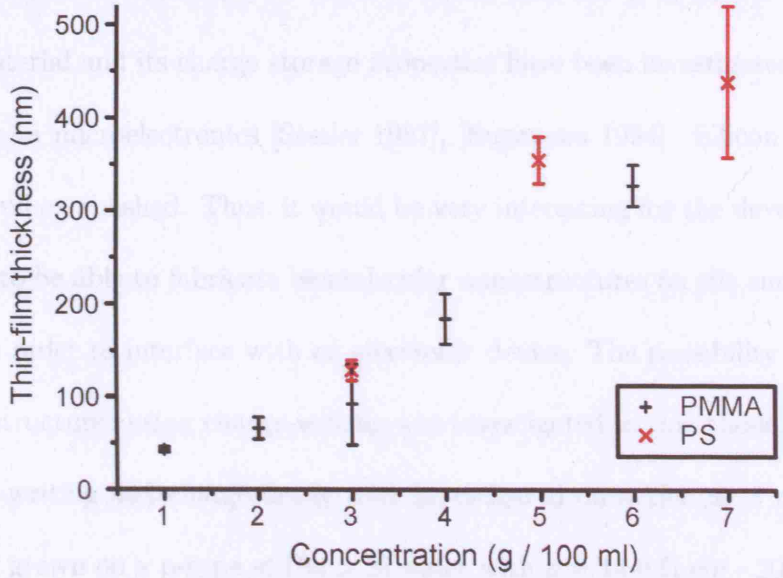

Figure 3.2: **PMMA and PS thin-film thickness.** Increasing the concentration of polymer in the solution used for spin-coating produced thicker films.

The standard deviation of the thickness of the films ranged from 10 % to 60 %. The reason for the variation in the film thickness measured in different samples could be related to the fact that the Si substrates used were not exactly the same size and the volume of solution deposited on the surface for spin-coating was not the same. A certain variation was also expected within each sample. However, polymer films

of significantly different thicknesses could be fabricated by controlling the polymer concentration and the thickness of each film could be measured in the proximity of the area to be charged.

3.1.1.2 Silicon dioxide

Thermal oxide

Silicon dioxide is a key material in microfabrication and electronic devices as it is an insulator that makes a very good interface with Si. It is also a well known electret material and its charge storage properties have been investigated due to its importance in microelectronics [Sessler 1987], [Sugawara 1994]. Silicon microtechnology is well established. Thus, it would be very interesting for the development of biosensors to be able to fabricate biomolecular nanostructures on the surface of this material in order to interface with an electronic device. The possibility of creating such nanostructures using charge-writing was investigated in this thesis.

Charge-writing and charge decay were investigated on a 194 $\pm$ 3 nm thermal oxide layer grown on a p-type $< 100 >$ Si wafer with $\rho = 14.0\ \Omega$·cm - 20.0 Ω·cm. It was manufactured by the Scottish Microelectronics Centre (Edinburgh University, Edinburgh, UK). Pieces of approximately 0.25 cm^2 were cut from the wafer and ultrasonicated in ethanol and in UHQ-water for 10 min consecutively. They were dried under a stream of N_2 and fixed on a metallic specimen disc using silver paint.

Samples are usually stored for a long time after their fabrication and water can diffuse into the oxide and lead to faster charge decay times. Thus, the samples were dehydrated before charge-writing by performing a 200°C heat treatment on a hot

plate. The relationship between the length of the heat treatment and charge-pattern stability is shown in section 3.2.3.1.

OTS modified oxide

Surface coatings are typically used to selectively promote or minimise protein attachment. Proteins exhibit different affinity for adsorbing on self-assembled monolayers (SAMs), depending on their termination group. Many proteins show low absorption to methyl-terminated SAMs [Wadu-Mesthrige 2000]. On the other hand, terminating groups such as carboxilic acid, aldehydes [Wadu-Mesthrige 1999] or biotin [Lee 1994] are known to promote protein adhesion by electrostatic interactions, covalent binding or biospecific interactions. In this section a surface coating was layered on a SiO_2/Si substrate to explore the combination of surface functionalisation of the electret substrate and charge-writing.

The SiO_2 pieces prepared as described in section 3.1.1.2 were used as substrate. The samples were dried at 200°C for 3 h on a hot plate and the cleaning procedure was completed with 120 s plasma-cleaning in air at 1-5 mbar pressure using a ILMVAC PLASMA-clean 4 plasma-cleaner (Agar Scientific Ltd., Stansted, UK).

The clean SiO_2 substrates were coated with a layer of methyl-terminated n-octadecyltrichlorosilane (OTS) (Sigma-Aldrich Company Ltd., Poole, UK) following Sagiv's methodology [Maoz 1999]. The samples were immersed in a 10 mM solution of OTS in hexane for 30 s followed by ultrasonication for 2 min in pure hexane in the flow-hood. This process was repeated eight times. Finally the samples were thermally annealed at 110°C for 10 min on a hot plate. Figure 3.3 shows an

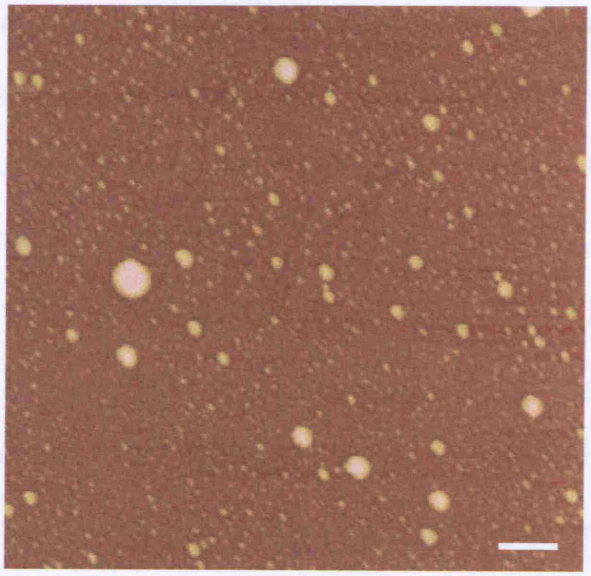

Figure 3.3: **Topography image of the OTS/SiO_2 sample surface.** AFM topography image showing aggregates on the surface of the OTS/SiO_2 sample. Image scanned in tapping mode. Scale bar = 2 μm, z-scale range = 200 nm.

AFM image of the OTS layer on SiO_2. In the topography image, many aggregates can be observed of sizes ranging between 10 nm up to 200 nm. Thus, it was not possible to assume that the surface was methyl-terminated. However, since the surface conductivity of SiO_2 is very sensitive to surrounding humidity [Olthuis 1992], [Kressmann 1996], the OTS layer may reduce the influence of ambient moisture in the charge-pattern decay. The influence of the OTS layer on charge-writing and subsequent biomolecule deposition was thus investigated.

3.1.2 AFM charge-writing

The instrument used for charge-writing and for surface potential and topography imaging was a NanoScope MultiMode SPM (Digital Instruments Inc., Santa Barbara CA, USA) equipped with IV Controller. Quadrex phase imag-

ing with lock-in detection is implemented in the controller to map the phase and amplitude of the cantilever oscillation during a scan. The detection of the amplitude and phase of the ω-component of the force is necessary for the KFM measurement of the surface potential (section 2.3).

The piezo-scanner used for the translational movement of the AFM tip was a 5834 JVH scanner with x-y range of 150 μm. This allows writing and imaging patterns ranging from hundreds of nanometres size to the upper limit of the scanner. Charge-writing was performed by applying a voltage between the cantilever tip and the sample substrate as the tip was moved over the sample drawing the desired pattern. The bias was turned on and off to create charged and non-charged areas. After charge-writing, the surface potential of the area was measured by KFM. The tip must be conductive for charge-writing and charge detection. The same tip was used for both actions to facilitate imaging the surface potential in the same location, immediately after charge-writing. Highly-doped plain Si and W_2C-coated tips were used: NONCONTACT silicon cantilevers NSC12/50 and NSC12/W2C/15 (Mikromasch, Madrid, Spain). The specifications of the tips are shown in table 3.2. Plain Si tips were conductive enough for charge-writing. They were significantly cheaper and the resolution was better as the radius of curvature was smaller. The charge-patterns were written either in contact or in tapping mode. Cantilevers A or B were used generally for tapping mode and cantilever E for contact mode scanning. The specifications are shown in table 3.3.

The connection of the signal access module III (SAM) (DIGITAL INSTRUMENTS INC., Santa Barbara CA, USA) between the microscope and the controller permit-

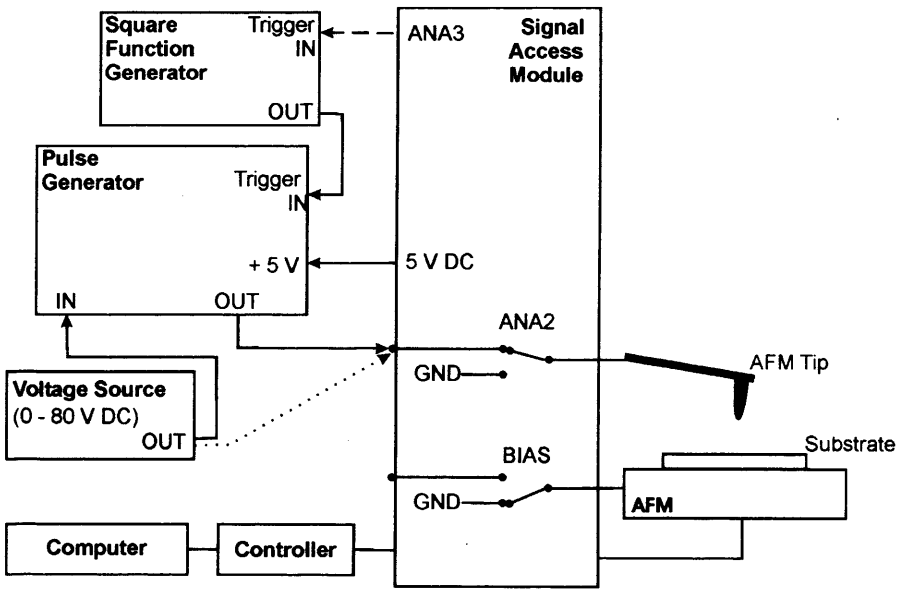

Figure 3.4: **Charge-writing experimental set-up.** The controller was connected to the microscope through the signal access module (SAM). The SAM allowed access to the substrate through BIAS and to the tip through ANA2. During charge-writing the tip or the substrate were disconnected from controller and connected to an external voltage. If the voltage was introduced via BIAS, the substrate was positively biased and the tip was grounded. This resulted in a negative surface potential pattern. If the voltage was introduced via ANA 2 with the substrate grounded, then the polarity was inverted and the pattern was positively charged. The external voltage was either a pulsed voltage of a DC voltage (dotted line). The pulse generator (PG) was triggered by each downwards flank of a + 5 V. 50 Hz square function. The square function was either operated in continuous mode or in trains of 5 V pulses triggered by the AFM lithography software via ANA3 (dashed line). The magnitude of the output PG pulses was selected from 0 - 80 V by the voltage source. + 5 V DC fed the PG. During KFM imaging the tip and the sample substrate were connected to the controller.

ted the introduction of external signals into the microscope and monitoring signals coming from both the microscope and the controller (Fig. 3.4). A custom-built pulse generator (PG) was connected to the tip of the AFM through the SAM, with the sample mount grounded, to inject holes into the electret. To inject electrons, the polarity of the voltage applied was inverted by introducing the signal coming from the PG output into the sample mount. Instead of a pulsed voltage, a DC voltage could also be directly applied for charge-writing. The PG was tuned to generate pulse voltages of 500 μs length. The magnitude of the pulse, Up, was selected by

regulating the DC power supply feeding the PG. The patterns were written by triggering the pulsed voltages to occur in the desired locations. This was programmed using the lithography software implemented in the AFM. For large and simple features, such as tens of micrometre-size charge-lines, voltage pulses were applied by triggering the PG with a 5 V, 50 Hz square signal turned on and off manually.

Tip	Plain Si	W_2C-coated Si
Radius of curvature (μm)	< 10	< 35
Tip height (μm)	15 - 20	15 - 20
Top side coated with Al	yes	yes
Full tip cone angle	$< 20°$	$< 20°$

Table 3.2: **Specifications of the plain Si and W_2C coated tips**

Cantilever	A	B	E
Length (μm)	110 ± 5	90 ± 5	350 ± 5
Width (μm)	35 ± 3	35 ± 3	35 ± 3
Thickness (μm)	$< 2.0 \pm 3$	$< 2.0 \pm 3$	2.0 ± 3
Resonance frequency (KHz)	165 - 240	240 - 405	17 - 24
Force constant (N/m)	3.5 - 12.5	6.5 - 27.5	0.1 - 0.3

Table 3.3: **Specifications of the cantilevers**

The charge-patterns were imaged by KFM after AFM-CW at scanning rates ranging from 0.5 Hz to 2 Hz. Nanoscope 6.12 software was used for the analysis of the AFM images. The surface potential images obtained in KFM mode were X-Y plane-fitted (1^{st} order) and the topography images were flattened (1^{st} order) off-line excluding any aggregates or dirt from the calculations.

3.2 Surface potential measurements

The magnitude of charge trapped in the electrets after charge-writing, the lateral spread of the charge and the charge decay determine the quality, the fidelity and the stability of charge-patterns to be used as electrostatic templates. These values depend on the electret used, its preparation, the charge-writing parameters employed as well as the ambient humidity. Different electrets have different concentrations of trapping states and those can be located at different distances with respect to the surface. These factors influence the shape and magnitude of the patterned surface potential obtained after charge-writing. Different materials may also have different detrapping mechanisms that would influence the charge decay. Decay and lateral spread of the injected charge could be a restricting factor on the attachment of charge nano-objects to charge-patterns. Therefore, the charge-patterns were evaluated, for each material used, by KFM.

3.2.1 Charge-patterning and charge decay on PMMA

3.2.1.1 Charge-pattern decay in air

The first approach was to evaluate the charge-patterns and the charge-decay in air. The charge-pattern consisted in two parallel arrays of eight charge-spots each. The first array was charge-written applying a positive voltage and the second one applying a negative voltage to obtain positively and negatively charged spots (Fig. 3.5). Each array of spots was charge-written using a lithography program that scanned the AFM tip at 10 μm/s tip velocity over each 1 μm^2 spot applying voltage pulses at 50 Hz rate. Subsequently, the tip moved 6 μm laterally, applying no voltage, to

reach the area where the next adjacent spot was to be charge-written. Selecting a scan size of 60 μm and aspect ratio = 4, the charge-writing program was run, at the top of the image frame with Up = + 70 V and subsequently, at the bottom of the image frame with Up = - 70 V (Source Code: Appendix D.1). After charge-writing the aspect ratio was changed to 2 and the pattern was imaged at regular intervals of time to monitor the charge decay. Figure 3.5 shows the charge-patterns written in tapping and in contact mode. The pattern written in contact mode shows higher surface potential contrast between charged and non-charged areas. This was expected as charge-writing in contact mode, the tip is in contact with the surface longer than in tapping mode allowing more electron transfer.

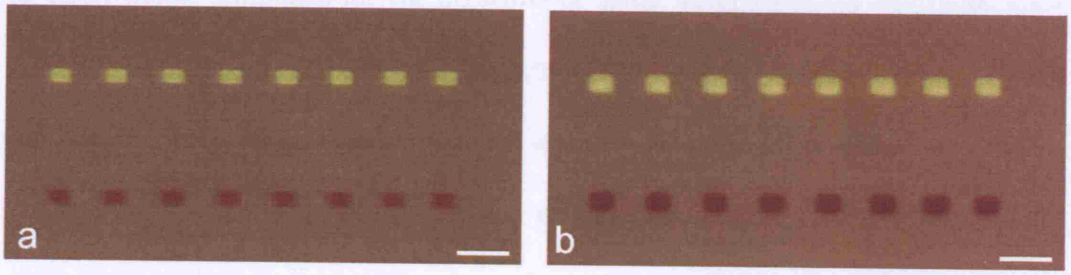

Figure 3.5: **Positive and negative charge-spots on PMMA.** KFM images of the charge-patterns written on PMMA using a thin-film of 66 ± 12 nm thickness. a) Charge-pattern written in tapping mode. b) Charge-pattern written in contact mode. Scale range = 10 V. Scale bars = 6 μm.

The charge decay time constant calculated for the positive charge-pattern was $t_d = 12 \pm 2$ min when written in tapping mode and $t_d = 10 \pm 4$ min when written in contact mode. For the negative charge-patterns, the decay time constant was $t_d = 10 \pm 2$ min when written in tapping mode and $t_d = 12 \pm 2$ min when written in contact mode (Fig. 3.6). Thus, the charge-pattern decayed at a similar rate for both writing methods, but the initial surface potential is higher when writing in

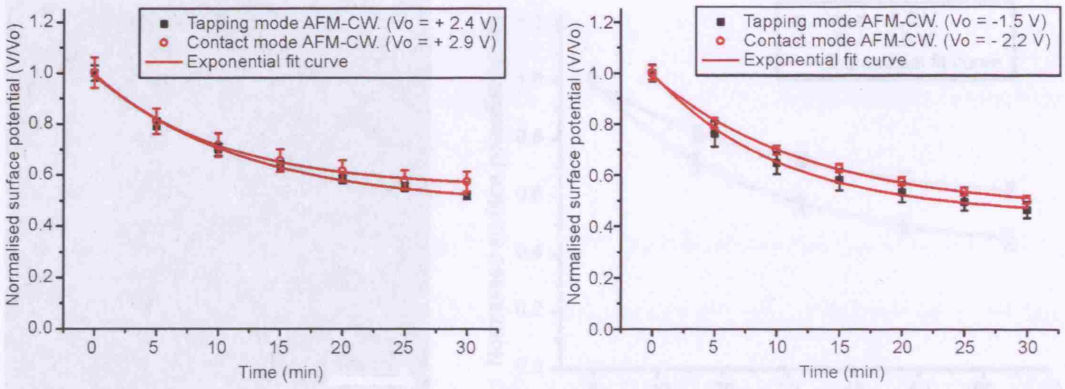

Figure 3.6: **Decay of positive and negative charge-spots on PMMA.** Left: Decay of the positively charged spots written in tapping and contact mode. Right: Decay of the negatively charged spots written in tapping and contact mode. The data was fitted to an exponential decay curve $\propto e^{-t/t_d}$ where t_d is the time decay constant.

contact mode, as expected. The charge-patterns are thus stable enough to be used as electrostatic templates for the attachment using water-in-FC-77 emulsions since only a few minutes are needed for the attachment and the dielectric oil FC-77 has a minimal effect over the charge-pattern stability [MesquidaDiss 2002].

In order to extend the study to other charge-pattern geometries, 40 μm x 4 μm areas were written in tapping mode with positive and negative charges. The tip velocity during writing was 10 μm/s and 12 lines were scanned in each of the rectangular areas applying a continuous train of voltage pulses turned on and off manually. Figure 3.7 shows the surface potential decay measured at the centre of the charged areas.

In air, under normal conditions, the charge decay time constant calculated by fitting the data to an exponential decay curve was $t_d = 30 \pm 10$ min for the positively charged area and $t_d = 25 \pm 7$ min for the negatively charged-area (Fig. 3.7). After 1 h, the positive peak surface potential had decayed to 60 % of its initial value and the

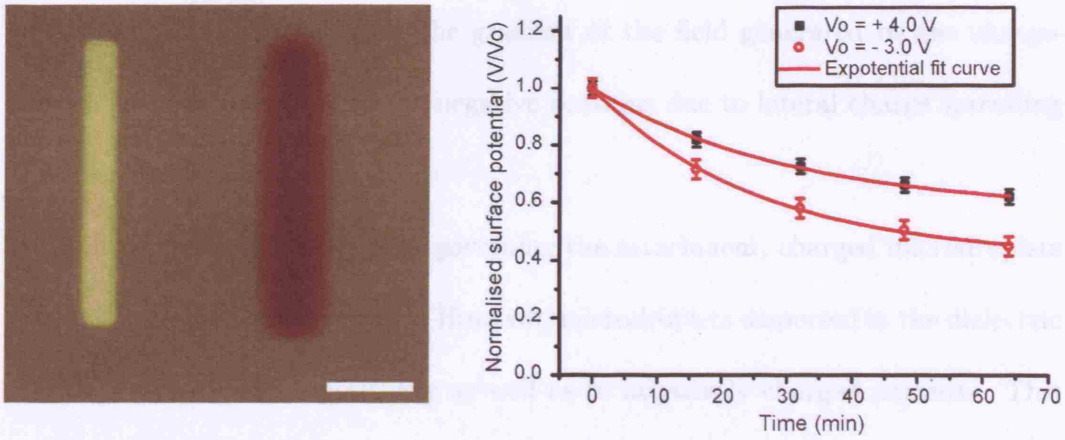

Figure 3.7: **Positively and negatively charged rectangular areas on PMMA.** Left: KFM image of a positively charged 40 μm x 4 μm areas on a 66 $\pm$ 12 nm PMMA thin film. The areas were charge-written at tip velocity = 10 μm/s, in tapping mode, applying $\pm$ 70 V voltage pulses. Scale range = 10 V. Scale bar = 12 μm. Right: Normalised surface potential decay of the positively and negatively charged areas. The lines are 1st-order-exponential fits $\propto e^{-t/t_d}$ of the normalised surface potential where t_d is the time decay constant.

negative peak surface potential had decayed to 45 %. The negatively charged pattern also showed lower pattern definition than the positively charged one. The lack of definition could be explained by the charge spreading laterally during charge-writing. The negatively charged traps could be closer to the surface than the positively charged ones and thus be more influenced by surface conduction [Hori 2000].

Positive charge-patterns are thus more suitable to be used as high resolution electrostatic templates than the negative ones in PMMA. Moreover, in the case of polarisable particles, due to the contribution of dielectrophoretic forces to the attachment, sharper changes in the surface potential are expected to drive more attachment. This result is confirmed by previous research where high resolution attachment of charged objects, from air or suspended in dielectric solvents, to positive charge-patterns was demonstrated [Barry 2003], [Naujoks 2005]. The negative charge-patterns drove less attachment than positive ones [Naujoks 2005]. This

was attributed to the fact that the gradient of the field generated by the charge-pattern features was lower in the negative patterns due to lateral charge spreading [Naujoks 2005].

If only Coulombic forces were governing the attachment, charged microdroplets would only attach to one polarity. However, microdroplets dispersed in the dielectric oil FC-77 can attach to positively as well as to negatively charged patterns. This is due to the contribution of dielectrophoretic forces [MesquidaDiss 2002] which can be described by the equation 3.1 where R is the radius of a polarisable spherical particle and ϵ_p and ϵ_s are the corresponding dielectric constants of particle and solvent [Jones 1995].

$$\vec{F}_{Diel} = 2\pi R^3 \frac{\epsilon_p - \epsilon_s}{\epsilon_p + 2\epsilon_s} \epsilon_s \nabla E^2 \tag{3.1}$$

According to equation 3.1, the direction of the force is determined by the sign of the factor $(\epsilon_p - \epsilon_s)$ and not by the polarity of the net charge of the microdroplets. For water microdroplets dispersed in FC-77, where $\epsilon_p > \epsilon_s$, the microdroplets would be driven towards higher electric fields. Sharper changes in the surface potential would thus drive more attachment of microdroplets independently of the polarity.

3.2.1.2 Charge-pattern decay in water

To attach nano-particles or biomolecules from aqueous liquids, the charge decay time constant in water needs to be investigated as charge-patterns are expected to decay faster in mediums with higher conductivity. A 20 μm x 4 μm area was charge-written in tapping mode applying - 80 V and + 80 V pulses on a PMMA thin-film spin-coated using a 0.02 g/ml PMMA in chlorobenzene solution. The thickness of the film

was 61 ± 8 nm. Surface potential imaging could not be performed in water because the conductivity of the medium would produce a short-cut between the cantilever and the sample substrate. In order to measure the surface potential, the water was removed approximately after every ten seconds of immersion. The sample was immersed in water again after each measurement. The time invested in measuring the surface potential was not counted as immersion time. The decay of the surface potential during immersion in deionized water (UHQ-water $\rho = 14 \cdot 10^6\ \Omega \cdot \mathrm{cm}$) is shown in figure 3.8.

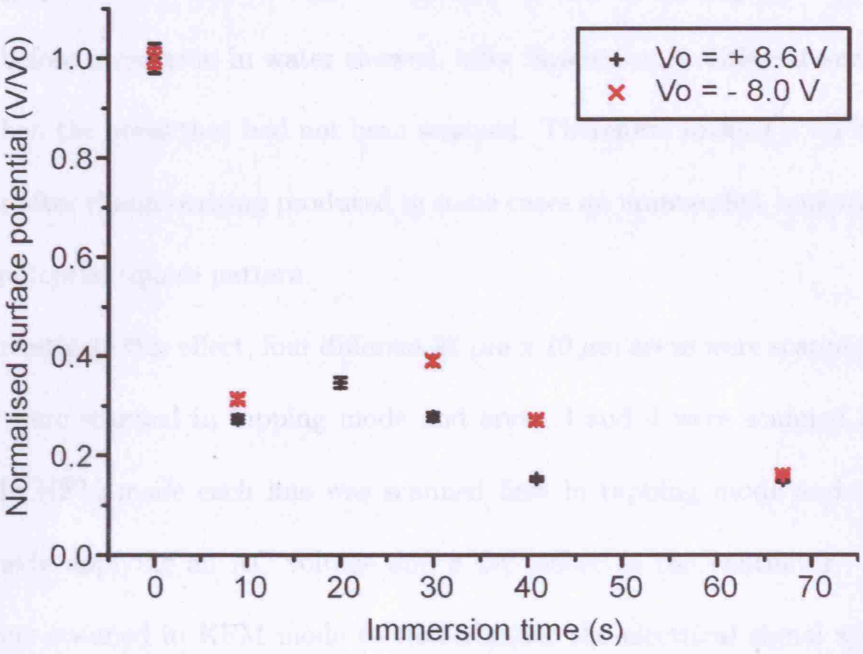

Figure 3.8: **Decay of charge-patterns written on PMMA in water.** (+) Positively-charged area. (×) Negatively-charged area. The surface potential was normalised to the surface potential value measured immediately after charge-writing, before immersion.

After 9 seconds of immersion in pure water 27 % of the initial charge was measured in the positively charged area and 31 % in the negatively charged area. After 1 min, 15 % of the initial charge remained for both polarities. The charge decay was

therefore faster than in air. This was expected as PMMA is a polar material and thus sentitive to humidity changes. The methyl ester side-chain group in PMMA is polar and can react with the H^+ in water leading to water absorption in the surface and bulk of the PMMA increasing its conductivity [Cui 1998].

3.2.1.3 Influence of scanning in surface potential

Some of the KFM images made after immersion of the charge-written PMMA samples in water did not show a homogeneous background potential in the proximity of the charge-patterns. Areas that had been scanned without the application of a bias voltage before immersion in water showed, after immersion, a different surface potential than the areas that had not been scanned. Therefore, making a KFM image before or after charge-writing produced in some cases an unintended, superimposed, surface potential square pattern.

To investigate this effect, four different 20 μm x 20 μm areas were scanned. Areas 1 and 2 were scanned in tapping mode and areas 3 and 4 were scanned in KFM mode. In KFM mode each line was scanned first in tapping mode and secondly in lift mode applying an AC voltage and a DC offset to the cantilever. Areas 3 and 4 were scanned in KFM mode to test whether the electrical signal applied to the cantilever during the KFM imaging had any influence on the sample surface potential. A scratch made on the polymer surface was used as reference to find the scanned areas after the immersion (Fig. 3.9). The thickness of the PMMA film used was 66 $\pm$ 12 nm.

After scanning the 20 μm x 20 μm areas in their corresponding modes, a larger

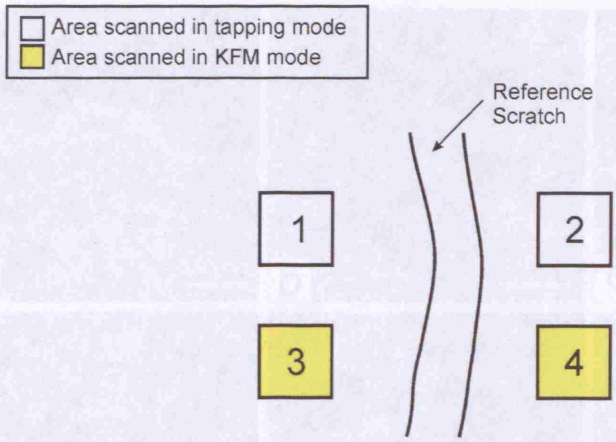

Figure 3.9: **Diagram of the areas scanned on a PMMA thin-film to investigate their effect on the surface potential.** Areas 1 and 2 were scanned in tapping mode. Areas 3 and 4 were scanned in KFM mode. Scanning parameters: plain Si tip, cantilever A, scan rate = 0.5 Hz.

KFM image was made to compare the surface potential in the originally scanned and non-scanned areas. The scanned areas 1 and 3 were imaged before and after immersion in pure water. The scanned areas 2 and 4 were imaged after immersion only. The surface potential images are shown in figure 3.10. The immersion was performed by placing a droplet of water on the surface with a pipette and removing it after 15 s. Before KFM imaging, the surface was dried under a stream of N_2.

The KFM images showed a larger contrast between the scanned and non-scanned areas when the area was originally scanned in tapping mode rather than in KFM mode (Fig. 3.10, (a), (d)). The surface potential of the scanned areas was more negative than the surrounding non-scanned areas. After immersion in water, the contrast increased in all cases. This effect seemed to be an adding effect since when an area was scanned twice (Fig. 3.10, (c), (f)), the surface potential became more negative than when it was scanned only once (Fig. 3.10, (b), (e)). The same

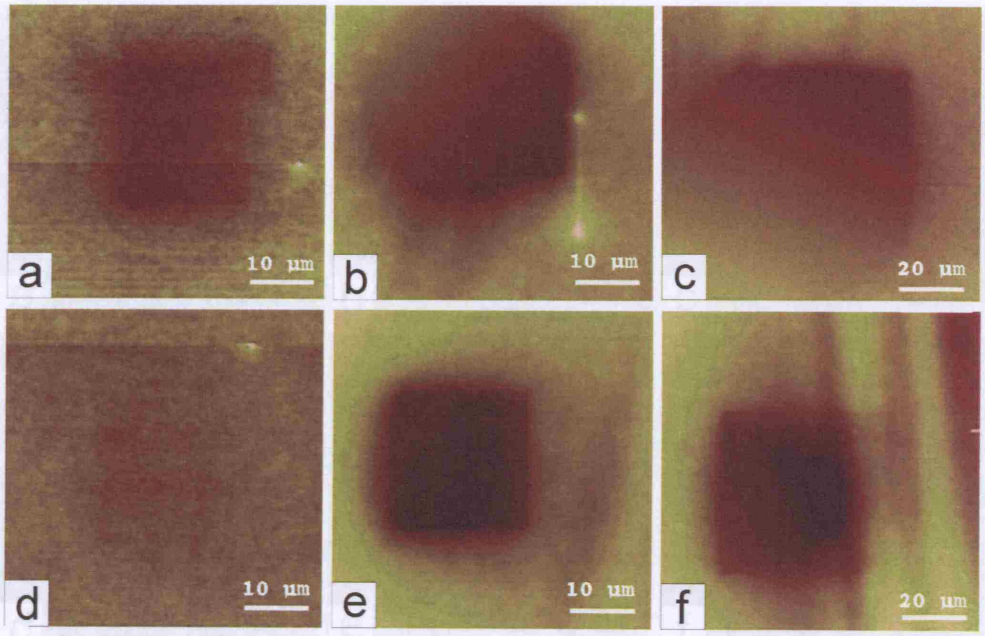

Figure 3.10: **Influence of scanning with a Si tip, on the surface potential of a PMMA thin-film.** Top images: initial 20 μm x 20 μm areas 1 and 2 scanned in tapping mode: a) KFM image of the scanned area 1 before immersion of the sample in water. Scale range = 0.3 V; b) KFM image of the scanned area 2 after immersion. Scale range = 3 V; c) KFM image of the scanned area 1 after making the KFM image (a), immersing the sample in pure water for 15 s and drying it. Scale range = 3 V. Bottom images: initial 20 μm x 20 μm areas 3 and 4 scanned in KFM mode: d) KFM image of the scanned area 3 before immersion. Scale range = 0.3 V; e) KFM image of the scanned area 4 after immersion. Scale range = 3 V; f) KFM image of the scanned area 3 after making the KFM image (d), immersing the sample in water for 15 s and drying it. Scale range = 3 V.

experiment was performed on another PMMA thin film 90 ± 20 nm thick reducing by 30 % the force applied over the sample during scanning. The results are shown in figure 3.11. The results were qualitatively the same as in figure 3.10. The values of the surface potential of the scanned areas before and after immersion are shown in table 3.4.

To investigate whether the surface potential modification decayed in time, KFM images were made 7 and 8 days later on area 4. The surface potential values are shown in table 3.5. Eight days after immersion in water there was still a significant

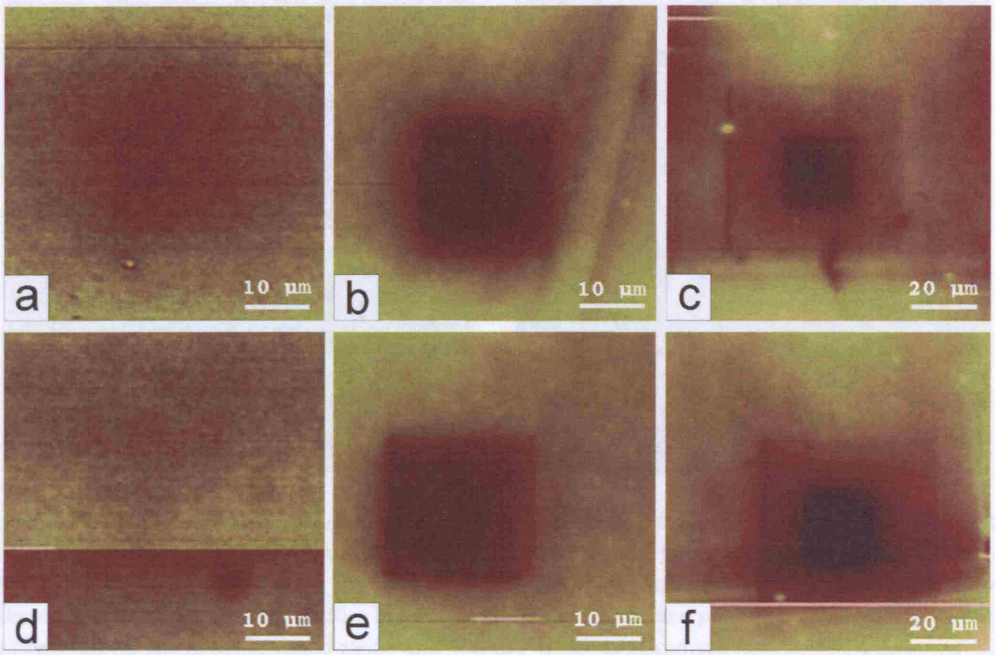

Figure 3.11: **Influence of scanning with a Si tip, with lower applied force, on the surface potential of a PMMA thin-film.** The applied force is 30 % lower than in figure 3.10. Top images: initial 20 μm x 20 μm areas 1 and 2 scanned in tapping mode: a) KFM image of the scanned area 1 before immersion. Scale range = 0.3 V; b) KFM image of the scanned area 2 after immersion. Scale range = 3 V; c) KFM image of the scanned area 1 imaged before and after the immersion. Scale range = 3 V. Bottom images: initial 20 μm x 20 μm areas 3 and 4 scanned in KFM mode: d) KFM image of the scanned area 3 before immersion. Scale range = 0.3 V; e) KFM image of the scanned area 4 after immersion. Scale range = 3 V; f) KFM image of the scanned area 3 imaged before and after the immersion. Scale range = 3 V.

	Before immersion	After immersion only	Before and after immersion
20 μm x 20 μm area initially scanned in tapping mode	(Area 1) -30 mV	(Area 2) -1050 mV	(Area 1) -1320 mV
20 μm x 20 μm area initially scanned in KFM mode	(Area 3) -20 mV	(Area 4) -830 mV	(Area 3) -2050 mV

Table 3.4: **Surface potential contrast between scanned and non-scanned areas on PMMA measured before and after immersion in pure water.**

surface potential contrast between the area that was originally scanned and the surrounding area.

Using different tips, surface contrasts of magnitudes ranging from a few tens of millivolts to 200 mV were generated after immersion in water. The cantilevers were

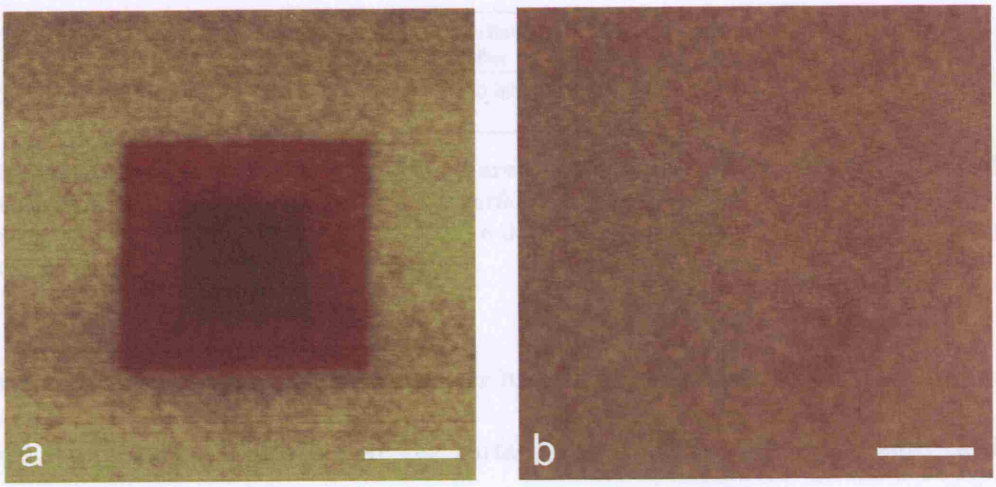

Figure 3.12: **Influence of NH_4F treatment of Si AFM tips on the surface potential contrast generated by scanning.** a) Area scanned using an non-cleaned tip. KFM image of a PMMA film in which a 5 μm x 5 μm area and a 10 μm x 10 μm area were scanned consecutively at the centre of the image. After 15 s immersion in water, a surface potential contrast of - 200 mV was observed on the areas scanned twice and 100 mV in areas scanned once. b) Area scanned using a tip cleaned with NH_4F. KFM image showing no surface potential contrast between the scanned and non-scanned areas after immersion in water. Scale range = 0.5 V. Scale bars = 4 μm.

then cleaned with NH_4F. During the cleaning procedure the cantilever chip was held with tweezers clamped vertically during the immersion in 40 % NH_4F aqueous solution (FLUKA, Buchs, Switzerland). After immersion the cantilever chip was lifted out and dried under a gentle stream of N_2. Any remnants of the reaction were cleaned by immersion in UHQ-water and the cantilever was gently dried under N_2 again. Scanning with NH_4F-treated tips did not lead to any surface potential contrast after immerison in water (Fig. 3.12, (b)). The H-passivation created by treating the Si-tips with NH_4F could have thus, contributed to the reduction of the tip-surface interaction producing the surface potential contrast.

The nature of the enhancement of the surface potential contrast after immersion in water is not clear. The tip and PMMA have different work functions, thus some electron transfer is expected by contact electrification. However, the fact that the

Time after immersion	Immediately after	7 days after	8 days after
Surface potential of area 4	-830 mV	-610 mV	-670 mV

Table 3.5: **Surface potential contrast of an area scanned on PMMA, measured at different times after immersion in water.** The surface potential of the scanned area 4 was measured immediately after immersion, 7 days after and 8 days after immersion. After eight days a surface potential contrast could still be measured.

surface potential contrast increased after immersion and remained stable during at least 8 days could indicate that the surface underwent a physical change during scanning. The response of PMMA surfaces to local mechanical stimulation by AFM scanning is known to be larger in solvents such as water, methanol, ethanol and aqueous alcohol solutions [Leach 2003]. This effect could be a determining factor during the attachment of proteins to charge-patterns using aqueous solutions. AFM charge-writing requires a mechanical contact between tip and sample surface during charge injection. A latent, scanning-related modification of the surface could thus be generated during charge-writing. After immersion in water, the surface potential features created by the injected charge would decay rapidly. However, the scanning-related surface potential contrast would be enhanced and could drive preferential protein attachment.

3.2.2 Charge-patterning and charge decay on PS

The polystyrene thin-films were spin-coated using a 0.05 g/ml in xylene solution. Charge-patterns consisting of 6 positive and negative charge-spots were charge-written in contact and tapping mode applying voltage pulses using the lithography program described in section 3.2.1.1, (Source Code: Appendix D.1). The charge-

patterns written in contact and tapping mode are shown in figure 3.13

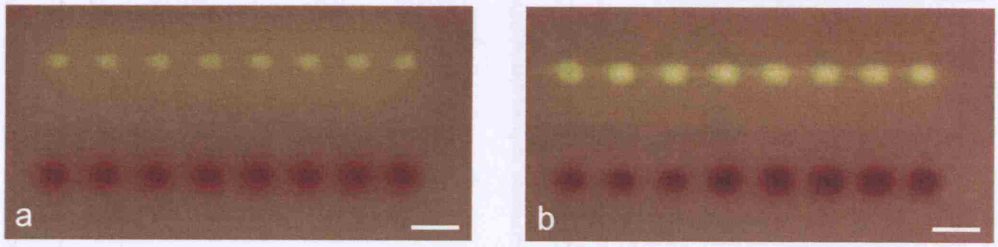

Figure 3.13: **Positive and negative charge-spots on PS.** a) KFM image of a the charge-pattern written in tapping mode on a 350 ± 25 nm PS thin film. b) KFM image of the charge-pattern written on the same PS thin-film in contact mode. Scale range = 10 V. Scale bars = 6 μm.

The patterns written in contact mode showed larger surface potential difference than the ones written in tapping mode. This effect was also observed when the charge-patterns were written on PMMA. It was associated with a longer contact time between tip and substrate in contact mode, which resulted in an increased electron transfer. However, the charge-pattern definition on PS was not as good as on PMMA possibly due to a higher degree of lateral charge spread. The charge decay was investigated measuring the surface potential at regular intervals after charge-writing. The normalised average surface potential peaks measured are shown in figure 3.14.

The data could not be fitted to an exponential decay (Fig. 3.14). Negatively-charged spots decayed at a faster rate than positively-charged ones. In the case of the positive charge-pattern, After 30 min, 70 % of the charge remained if the sample was charge-written in tapping mode and more than 80 % if the pattern was charge-written in contact mode. In the case of the negative charge-pattern, 30 % remained after 30 min when charge-writing in tapping mode and 60 % if the pattern was written in contact mode.

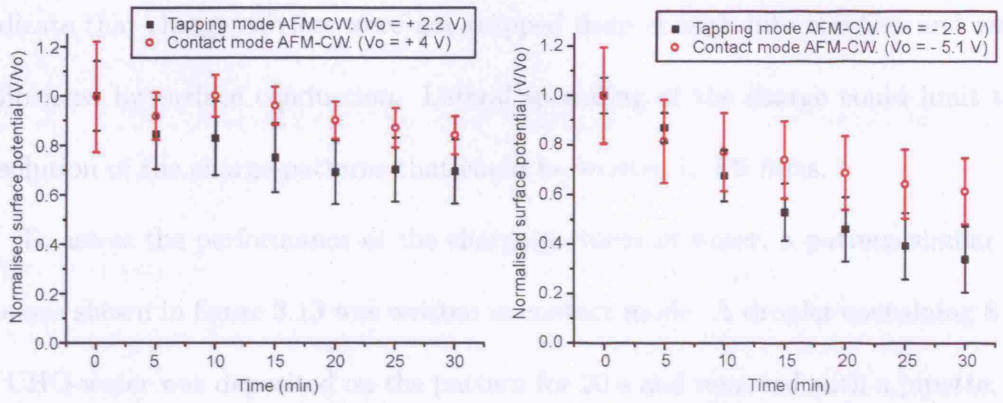

Figure 3.14: **Decay of positive and negative charge-spots on PS.** Left: Decay of the positively charged spots written in tapping and contact mode. Right: Decay of the negatively charged spots written in tapping and contact mode.

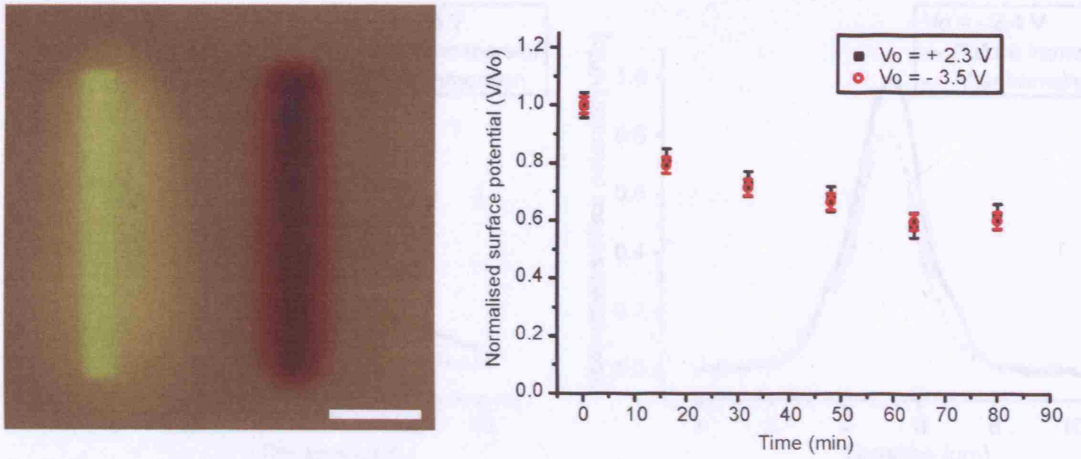

Figure 3.15: **Positively and negatively charged rectangular areas on PS.** Left: KFM image of a positively charged 40 μm x 4 μm areas on a 350 $\pm$ 25 nm PS thin film. The areas were charge-written at tip velocity = 10 μm/s, in tapping mode, applying $\pm$ 70 V voltage pulses. Scale range = 10 V. Scale bar = 12 μm. Right: Normalised surface potential decay of the positively and negatively charged areas.

When 40 μm x 4 μm areas were charge-written, both polarities decayed at similar rates and after 30 min more than 70 % of the charge remained (Fig. 3.15, right). The charge decay rates are thus slow enough to use the charge-patterns as electrostatic templates in air or in water-in-FC-77 emulsions. However, both charged areas showed poorer pattern definition than in PMMA (Fig. 3.15, left). This could

indicate that charge carriers were not trapped deep enough into the film and were influenced by surface conduction. Lateral spreading of the charge could limit the resolution of the charge-patterns that could be written in PS films.

To assess the performance of the charge-patterns in water, a pattern similar to the one shown in figure 3.13 was written in contact mode. A droplet containing 8 μl of UHQ-water was deposited on the pattern for 20 s and removed with a pipette. A KFM image was made before and after the immersion and the profile of the surface potential peaks is shown in figure 3.16.

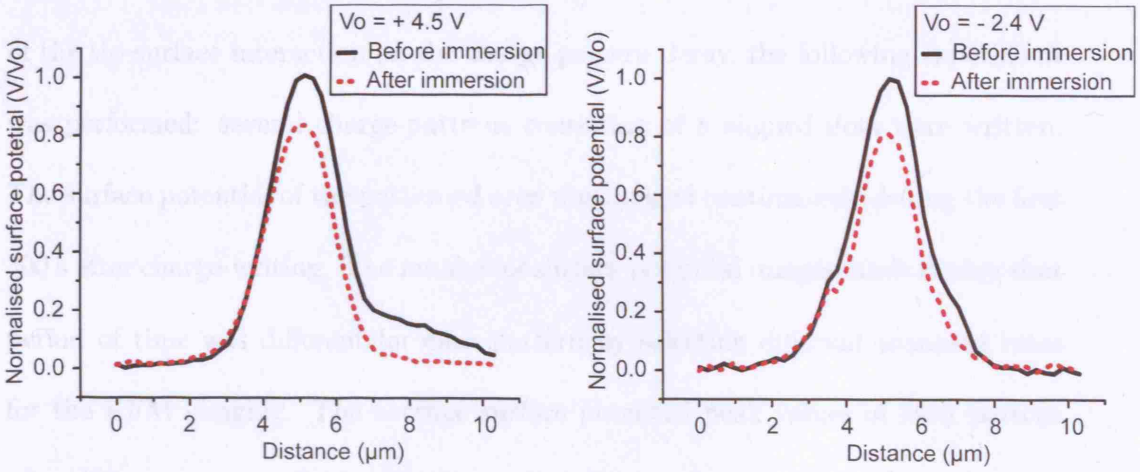

Figure 3.16: **Charge decay of charge pattern written on PS after 20 s immersion water.** Normalised surface potential peak of the positive (left) and negative (right) charge-patterns before and after 20 s immersion in UHQ-water.

According to the profiles in figure 3.16, for both polarities, approximately 80 % of the charge remained after 20 s immersion in water. Thus, the performance of charge-patterns was better in PS than in PMMA in which the charge decayed down to 30 % of the initial value in the first 10 s of immersion in water. Consequently, the electrostatic attachment was attempted directly from aqueous solution to charge-

patterns written on PS.

3.2.3 Charge-patterning and charge decay on silicon dioxide

3.2.3.1 Thermal oxide

Charge decay dependence on heat treatment of the sample

KFM images of the surface potential were made sequentially to trace the evolution of the surface potential difference between charged and non-charged areas. In the KFM technique the tip taps the sample surface to get a topographical image of the area before measuring the surface potential in lift mode. To determine the influence of the tip-surface interaction on the charge-pattern decay, the following experiment was performed: several charge-patterns consisting of 8 aligned dots were written. The surface potential of the patterned area was imaged continuously during the first 400 s after charge-writing. The number of surface potential images made during that period of time was different for each pattern by selecting different scanning rates for the KFM imaging. The average surface potential peak values of each pattern after 400 s was normalised with the peak surface potential measured immediately after charge-writing. The results were compared in figure 3.17 assuming that the charging and the decay does not depend on the position of the pattern.

There is no significant relationship between the number of scans and the charge decay within the first ten scans (Fig. 3.17). The variation of the data points could be a random effect due to changes on the shape of the tip during the experiments. Charge decay and lateral spread on silicon dioxide are also strongly related to the absorbed water layer on the surface. Performing a heat treatment can remove ph-

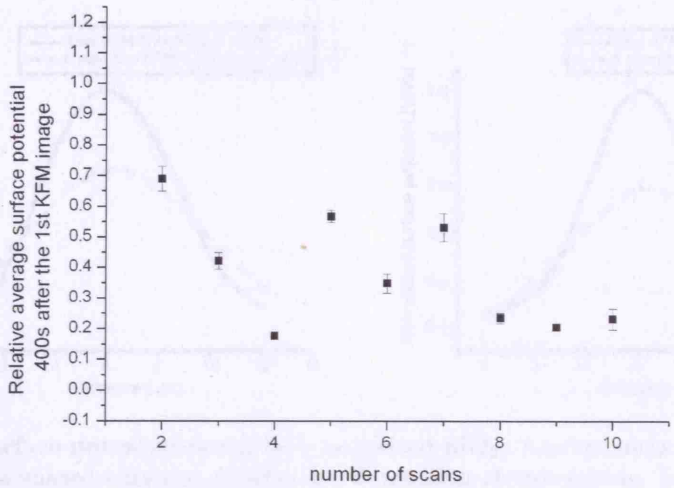

Figure 3.17: **Charge-pattern decay depending on number of scans on SiO_2.** Normalised average surface potential peak values recorded 400 s after charge-writing. Different number of scans were performed during the 400 s after charge-writing for each pattern.

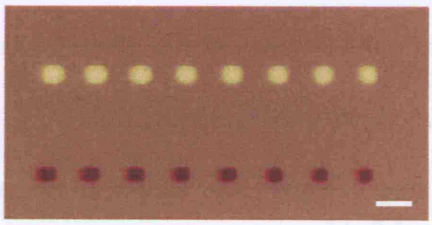

Figure 3.18: **Charge-pattern used for charge decay analysis on SiO_2.** KFM image of the charge-pattern written on a SiO_2 sample. 7 h heating pretreatment at 200°C. Scale range = 20 V, scale bar = 5 μm.

ysisorbed water from the oxide and thus improve the stability of the charge-patterns [Uchihashi 1994]. To determine the influence of the length of the heat treatment over charge-pattern decay, 4 SiO_2 samples were used; one of them was not heated and the other 3 were heated 1 h, 3 h and 7 h respectively at 200°C on a hot plate. Immediately after heating, each sample was charge-written with a charge-pattern consisting of 8 positively and 8 negatively charged spots (Fig. 3.18) and imaged at regular intervals of time to monitor the charge decay. The average surface potential profile of

similar charge-spots written on the non-heated sample is shown in figure 3.19.

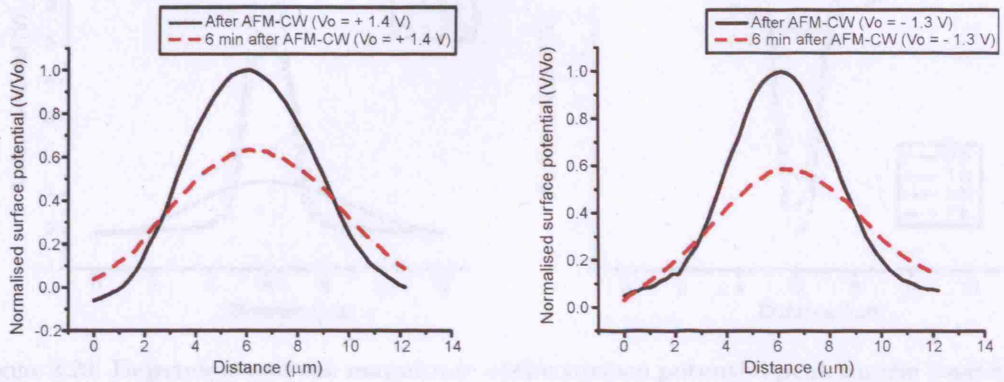

Figure 3.19: **Surface potential decay in non-heated SiO_2.** Average surface potential profile of the charge-spots imaged immediately after and 6 min after charge-writing. Left: Positive charge-pattern. Right: Negative charge-pattern.

For both polarities the pattern had poor definition and decayed rapidly. The surface potential achieved after AFM-CW was on the order of ± 1.4 V and after 6 min had decayed to 50 % of that value. Comparing these values with the surface potential achieved in the samples that underwent a heat treatment (Fig. 3.20), a great inprovement can be observed in pattern definition and magnitude of the surface potential peaks for both polarities.

The average surface potential profiles of the charge-spots measured immediately after and 90 min after charge-writing on the heated samples are shown in figure 3.21. Each peak was normalised to the peak values measured immediately after AFM-CW to directly show the percentage of charge remaining. The negative charge-patterns became more stable and well defined after the heat treatment but after 90 min, only minor differences in spreading and peak value were observed for different heat treatment times. However, a significant improvement was observed with longer heat treatments on the decay and spreading of the positive charge-pattern. These

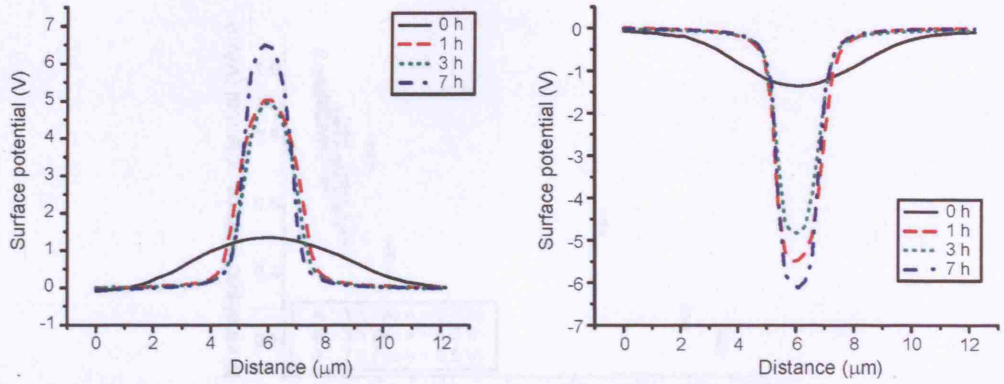

Figure 3.20: **Dependence of the magnitude of the surface potential peak on the length of the heat treatment.** One sample was not heated and three were heated at 200° for 1 h, 3 h and 7 h respectively. Left: Average surface potential profile of the charge-spots in the positively charged array. Right: Average surface potential profile of the charge-spots in the negatively charged array.

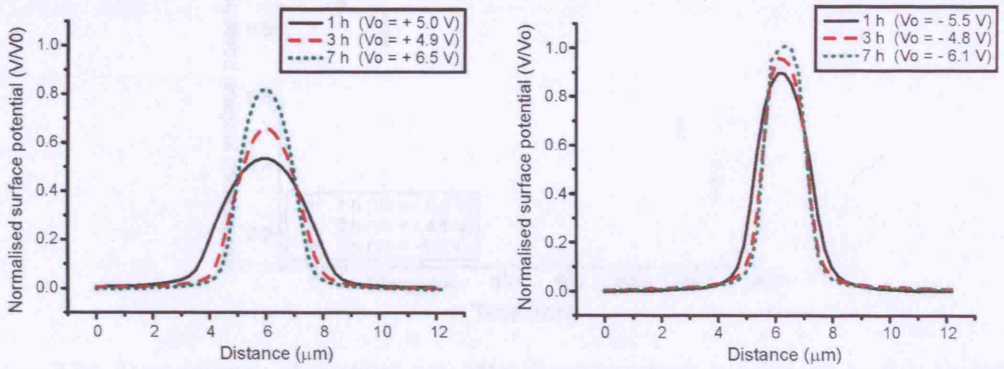

Figure 3.21: **Surface potential decay 90 min after charge-writing on heated SiO_2.** Normalised average surface potential profile of the charge-spots. Left: Positive charge-pattern. Right: Negative charge-pattern.

improvements facilitated the use of both polarities for electrostatic attachment.

The dependence of the surface potential decay on the length of the heat treatment is shown in figure 3.22. The positive and negative polarities decayed very differently. In general, for the positive patterns the decay became gradually slower with time, however, it could not be fitted well to an exponential decay. The patterns decayed slower for longer heat treatments. There was no significant difference in the decay of the negative patterns in the first 100 min after charge-writing. All pre-heated

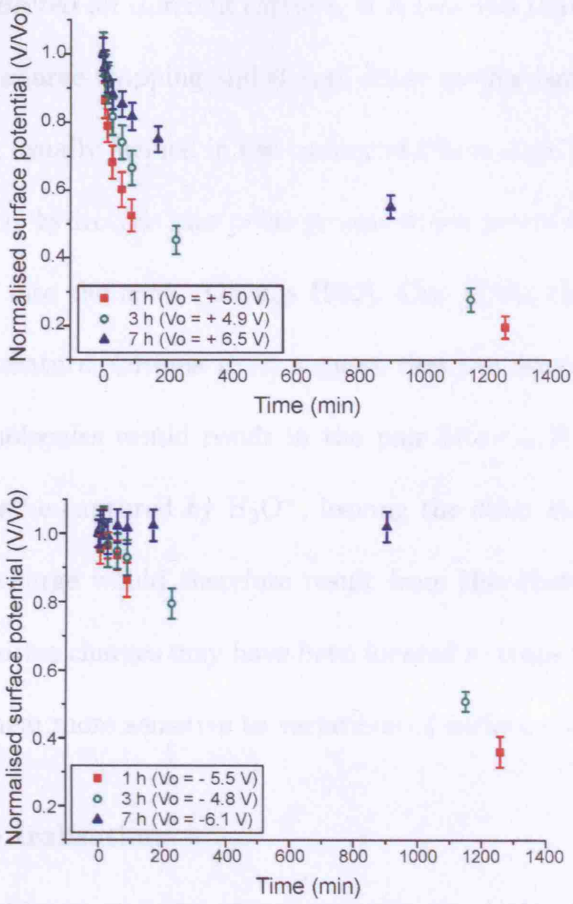

Figure 3.22: **Dependence of surface potential decay on heat treatment length in SiO_2.** Top: Normalised decay of the surface potential peaks in the positive charge-pattern. Bottom: Normalised decay of the surface potential peaks in the negative charge-pattern.

samples decayed at a very slow rate. For longer times, a significant improvement in the decay was observed in the sample heated for 7 h which did not show any decay when the other samples had decayed already to 50 % and 35 % of their inital value. The charge-pattern stability was thus improved by performing a heat treatment.

Electrically neutral charge traps in the oxide layer can be charged negatively or positively by injecting electrons or holes into the oxide [Olthuis 1992]. The origin and location of these traps can be very varied and different charging and decay

mechanisms are expected for different carriers. It is believed that water plays an important role in the charge-trapping and charge decay mechanisms in silicon dioxide. The silanol groups, usually formed in the surface of silicon dioxide shortly after fabricating the oxide by hydrolysis, are polar groups which promote the physisorption of water molecules into the oxide [Olthuis 1992]. One of the charging mechanisms proposed in the literature [Olthuis 1992] suggest that the deprotonation of silanol groups by water molecules would result in the pair SiO^- + H_3O^+. An incoming electron would thus be captured by H_3O^+, leaving the other fragment of the pair. A stable negative charge would therefore result from this chain of reactions. On the other hand, positive charges may have been located in traps nearer the air/SiO_2 interface making them more sensitive to variations of surface conductivity.

Rapid charge neutralisation

One of the advantages of using charge-patterns as electrostatic templates for biomolecular patterning was, that after having fulfilled their goal, they could be easily neutralised using a Zerostat® anti-static gun (Aladrich, Gillingham, UK) and after neutralisation, new charge-patterns could be written in the same substrate (Fig. 3.23). This allowed the use of electrostatic templates to sequentially attach different biomolecules without cross contamination. After neutralisation, no further electrostatic attachment is expected in the areas where biomolecules have already been attached.

Charge decay in polar and non polar liquids: water and FC-77

An experiment was carried out to determine the stability of the charge-pattern

Figure 3.23: **Charge-pattern neutralization.** A) KFM image after charge-writing on SiO_2. Scale range = 20 V. B) KFM image after neutralisation of the area previously charge-written. Scale range = 2 V. C) KFM image after charge-writing on the neutralised sample. Scale range = 20 V. Scale bars = 5 μm.

written on SiO_2 immersed in water. A SiO_2 substrate heated for 3 h at 200°C was patterned with a line of eight dots in tapping mode applying a single pulsed voltage 0.5 ms long and - 80 V magnitude per dot. The surface potential pattern is shown in figure 3.24.

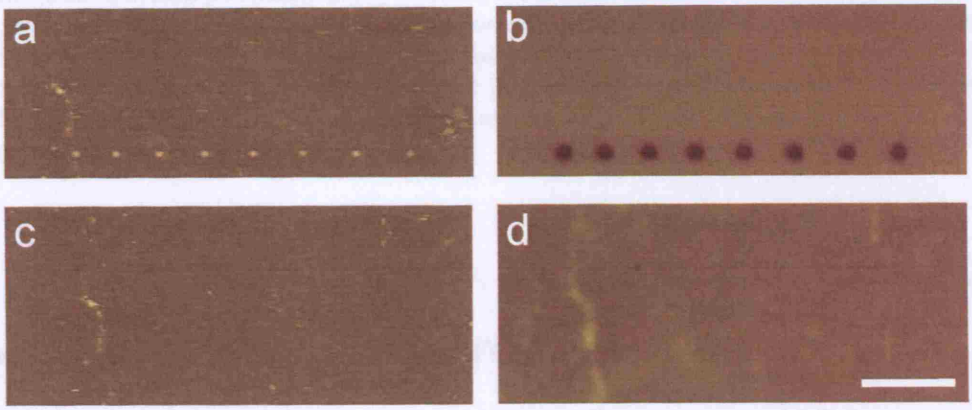

Figure 3.24: **Charge-pattern written on SiO_2 before and after immersion in water** a) AFM topography image corresponding to the area charge-written before immersion in water, z-scale range =35 nm. b) KFM surface potential image of a line of negatively charged dots written in tapping mode applying a single - 80 V pulse per dot. Average surface potential peak = 3.6 ± 0.1 V. Scale range = 5 V. c) AFM topography image of the area charge-written imaged after 24 s immersion in water, z-scale range =35 nm. d) KFM surface potential image of the area charge-written after 24 s immersion in water. Scale range = 5 V. Scale bar = 7 μm.

Immediately after charge-writing, a droplet of pure water was placed on the surface with a pipette and was removed after 24 s. The KFM image of the area

corresponding to the charge-pattern is shown in figure 3.24, (d). No electrical pattern can be distinguished from the background. This could be an indication of the water, or ions solved in the water, rapidly neutralising the charge-pattern. An increase of the surface conductivity of the oxide is also expected due to absorption of water.

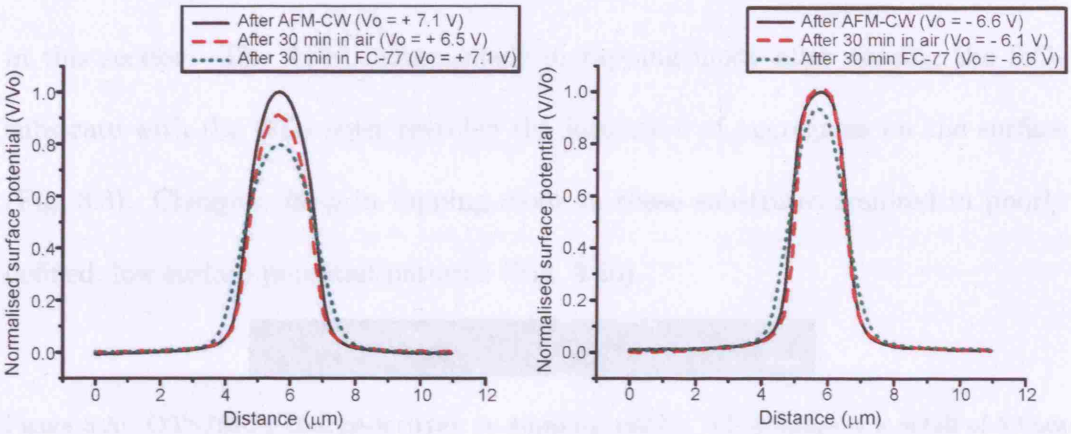

Figure 3.25: **Surface potential decay in SiO_2 after immersion in FC-77.** Normalised average surface potential profiles of the charge-spots measured immediately after AFM-CW and after 30 min immersion in FC-77. The profile of a similar pattern measured after 30 min in air is also shown and normalised to the value measured immediately after charge-writing for comparison. Left: Profiles corresponding to the positive charge-pattern. Right: Profiles corresponding to the negative charge-pattern.

To assess the charge decay in FC-77, the surface potential was measured before and after 30 min immersion in pure FC-77. The charge-pattern consisted of 8 positively and 8 negatively charged spots written by scanning 1 μm^2 areas in tapping mode applying + 70 V or - 80 V voltage pulses. Figure 3.25 shows the normalised average surface potential profiles of the positive (A) and the negative (B) charge-spots. After 30 min immersion in FC-77, the peak value of the surface potential was 80 % of the value measured immediately after charge-writing in the positive charge-pattern and more than 93 % in the negative charge-pattern. Hence, in the case of silicon dioxide substrates, water-in-FC-77 emulsions were used to perform

the attachment experiments instead of aqueous solutions since the charge-patterns remained sufficiently stable during the immersion in FC-77 and not in water.

3.2.3.2 OTS modified oxide

The OTS/SiO_2 substrates described in section 3.1.1.2 were assessed for AFM-CW in this section. The AFM images made in tapping mode after coating the SiO_2 substrate with the OTS layer revealed the formation of aggregates on the surface (Fig. 3.3). Charge-writing in tapping mode in these substrates resulted in poorly defined, low surface potential patterns (Fig. 3.26).

Figure 3.26: **OTS/SiO_2 charge-written in tapping mode.** KFM image of a detail of 5 lines charge-written in tapping mode at 10 μm/s tip velocity applying - 80 V voltages pulses at a 50 Hz rate. Scale bar = 3 μm, scale range = 10 V.

However, scanning in contact mode over the surface swept the aggregates to the edges of the scanning area producing a smoother area (Fig. 3.27). Positively- and negatively-charged lines were written in the smoother areas, created by previously scanning in contact mode. Different voltage magnitudes were used and surface potential differences ranging from - 2.7 V to + 3.5 V were achieved (Fig. 3.28).

Higher surface potential differences were achieved when charge-writing several adjacent lines covering a 20 μm x 1 μm surface area instead of a single line. In this case, no previous smoothing of the surface was performed. Scanning in contact mode, charge-writing and aggregate sweeping took place simultaneously, creating topographical features as well as charge-patterns (Fig. 3.29).

To compare the decay on OTS-coated and non-coated SiO_2 substrates, similar

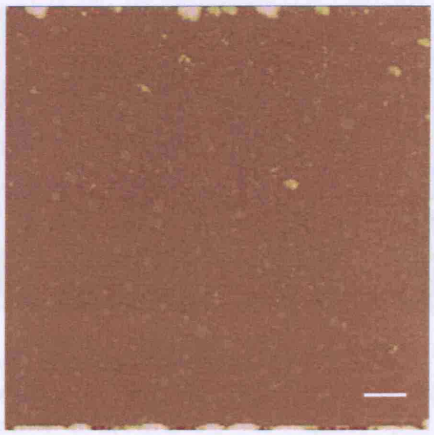

Figure 3.27: **Surface topography of the OTS/SiO_2 sample after scanning in contact mode.** AFM topography image made in tapping mode after previously scanning the area in contact mode. The aggregates are mainly accumulated on the edges of the image. Scale bar = 3 μm, z – scale range = 200 nm.

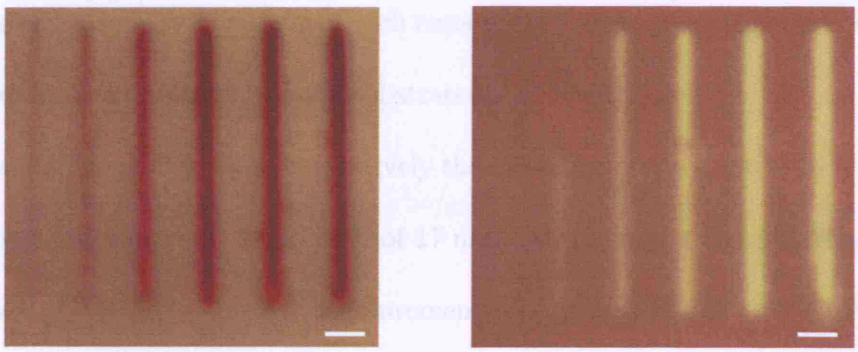

Figure 3.28: **Contact mode charge-writing on OTS/SiO_2 on areas previously scanned in contact mode.** KFM images of a set of charged lines written in contact mode, at 10 μm/s tip velocity, applying voltage pulses at 50 Hz pulse rate. Left: from left to right Up = - 40 V, - 50 V, - 60 V, - 70 V, - 80 V, - 80 V. Right: from left to right Up = + 30 V, + 40 V, + 50 V, + 60 V, + 70 V, + 80 V. Scale bars = 3 μm, scale range = 10 V.

20 μm x 1 μm positive and negative charge-patterns were also written on a bare SiO_2 substrate pre-heated for 3 h at 200°C. Four consecutive surface potential images were made to monitor the pattern decay, each image taking 17 min to be completed. It was assumed that the charge distribution was homogeneous and that the decay mechanisms were similar along the charge-pattern. A cross-section of each pattern

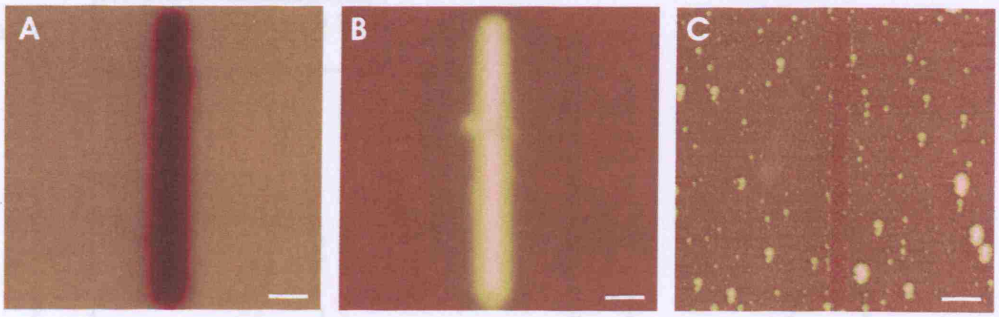

Figure 3.29: **Contact mode charge-writing on OTS/SiO_2.** A) KFM image showing a 20 μm x 1 μm area charge-written by scanning, in contact mode, 26 lines in that area at 0.1 Hz scan rate, applying voltage pulses at 50 Hz pulse rate. Up = - 80 V. Maximum surface potential difference = - 8.5 V, scale range = 20 V B) KFM image of a charge-pattern written as in (A) with Up = + 80 V. Maximum surface potential difference $\geq$ + 10 V, scale range = 20 V. C) AFM topography image of the area previously charge-written negatively, (A), showing aggregate accumulation on the edges of the patterned area, z – scale range = 300 nm. Scale bars = 3 μm

was thus measured in the middle of each consecutive image to monitor and compare the decay for each polarity in both substrates.

Figures 3.30 and 3.31 show respectively the evolution of the negative and positive charge-patterns measured in intervals of 17 min. In the case of the negative charge-patterns on OTS/SiO_2, the first measurement was truncated due to a limitation in the compensating potential of the KFM technique. The shape of the profile was extrapolated in this case to the expected shape.

The peak value and the full width at half the maximum value of the profiles are shown in figure 3.32. The peak values of the negative charge-patterns decayed at the same speed for SiO_2 with or without OTS layer. The FWHM increased at the same rate. After 51 min the peak value was more than 75 % of the initial value and the FWHM had increased 30 % of its initial value in both susbtrates. A significant difference between bare SiO_2 and OTS/SiO_2 was observed in the case of positively-charged patterns. The peak values decreased slower in the case of OTS-

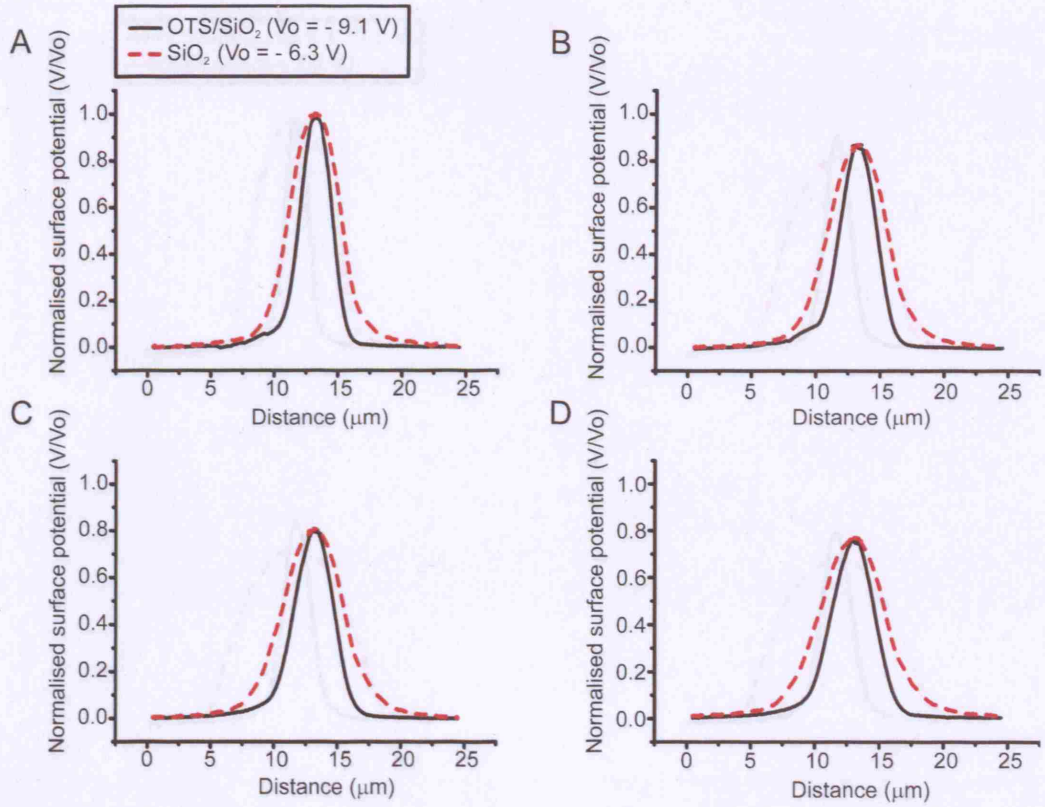

Figure 3.30: **Time evolution of negative charge-patterns in OTS/SiO_2 and SiO_2.** Normalised surface potential profiles measured A) after charge writing, B) 17 min after (A), C) 34 min after (A), D) 51 min after (A).

coated samples. After 51 min, the peak value of the surface potential was above 80 % of the initial value for OTS-coated samples and lower than 70 % for bare SiO_2. Furthermore, the FWHM was significatly narrower in OTS/SiO_2 than in non-coated SiO_2 immediately after charge-writing. Moreover, after 51 min, the FWHM increased 30 % of its initial value in the OTS/SiO_2 sample, an increase comparable to that observed in the negative charge-patterns. On the other hand, the FWHM of the positive charge-pattern written on bare SiO_2 increased almost 50 % of its initial value. The area under the profiles did not change significantly with time during the experiment (Table 3.6). The area under the profile of the positive charge-pattern

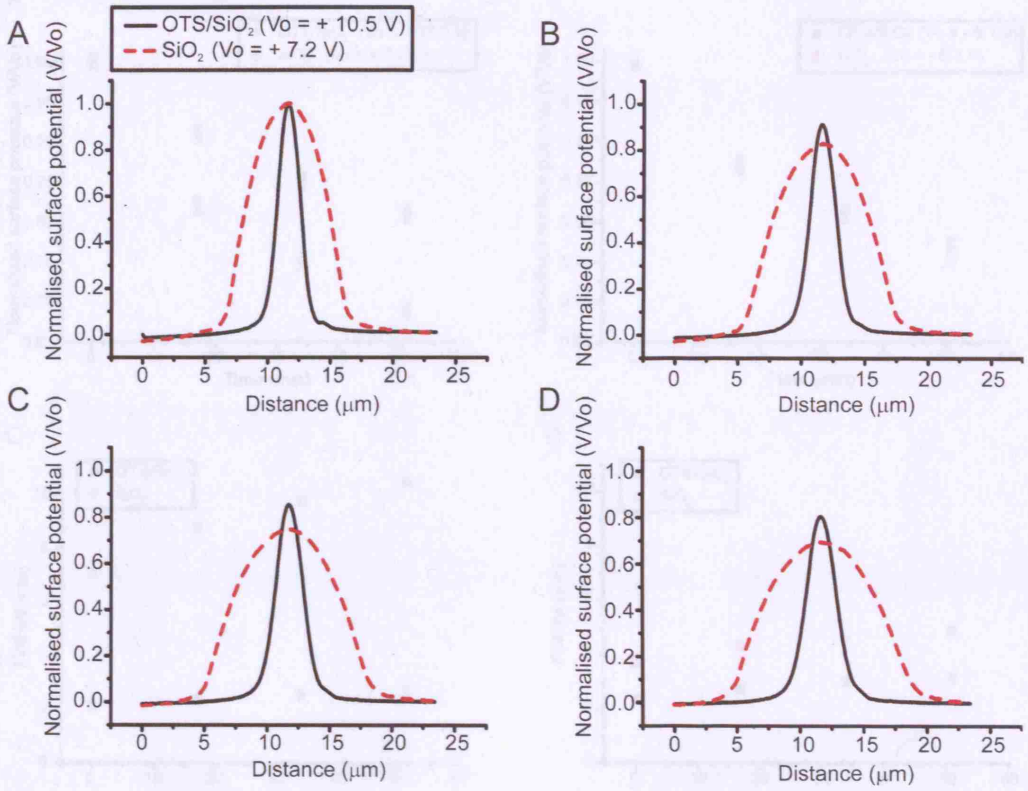

Figure 3.31: **Time evolution of positive charge-patterns in OTS/SiO_2 and SiO_2.** Normalised surface potential profiles measured A) after charge writing, B) 17 min after (A), C) 34 min after (A), D) 51 min after (A).

written on bare SiO_2 was significantly larger than in the other cases.

Substrate	Pattern polarity	Area under surface potential profile (V·μm)
SiO_2	negative	26 ± 1
SiO_2	positive	49 ± 1
OTS/SiO_2	negative	25 ± 1
OTS/SiO_2	positive	26 ± 1

Table 3.6: **Area under the surface potential profile of positive and negative charge spots in OTS/SiO_2 and bare SiO_2.** The areas were calculated using the non-normalised values.

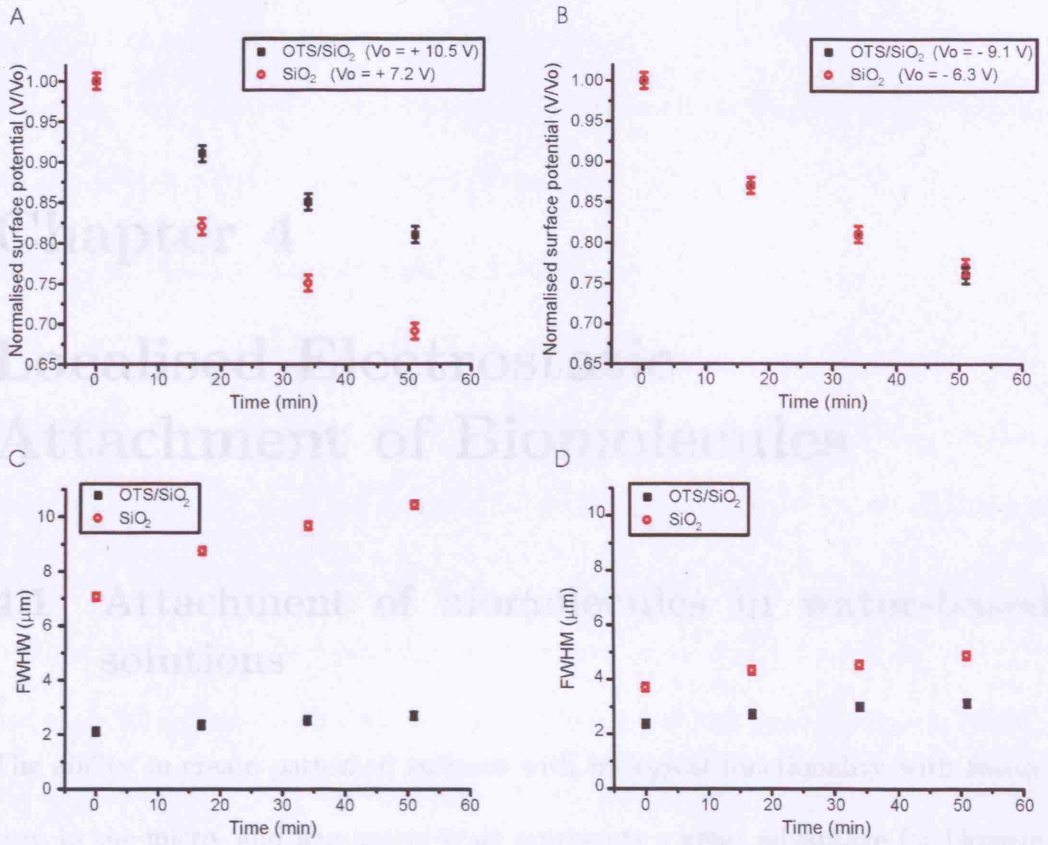

Figure 3.32: **Surface potential decay in OTS/SiO_2 and SiO_2.** Left panels: Positive charge-pattern decay. A) Normalised surface potential peak values. C) FWHM of the profiles. Right panels: Negative charge-pattern decay. B) Normalised surface potential peak values.D) FWHM of the profiles.

These results show that the stability and definition of the positive charge-patterns on SiO_2 can be improved dramatically by covering the surface with a hydrophobic layer. The adsorption of water on the surface may have been reduced leading to the reduction of ion mobility [Olthuis 1992]. However, the use of a hydrophobic layer did not influence the quality of the negative charge-patterns. This could indicate that the positive charges were trapped nearer the surface and thus, any surface treatment had a greater influence on them than in the negative charge-patterns.

Chapter 4

Localised Electrostatic Attachment of Biomolecules

4.1 Attachment of biomolecules in water-based solutions

The ability to create patterned surfaces with biological functionality with feature sizes in the micro- and nanometre scale represents a great advantage for biomedical applications such as genome or proteome analysis. Higher throughput can be achieved with less volume of reagents by downscaling the feature size of the patterns. The use of electrical patterns is an attractive approach to drive the localised attachment of biomolecules since charge-patterns with nanometre scale feature sizes can be written on a wide variety of substrates. In 1996, M N Wybourne et al. reported the patterned attachment of avidin-fluorescein from an aqueous solution to a polystyrene thin-film by electrostatic means. The polystyrene thin film was locally irradiated using an e-beam producing a charge distribution. The charge-patterned polymer was subsequently incubated in an aqueous solution containing avidin-fluorescein. A preferential attachment of such protein to the irradiated areas was observed using fluorescence microscopy [Wybourne 1996]. In the following experiments, an AFM

instead of an e-beam was used to create the charge-patterns. Following Wybourne's procedure, the charge-patterns were directly immersed in the protein solution and subsequently imaged by fluorescence microscopy.

4.1.1 Preliminary considerations

Nanoxerographic approaches have been previously used for patterning using either charged particles suspended in air or in non-polar liquids [Barry 2003], or using particles encapsulated in water droplets which are dispersed in non-polar liquids [Mesquida 2001]. One of the goals of this project is to achieve electrostatic attachment using aqueous solutions, since biomolecules cannot usually be solved in non-aqueous solvents. This is not straightforward as charges written on insulating thin films decay very quickly in the presence of water [MesquidaDiss 2002] and because of the electrostatic screening effect in electrolyte solutions.

4.1.1.1 Charge stability in liquid

Charge stability in pure water was discussed in sections 3.2.1.2 and 3.2.2. After 10 s immersion, 30 % of the initial surface potential remained in PMMA. In the case of PS, after 20 s immersion, 80 % of the surface potential remained. In SiO_2 no charge-pattern could be observed after a few seconds immersion in pure water. However, molecular adsorption onto a charged surface can take place within seconds [Brayshaw 2004]. Thus, it needs to be investigated whether the electrical field created by the charge-pattern is strong enough in water during the minimum time required for the attachment.

4.1.1.2 Screening effect

Another factor to take into consideration is that the ideal environment for biological molecules is not pure water. They are usually diluted in buffered solutions in order to provide the right pH conditions that allows molecular functionality. This involves a high number of ions that will screen the electrostatic interactions between the charge-patterned surface and the charged biomolecules. The Debye screening length was used to estimate the distance from a charged surface at which the Coulomb electrostatic interaction becomes small [Oshima 1998].

The Debye length is calculated considering a plane surface immersed in an electrolyte composed of N ionic mobile species of valence z_i and bulk concentration $n_i(i = 1, 2, ...N)$ where $\sum_{i=1}^{N} z_i n_i = 0$ since the bulk of the solution is electrically neutral. Then, taking an h axis perpendicular to the plane with its origin $h = 0$ at the surface and $h > 0$ corresponding to the solution phase, the Poisson equation which relates the electric potential $\Psi(h)$, to the charge density of free mobile charged species $\rho(h)$ can be written as shown in equation 4.1. The origin of the electric potential is set at the bulk solution phase.

$$\frac{\partial^2 \Psi}{\partial h^2} = -\frac{\rho(h)}{\epsilon_r \epsilon_0} \tag{4.1}$$

where ϵ_r is the relative permittivity of the electrolyte solution and ϵ_0 the permittivity of vacuum.

Assuming that the distribution of the electrolyte ions obeys Boltzmann's law (Eq 4.2), where e is the elementary electrical charge,

$$\rho(h) = \sum_{i=1}^{N} e z_i n_i exp\left(-\frac{z_i e \Psi}{k_\beta T}\right) \tag{4.2}$$

if the potential is low (Eq 4.3)

$$\left|\frac{z_i e\Psi}{k_\beta T}\right| << 1 \tag{4.3}$$

then, equation 4.1 can be linearized:

$$\frac{\partial^2\Psi}{\partial h^2} = \kappa^2\Psi \tag{4.4}$$

where

$$\kappa = \left(\frac{1}{\epsilon_r\epsilon_0 k_\beta T}\sum_{i=1}^{N} e^2 n_i z_i^2\right)^{1/2} \tag{4.5}$$

The solution of the linearized Debye-Huckel equation 4.4 is

$$\Psi = \Psi_0 exp(-\kappa h) \tag{4.6}$$

using the following boundary conditions where Ψ_0 is the surface potential

$\Psi = \Psi_0$ at $h = 0$

$\Psi = \frac{d\Psi}{dx} = 0$ at $h = \infty$

The potential decreases exponentially, at $h = 1/\kappa$, $\Psi \approx \Psi/3$ (Fig.4.1). This distance is defined as the Debye length, λ, and for $h > \lambda$ the influence of the surface potential over a charged particle will be considered negligible.

ImmunoPure Avidin, fluorescein isothiocyanate (FITC) conjugated , 5 mg/ml (buffer: 10 mM HEPES, 0.15 M NaCl, pH 8.5, 0.08 % sodium azide) (Pierce, Cramlington, UK) was used in the following concentrations for the experiments:

-0.1 mg/ml (buffer: 10 mM HEPES, pH 8.5).

-0.1 mg/ml (buffer: 10 mM MES, pH 5).

The Debye length was estimated for the buffered solutions used during the incubation. In order to do so, the concentration of the ions involved had to be calculated.

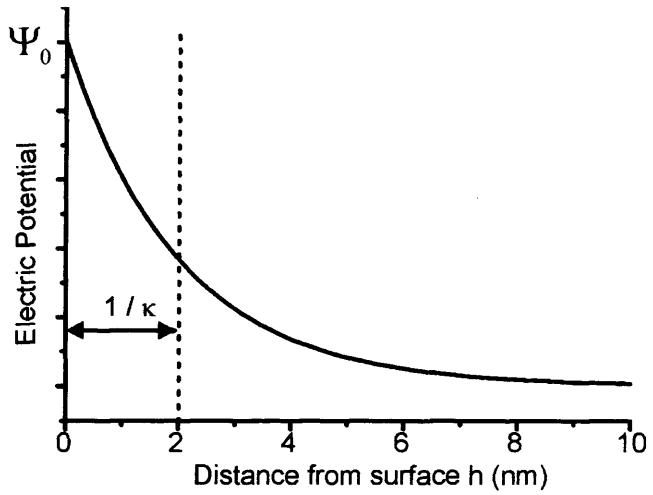

Figure 4.1: **Debye length diagram.** The diagram shows the exponential decay of the electric potential in the presence of an electrolyte solution. Debye length = $1/\kappa$.

Both HEPES and MES buffers have a zwitterionic form, with neutral net charge, corresponding to the acid form of the buffer (Fig. 4.2). Therefore, only the basic form will be taken into account for the calculation of the Debye length.

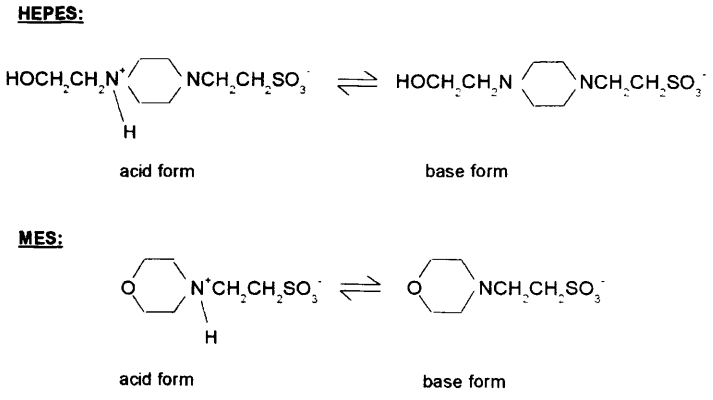

Figure 4.2: **Acid and base forms of buffers MES and HEPES.**

The MES buffer has a pKa = 6.15 at 20°C and HEPES pKa = 7.5. Therefore, introducing this value in the Henderson-Hasselbalch equation (Eq 4.7), the concen-

tration of the conjugated base of MES and HEPES can be calculated knowing the pH and the concentration of buffer used. The concentration of NaOH used for titration of the buffer and the concentration of NaCl was also taken into account. They will provide ions to the solution when dissociated.

$$pH = pKa + log\frac{[baseform]}{[acidform]} \tag{4.7}$$

An estimation of the Debye length was made using equation 4.5. The resulting Debye screening length was $\lambda = 8.5$ nm for HEPES buffer and $\lambda = 4.13$ nm using MES buffer. The charged molecules beyond this distance would be considered as not to be affected by the charged surface.

4.1.1.3 Unintended interactions

In the context of this project, the intended interactions take place ideally in the charge-patterned area and due to electrostatic interactions only. Molecules or particles deposited on the surface independently from the charged-pattern are considered unintended attachment.

Two main sources of unintended interactions are hydrophobic interactions and electrostatic interactions not related to the charge-pattern, as surfaces are typically charged in solution [Oshima 1998]. These interactions could lead to the appearance of a non-desired background or block the intended attachment.

a) Unintended attachment due to background charge.

To determine the polarity of the PMMA surface it was immersed in solutions of polyelectrolytes or particles of known net charge polarity. Positively-charged poly-L-

lysine (M_w: 150000-300000, 0.1 g/ml in water) and gold colloid solution containing negatively-charged gold nanoparticles of 20 nm diameter [Weiser 1933], were thus used for this purpose. Both solutions were obtained from Sigma (Sigma-Aldrich Company Ltd., Poole, UK).

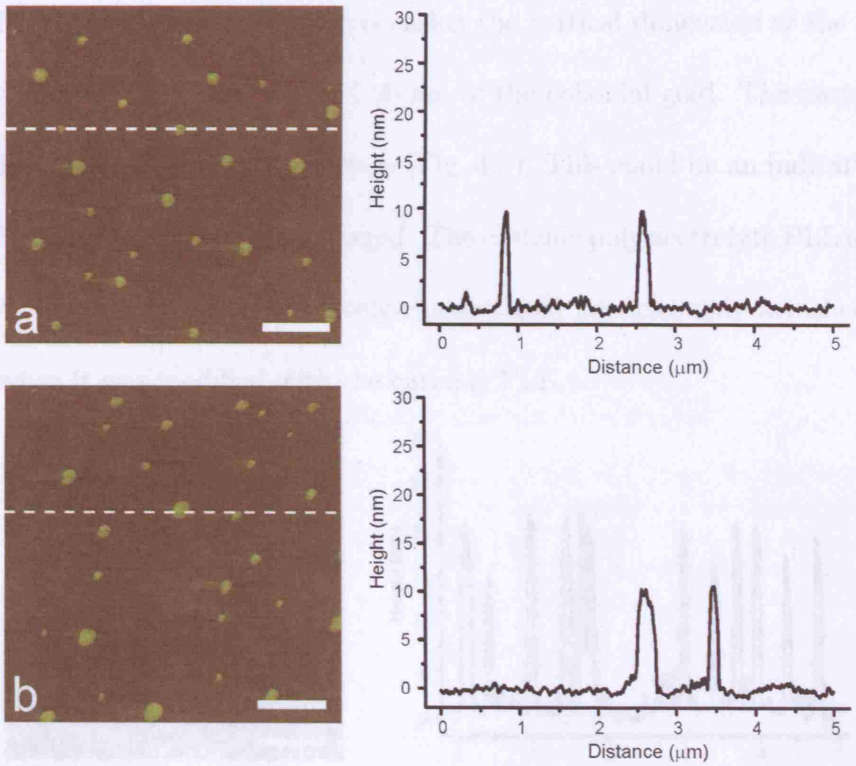

Figure 4.3: **PMMA surface before and after 2 min incubation in gold colloid solution.** (a) Left: AFM topography image of the PMMA surface before incubation, z-scale range = 70 nm, scale bar = 1 μm. Right: Cross-section of the topography image on the left. (b) Left: AFM topography image of the PMMA surface after 2 min incubation, z-scale range = 70 nm, scale bar = 1 μm. Right: Cross-section of the topography image on the left. The images were made in tapping mode using a plain Si tip, plane-fitted in XY directions and 1st order flattened.

The PMMA surface was firstly incubated for 2 min in the gold colloid solution, then rinsed with pure water, dried with N_2 and imaged with an AFM. No gold particles could be detected on the surface (Fig. 4.3). The cross-sections showed inhomogeneities on the PMMA surface before and after the incubation, however

their height was significantly lower than 20 nm which was the expected dimension of the gold particles. Using another PMMA thin-film, the surface was incubated for 90 s in the PLL solution, rinsed with pure water and then incubated in the gold colloid solution for 2 min. After the incubation time the surface was rinsed with pure water, dried with N_2 and imaged. On this occasion the vertical dimension of the features observed coincide with the expected 20 nm of the colloidal gold. The particles are randomly deposited all over the surface (Fig. 4.4). This could be an indication that the PMMA surface is negatively-charged. The cationic polyelectrolyte PLL attached to the PMMA surface. The negatively-charged gold particles only attached to the surface when it was modified with the cationic PLL.

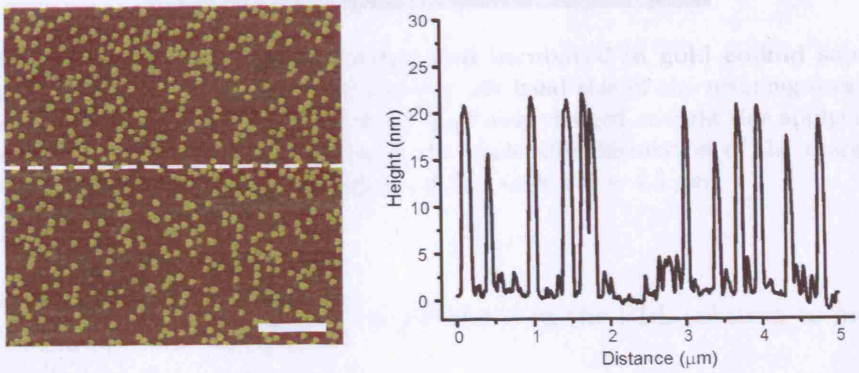

Figure 4.4: **PMMA surface incubated in PLL solution and in gold colloid solution** Left: AFM topography image of the PMMA after the incubation in gold colloid. Scale range = 70 nm. Scale bar = 1 μm. Right: AFM topography cross section.

Positively- and negatively-charged 20 μm x 5 μm areas were written on the PMMA film. The surface was then incubated in the gold colloid solution for 1 min and rinsed in pure water. No gold particles could be detected (Fig. 4.5). A topographical feature can be seen in the area negatively charge-written. This could be due to mass transport of melted polymer during charge-writing. It has been

reported in the literature that risen structures can be made on PMMA by biasing the AFM tip negatively [Lyuksyutov 2003].

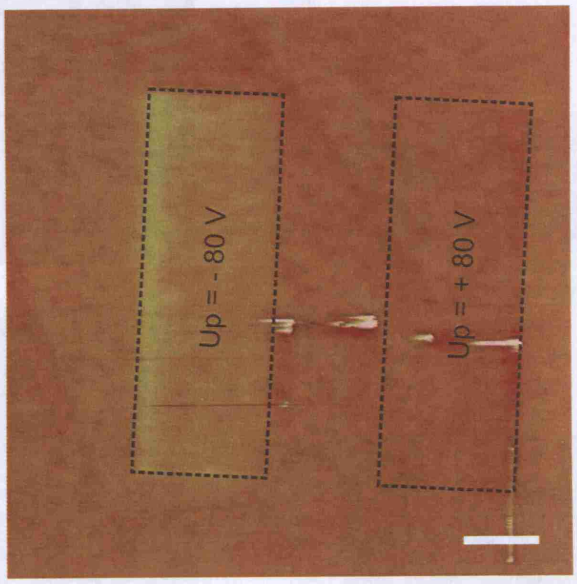

Figure 4.5: **PMMA surface charge written and incubated in gold colloid solution.** A negatively charged area was charge-written on the left hand side of the scanning area applying - 80 V voltage pulses and a similar size area was positively charged on right side applying + 80 V voltage pulses. The AFM topography image was made after incubation of the charge-written surface in gold colloid solution, z-scale range = 70 nm, scale bar = 4.5 μm.

The surface was then modified, incubating it in the PLL solution to modify its polarity. After the incubation, 50 μm x 6 μm areas were positively and negatively charge-written achieving + 8 V and - 8 V surface potential respectively. After charge-patterning, the surface was incubated in the gold colloid solution for 1 min, rinsed in pure water, dried and imaged. The gold particles were attached and distributed randomly over the surface (Fig. 4.6). The charge-pattern did not affect the deposition of the nanoparticles. The positive background-charge from the PLL layer deposited on the surface was thus dominating the attachment. The PLL positive charge is a permanent charge whilst the charge-pattern decays rapidly in aqueous

solutions.

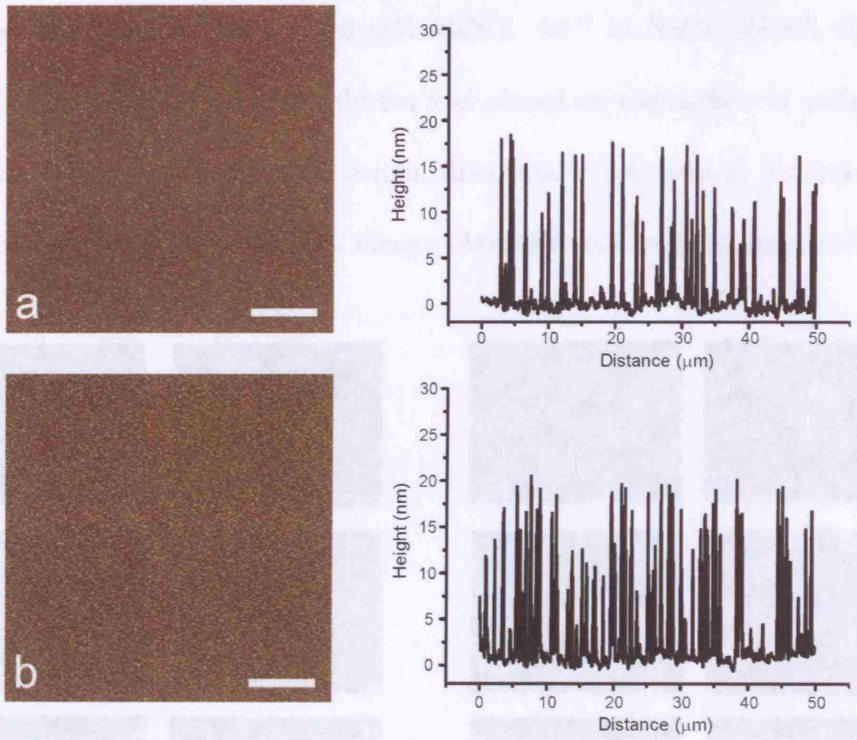

Figure 4.6: **PMMA surface incubated in PLL solution, charge written and incubated in gold colloid solution.** The images were made in tapping mode with a plain Si-tip, plane-fitted in XY directions and 1st order flattened, z-scale range = 70 nm, scale bar = 10 μm.(a) Left: AFM topography image made after incubation in gold colloid solution of the positively charged area. Right: cross-section of the topography image on the left. (b) Left: AFM topography image made after incubation in gold colloid solution of the positively charged area. Right: cross-section of the topography image on the left.

b) Reducing the hydrophobicity-related attachment with a plasma treatment.

Hydrophobic interactions between the surface and the particles are another source of unintended attachment. Two approaches were taken to reduce this interactions: plasma treatment of the surfaces and the use of non-ionic surfactants.

Ten PS and ten PMMA samples were prepared as described in section 3.1.1.1.

Five of each were plasma-cleaned for 120 s with an air ILMVAC PLASMA-clean 4. A droplet of 0.1 mg/ml (buffer: 10 mM MES,$6 \cdot 10^{-5}$ M NaCl, pH 8.5, 0.0016 % sodium azide) avidin-fluorescein solution was placed on the surface of each sample and rinsed using pure buffer after 3 min, dried under a stream of N_2 and imaged using fluorescence microscopy. The images obtained are shown in figure 4.7.

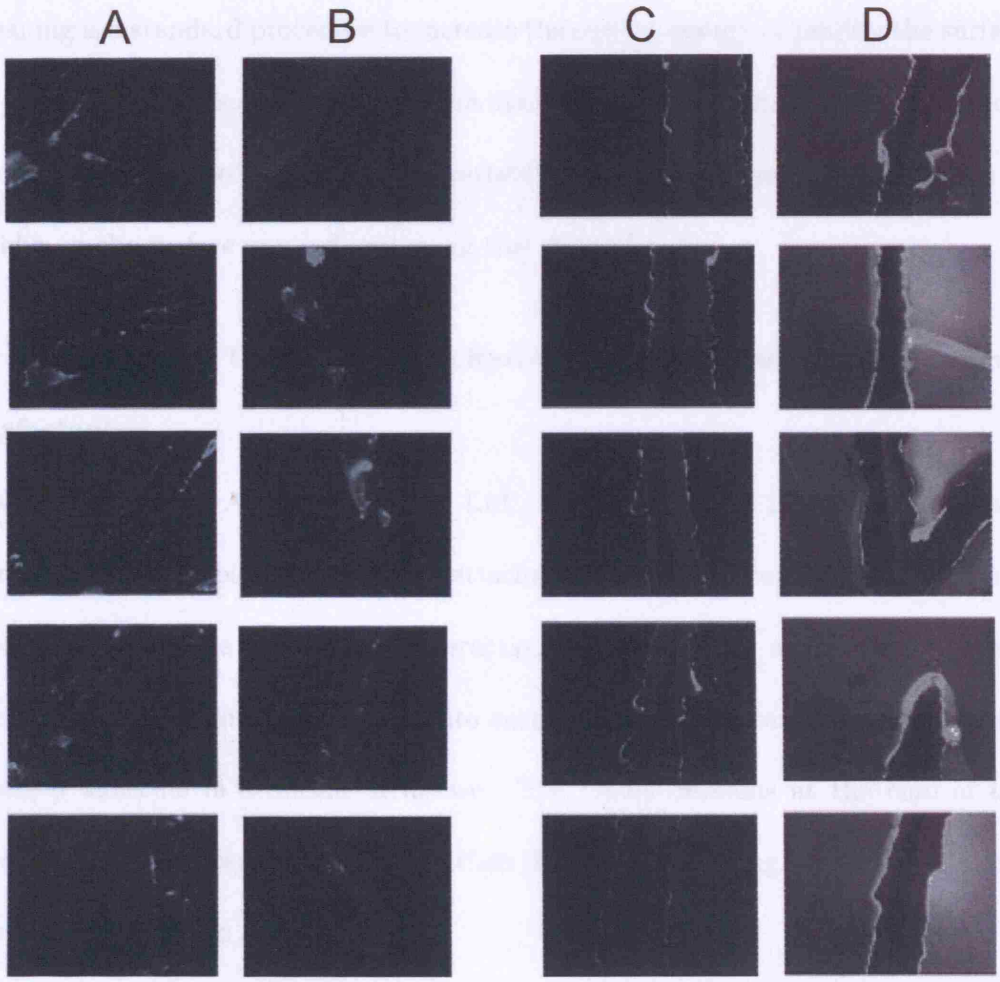

Figure 4.7: **Influence of plasma cleaning on the unintended attachment of avidin-fluorescein to PMMA and PS thin films.** A)PMMA thin-films plasma cleaned; B)PMMA thin-films not plasma cleaned; C) PS thin-films plasma cleaned; D) PS thin-films not plasma cleaned.

The scratch that can be seen in the images was made on the surface of the

sample before the incubation as a standard procedure to locate the charge-patterns when moving the sample from the AFM to the fluorescence microscope. In this experiment, though, no electrical pattern was written. No background improvement can be seen on the PMMA thin film. On the other hand, there is significantly less unintended attachment on the PS thin film after the plasma cleaning. Plasma cleaning is a standard procedure to increase the surface energy or modify the surface of polymer materials. Due to the plasma discharge, new oxygen-containing chemical groups were produced increasing the wettability of the thin-film. The adsorption of avidin on the surface was reduced using this method.

c) Reducing the hydrophobicity-related attachment using non-ionic surfactants.

Tween20® (Sigma-Aldrich Company Ltd., Poole, UK) is a non-ionic surfactant commonly used to block non-specific attachment due to hydrophobic interactions. Being non-ionic, the electrostatic interactions should not be altered but a possible screening effect has to be taken into account. The surfactant encapsulates the charged molecule in a micelle structure. The charge remains at the core of the micelle. If the encapsulation is thicker than the Debye screening length, the electrostatic forces will also be blocked.

Plasma-cleaned and non-plasma-cleaned PS and PMMA thin films were incubated in a solution of 0.1 mg/ml avidin-fluorescein in 10mM, 5.6 pH MES buffer containing 0.1 % Tween20®. After 3 min incubation time the surfaces were rinsed with clear buffer and pure water. The samples were dried under a stream of N_2 and

imaged under a fluorescence microscope. The unspecific attachment was blocked in all the thin films, plasma-cleaned or not. No fluorescence could be observed. Assuming that the PMMA film is negatively charged in this solution and knowing that avidin-fluorencein is positively charged at the pH used, if there was an attractive electrostatic interaction between them, their attachment was nevertheless blocked. This makes the use of this surfactant inappropriate in the context of this project.

4.1.2 Experimental method

To determine the attachment of charged molecules to charge-written areas, 60 μm x 6 μm lines were written with charges on PMMA and PS thin films. A scratch was made on the surface of the thin film using standard steel tweezers before charge-writing to facilitate locating the pattern.

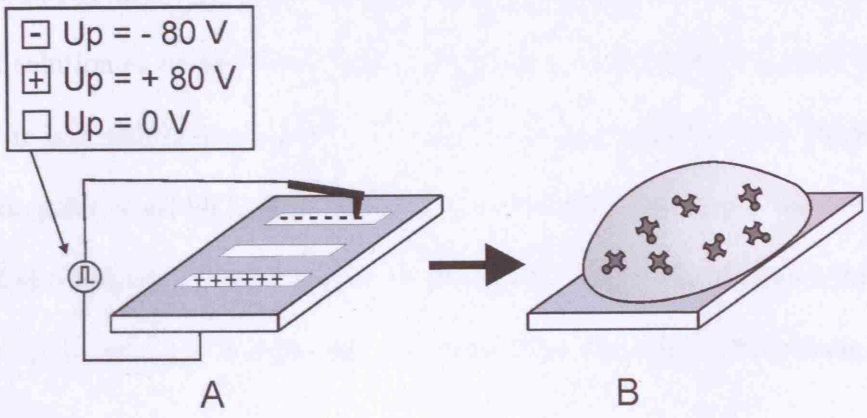

Figure 4.8: **Two step attachment procedure:** A) The polymer thin-film was charge-written positively and negatively applying a bias Up to the AFM tip during scanning. A control line was scanned at Up = 0 V. B) The charge-pattern was incubated in a solution containing 0.1 mg/ml avidin-fluorescein for 3 min.

The areas to be charged were scanned with a biased AFM tip. The tip velocity was 10 μm/s and the voltage was applied immediately after engaging. The voltage

applied was either DC, scanning in contact mode or pulsed, scanning in tapping mode. The voltage pulses were triggered by a 5 V, 50 Hz square signal. The magnitude was + 80 V or - 80 V to write positively or negatively charged areas. A third area with the same dimensions was also scanned applying no voltage. It acted as a control to detect molecule adsorption due to any surface modification generated on the scanned area not related to the electrical pattern written applying a voltage. The tip and sample surface are made of different materials. Therefore, contact electrification can occur just by scanning the surface [Saurenbach 1992]. Also, some mechanical damage can occur on the polymer surface during scanning. After charge-writing each line, a KFM measurement was made scanning perpendicular to the charged line to measure its surface potential.

Immediately after the KFM measurement, the sample was incubated with a buffered solution of avidin-fluorescein. This fluorescently-labelled protein was used because it is a well-known system. The electrostatic properties are known. The isoelectric point of avidin is approximately 10, therefore, for a given pH below 10, it is positively charged. Another reason to use labelled avidin is to detect the attachment using fluorescence microscopy. ImmunoPure Avidin, Fluorescein (FITC Conjugated)

5 mg/ml (buffer:10mM HEPES,0.15 M NaCl, pH 8.5, 0.08 % sodium azide) from Pierce was disolved in HEPES or MES buffer to be used in different pH conditions:

0.1 mg/ml (buffer: 10 mM HEPES, pH 8.5)

0.1 mg/ml (buffer: 10 mM MES, pH 5)

A droplet of the prepared solution was placed over the surface with a pipette. The incubation time was 3 min. After the incubation time, the sample was rinsed with clear buffer and pure water. The resulting patterned attachment was imaged using fluorescence microscopy. The fluorescence images were made using a Qimaging 3.3 micropublisher, cooled digital camera (Digital Pixel, Brighton, UK) installed in an Axioplan Universal Microscope for transmitted light and incident-light fluorescence (Zeiss, Gottingen, Germany).

4.1.3 Results and discussion

4.1.3.1 Attachment of avidin-fluorescein to charge-patterned PS thin films

Several 40 μm x 4 μm rectangular areas were charge-written on a plasma-cleaned PS thin-film using a plain Si tip (type B). A square was engraved on the film to be used as positional reference (Fig. 4.9). Two areas were charge-written in tapping mode with negative and positive charges respectively. Another two areas were charge-written in contact mode, one negatively and one positively. As a control, a third line was scanned in contact mode applying no voltage. The solution used for the incubation was 0.1 mg/ml avidin-fluorescein (buffer: 10 mM HEPES,pH 7). The fluorescence image taken after 3 min immersion in the solution is shown in figure 4.9.

In figure 4.9, preferential attachment of avidin-fluorescein can be observed in all the areas scanned in contact mode, no matter what the magnitude or the polarity of the voltage applied. Assuming that avidin-fluorescein was positively charged at pH below 10, it should have only attached to the negative surface potential lines if only electrostatic forces were governing the attachment. A possible explanation

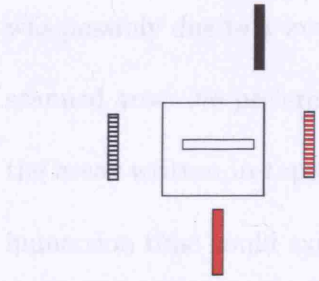

Voltages applied	mode
U_p = 0 V	Contact
U_p = + 80 V DC	Contact
U_p = - 80 V DC	Contact
U_p = + 80 V Pulsed	Tapping
U_p = - 80 V Pulsed	Tapping

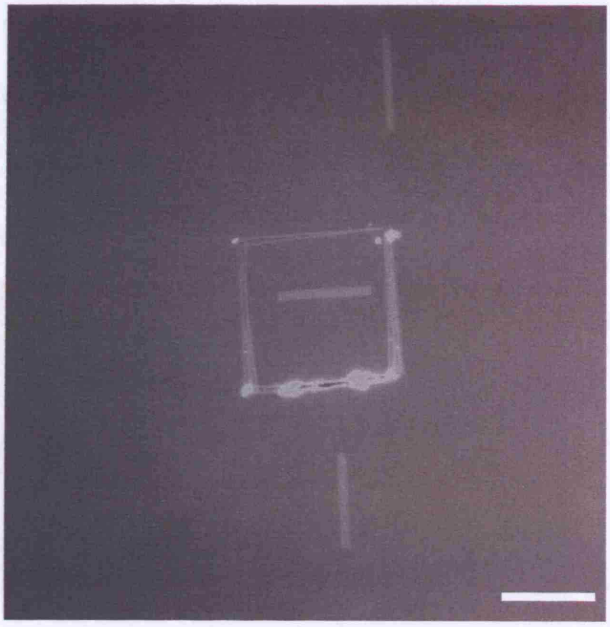

Figure 4.9: **Fluorescence images of the patterned attachment of avidin-fluorescein on PS.** Left: Diagram depicting the position and charge-writing mode of all the scanned areas. Right: Fluorescence image showing preferential attachment of avidin fluorescein to the areas scanned in contact mode on a plasma-cleaned PS film 570 pm 30 nm thick. Exposure time = 20 s. Scale bar = 40 μm.

for the observed behaviour could be a mechanical modification of the surface due to scanning as it can be observed that scratches on the film show a bright fluorescence after the attachment process on plasma cleaned PS surfaces (Fig. 4.9).

To assess the sample damage due to scanning in contact mode, rectangular areas were scanned applying positive, negative and no voltage. The forces were kept as low as possible during scanning. The incubation was performed in pure water in order to promote the decay of the charge-pattern. After the incubation in water the sample was dried under a stream of N_2 and an AFM topography image of the scanned area made. A topographical modification could be observed in the three lines scanned (Fig. 4.10). Thus, the preferential attachment observed in figure 4.9

was possibly due to a wetting effect caused by the topographical modification of the scanned area. No preferential attachment of avidin-fluorescein could be observed in the areas written in tapping mode. A rapid decay of the charge-pattern during the immersion time could explain this result.

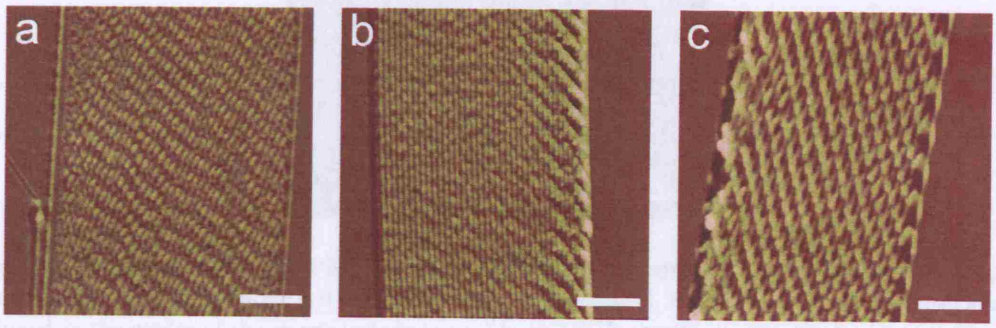

Figure 4.10: **Damage on the PS film due to contact mode scanning.** a)AFM tapping mode topography image of the area scanned in contact mode applying 0 V. b) Area scanned applying + 80 V. c) Area scanned applying - 80 V. Scale range = 30 nm. Scale bar = 0.5 μm.

In the literature a 500 nm-thick PS thin-film was charge-written using an e-beam with the aid of patterned masks [Wybourne 1996]. The charge-patterns were incubated in 4.5 mg/ml buffered avidin-fluorescein solution for 5 min and the fluorescence images showed the avidin-fluorescein preferentially attached to the irradiated areas. The attachment was attributed to electrostatic attachment but the irradiated patterns of only negative polarity were charge-written. However, the preferential attachment could be due to a surface modification introduced by the e-beam.

4.1.3.2 Attachment of avidin-fluorescein to charge-patterned PMMA thin films

To minimise any topographical modification due to scanning, charge-writing was performed in tapping mode using a PMMA thin film to hold the electrical pattern. No topographical modification of the surface could was observed after scanning a

20 μm $\times$ 20 μm area in tapping mode (Fig. 4.11).

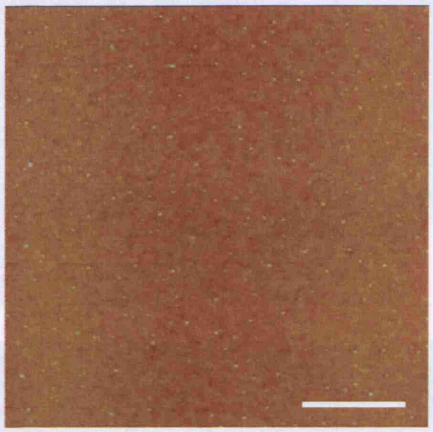

Figure 4.11: **No damage on PMMA after scanning in tapping mode.** AFM topography image made in tapping mode with a plain Si tip. A 10 μm x 10 μm area had been previously scanned in the centre of the image in tapping mode at 2.0 Hz scanning rate. Scale range = 20 nm. Scale bar = 6 μm.

The film used was spin-coated using a 0.02 g/ml PMMA in chlorobenzene solution (thickness = 66 nm $\pm$ 12 nm). After charge-writing the lines, the sample was incubated in 0.1 mg/ml avidin-fluorescein solution (buffer: 10mM MES, 3 mM NaCl, pH 5, 0.0016 % sodium azide). The fluorescence images taken of the resulting patterned attachment are shown in figure 4.12.

Attachment can be seen in the lines where voltage was applied. There is some non-homogeneous unintended attachment in the surrounding areas but there is an indication that there is more attachment at the negatively-charged line. This would be consistent with the hypothesis of electrostatic attachment as avidin-fluorescein is positively charged at pH 5.5. Some attachment can still be observed on the positively-charged line. A possible explanation could be the scanning-related effect described in section 3.2.1.3. A negative surface potential contrast appeared after im-

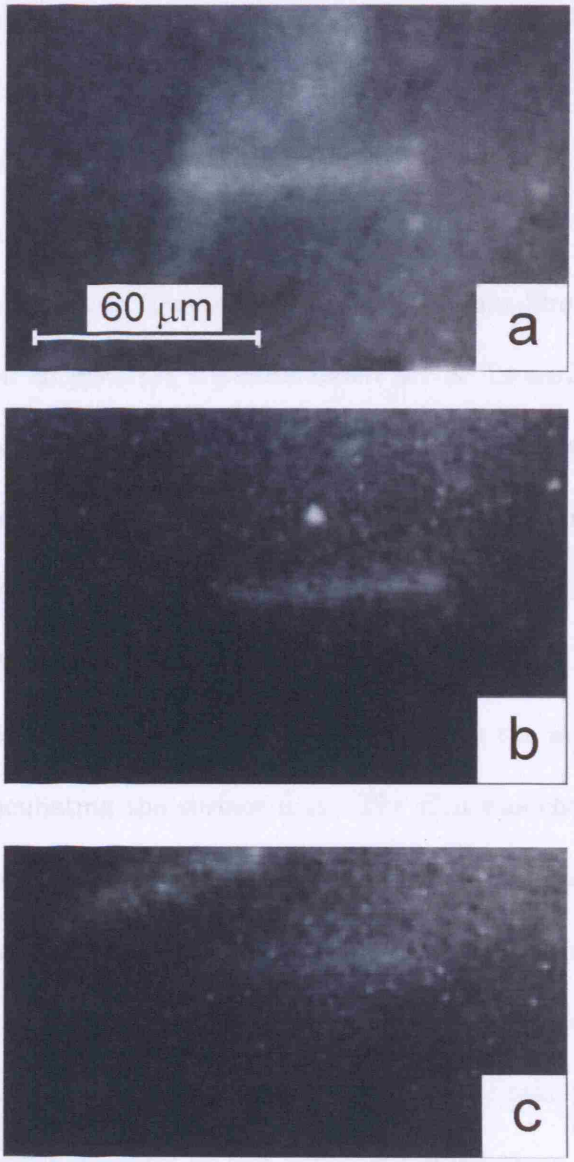

Figure 4.12: **Fluorescence images of the patterned attachment of avidin-fluorescein on PMMA** Top image (a): line charge-written applying -80 V pulses in tapping mode; Middle image (b): line charge-written applying + 80 V pulses in tapping mode, Bottom image (c): line scanned in tapping mode applying 0 V, scale bar = 60 μm

mersing scanned areas in water. Since charge-writing involves scanning the PMMA surface, a mechanical modification could have been introduced. Such mechanical modification could lead to an enhanced permanent negative surface potential con-

trast after immersion in the aqueous solution. Since charge-patterns decay rapidly in water, the scanning related negative surface potential contrast could be governing the attachment of the avidin-fluorescein.

To prevent the unintended attachment on the PMMA surface, several attachment experiments were tried using Tween20®. A PMMA thin film was immersed for 15 min in a solution 10 mM, pH 5.6 MES buffer 0.1 % Tween20®. After rinsing with pure water and drying under a stream of N_2, the film was negatively and positively charge-patterned in tapping mode applying voltage pulses. The charge-pattern was then incubated for 3 min in 0.1 mg/ml avidin, fluorescein conjugated in 10 mM, pH 5.6 MES buffer. No attachment was observed on the sample.

In another experiment the surfactant was solved with the avidin-fluorescein solution instead of incubating the surface first. The film was charge-patterned correctly but after the incubation with the solution containing avidin-fluorescein and Tween20®, no attachment was observed on the sample. It seems that the surfactant prohibits any electrostatic attachment. Due to the reduced Debye screening length ($\approx$ 4 nm), the electrostatic attachment would only take place if surface and particles were almost in contact. If the surfactant keeps them away from contact beyond the Debye length, no electrostatic attachment would be expected.

4.2 Attachment of biomolecules by electric droplet lithography

DNA and protein arrays provide a powerful tool for extracting large amounts of information from biological systems. These high throughput analysis techniques

are capable of separating, identifying and quantifying many biomolecules in parallel using a minimum volume of reagents, thus they are becoming more and more important in genomics and proteomics research and in other areas of the life sciences.

The use of antibodies in protein microarrays has its origins in the development of immunoassays for the precipitation and quantification of antigens [Heidelberger 1929]. Antigens are foreign macromolecules, normally proteins, carbohydrates and nucleic acids that trigger an immune response. Specific antibodies are produced against an antigen by B lymphocytes in mammals [Voet 1995]. Monoclonal antibodies can be obtained in virtually unlimited amounts and specific for almost any antigen by fusing myeloma (cancer) cells with lymphocites, raised in a mammal, against that antigen [Kohler 1976]. Monoclonal antibodies have become indispensable biomedical tools to assay and isolate extremely small amounts of nearly any specific biological substance. For example, they have made possible the routine testing of blood for the presence of HIV [Voet 1995]. In the late 1990's, with DNA microarray technology well established, the development of antibody microarrays for quantitative proteomics started to emerge showing that miniaturization of immunoassays not only reduced costs due to the lower volumes of reagents involved, but also achieved the sensitivity and specificity of the macroscopic assays using 1/100 of the capture antibodies [Silzel 1998].

Protein microarrays contain a large number of addressable protein spots, often specific antibodies, allowing the simultaneous analysis of the interaction of hundreds of proteins and peptides [Tomizaki 2005]. There are two main types of microarrays for protein profiling: forward microarrays and reverse microarrays [Becker 2006].

In the forward format different known proteins, typically antibodies, are immobilised in each spot of the microarray. The immobilised proteins discriminate their target affinity reagent (e.g., an antibody, a cell lysate, a recombinant protein or peptide, a drug) from a complex mixture sample solution. The bound molecules are detected directly by labelling the analytes with signal generating tags (Fig. 4.13, (A)) or indirectly via sandwich-type assays in which the bound analyte captures a secondary labelled antibody (Fig. 4.13, (B)). Thus, in the sandwich method, the analyte does not require labelling. This is an advantage as some proteins are preferentially labelled in their antigen-binding sites blocking their ability to be captured [MacBeath 2002]. In the reverse format microarrays (Fig. 4.13, (C)), each spot is a different sample containing a variety of analytes. The microarray is then queried with a solution containing known labelled biomolecules.

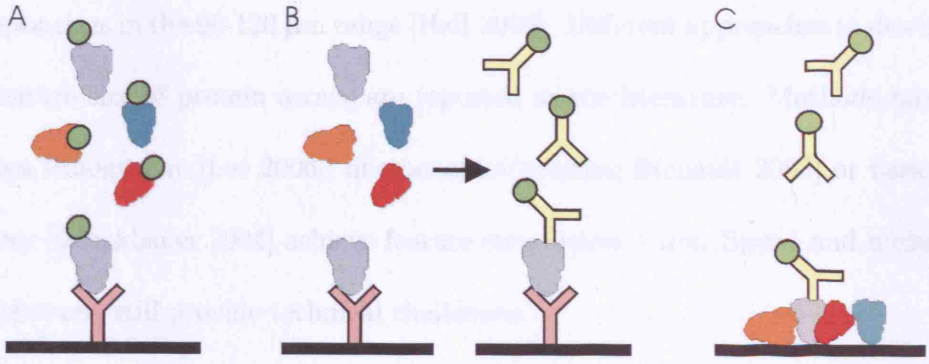

Figure 4.13: **Immunoassay methods used in protein arrays.** A)Forward assay, direct detection. The capture antibodies are immobilised on the substrate and the bound proteins, previously labelled, are detected directly. B) Forward assay, sandwich-type detection. The proteins immobilised on the substrate capture their target proteins from solution and these proteins are subsequently detected by specific interaction with a labelled biomolecule. C) Reverse assay. The sample that may contain the target protein is immobilised on the substrate. The target protein in the sample is detected by specific interaction with a labelled protein.

The development of microarray technology would also benefit research into tissue-

engineering and fundamental cell biology. Microarrays of extracellular matrix proteins (e.g. fibronectin. laminin, collagen) or biomaterials are used to screen the specificity of cell-matrix interactions [Kuschel 2004] or to promote cell adhesion [Anderson 2004], [Rozkiewicz 2006].

The most important requirements for the fabrication of protein arrays are the stable attachment of the biomolecules to the surface maintaining their biological functionality and the precise location of protein spots generated with minimal liquid volume. Gene microarrays, fabricated combining photolithography and combinatorial chemistry, with 11 μm feature size, are commercially available [Kreiner 2004]. However, commercial protein arrays are usually fabricated by automated spotting with piezoelectric arrayers and high-precision robots [Venkatasubbarao 2004]. Usually, small droplets of biomolecule solution are ejected out of a nozzle producing protein spot sizes in the 90-120 μm range [Hall 2006]. Different approaches to downscale the feature size of protein arrays are reported in the literature. Methods based in dip-pen lithography [Lee 2006], microcontact printing [Renault 2003] or nanopipet delivery [Bruckbauer 2004] achieve feature sizes below 1 μm. Speed and multiplexing, however, still provide technical challenges.

The method used in this section is based on electrostatically attaching microdroplets to a substrate instead of driving them out from a nozzle. This approach was developed in earlier works [Mesquida 2001], [MesquidaDiss 2002] and it is termed here as electric droplet lithography (EDL). EDL consists of two main stages: AFM charge-writing [Stern 1988], explained in detail in chapter 3, and microdroplet delivery [Mesquida 2001] in which the charged surface is immersed into a dispersion of

water droplets in a non-conductive liquid (a water-in-oil emulsion) [Mesquida 2001]. The dispersed droplets, containing any water-soluble material, are electrostatically attracted to the charge-pattern on the surface, where they deliver their contents [MesquidaDiss 2002].

The direct attachment of biomolecules to the AFM-CW charge-pattern from an aqueous solution has been explored in section 4.1. The rapid decay of the charge-pattern in water based solutions and the influence of hydrophobic/hydrophilic forces on the attachment, prevented the electrostatic forces from governing the attachment of biomolecules to the surface. However, the rapid charge decay can be prevented by using non-polar liquids, such as fluorocarbons [MesquidaDiss 2002]. Thus, using water-in-fluorocarbon emulsions is a good approach to simultaneously solve the problem of the rapid charge decay and provide the right environment for biomolecules to be functional [Naujoks 2003].

The emulsions were prepared by ultrasonication of the respective biomolecule solution in FC-77 [Mesquida 2001], [Naujoks 2003]. Figure 4.14 shows a fluorescence image of an emulsion created by dispersing the 3 μl of avidin-fluorescein (1 mg/ml dilution in 10 mM Hepes, pH 8 from Immunopure®Avidin, Fluorescein Conjugated 5 mg/ml in 10 mM HEPES, 0.15 M NaCl, pH 8.5, 0.08 % sodium azide, Perbio Science UK Ltd., Tottenhall, UK) in 1 ml FC-77 by 2 min ultrasonication. From the very low background fluorescence outside the spots (Fig. 4.14), it can be inferred that the proteins were well encapsulated in the water droplets and did not diffuse from the water phase into the FC-77 during the EDL process.

FC-77 is a dielectric fluorinated oil immiscible in water which is inert, leaves

Figure 4.14: **Avidin Fluorescein Emulsion.** Fluorescence image using an inverted light microscope (Olympus IX71, Middlesex, UK) with the 40x, NA 0.60 objective. The excitation/emission wavelengths of the FITC fluorophore was 490 nm/520 nm. Filters used to image the fluorescence emission: excitation filter: 460-490 nm, emission filter: 520 nm, dichromatic filter: 500 nm. The fluorescence image was recorded using a ORCA-ER digital camera (Hammamatsu, Welwyn Garden City, UK). Scale bar = 10 μm

no residue and is non-toxic [FC77]. The confinement conditions in which many biological processes take place can be emulated using water-in-FC-77 emulsions and they have thus been used for the study of protein dynamics [Reiner 2006]. Ultrasonically produced water-in-FC-77 emulsions are unstable. Very high interfacial tensions have to be overcome as fluorocarbons exhibit very weak intermolecular interactions compared with the very high associative character of water [Mukerjee 1981]. Suitable fluorinated surfactants (which are not commercially available) could possibly be employed in EDL to stabilize the emulsions, produce smaller droplets and a narrower droplet size range [Sadtler 1996]. However, for the purpose of fabricating biomolecule microarrays by EDL, surfactants could possibly cause denaturation of the biomolecules, affect their adsorption onto the charge-patterned surface and -

most importantly - impede their biomolecular function. Additional physical homogenization was attempted after ultrasonication instead, to produce a narrower range of droplet sizes.

The application of EDL with the protein avidin has been reported in the literature [Naujoks 2003]. Further work showed fluorescently labelled avidin from solution binding, through the well-known avidin-biotin interaction, to biotin-modified antibodies which had been patterned by EDL on a polymer substrate [Naujoks 2004]. However, microarrays for applications such as immunoassays often require different antibodies to be immobilised on the substrate and act as capture-molecules to detect and discriminate between different analytes in a solution by direct antibody-antibody or antibody-antigen interactions [Liotta 2003]. The immobilised antibodies are typically not biotinylated and should function in parallel [Liotta 2003]. Therefore, in multiple-protein microarrays different proteins must be placed on the same individual surface, maintaining their specific biological functionality without cross-contamination. Furthermore, to deposit the molecules on materials which potentially allow integration with state-of-the-art microtechnology, such as silicon dioxide, would also be attractive. These issues were addressed in this thesis using a variety of biomolecules including non biotinylated antibodies, serum and extracellular matrix proteins. Thus, a collagen array and a multiple-protein microarray with different immunoglobulin G antibodies and biotinylated bovine serum albumin (BSA) were fabriacted on silicon dioxide substrates. The ability of the attached proteins to capture their affinity biomolecules from solution was probed either directly using fluorescently labelled proteins or with a sandwich assay.

Often proteins are not directly physisorbed on bare solid substrates. Surface coatings are typically used to selectively promote or minimise protein attachment. Proteins exhibit different affinity for adsorbing on SAMs, depending on their termination group. Many proteins show low absorption to methyl-terminated SAMs [Wadu-Mesthrige 2000]. On the other hand, terminating groups such as carboxylic acid, aldehydes [Wadu-Mesthrige 1999] or biotin [Lee 1994] are known to promote protein adhesion by electrostatic interactions, covalent binding or biospecific interactions. The use of a surface coating in combination with EDL was explored aiming to minimise protein attachment in the non-patterned areas. For this purpose, a layer was coated on SiO_2/Si using methyl-terminated n-octadecyltrichlorosilane. It was shown in section 3.2.3.2 that contact mode AFM-CW can create a charge-pattern on the underling silicon dioxide and simultaneously engrave the OTS layer. The implications of this on the EDL attachment and protein functionality were explored in this chapter using mouse immunoglobulin G (IgG) in phosphate-buffered saline (PBS) microdroplets and, as a control, plain PBS microdroplets. After the delivery EDL step, the attached microdroplets were probed with anti-mouse IgG-FITC.

4.2.1 Experimental method

EDL consists of two main steps (Fig. 4.15): AFM charge-writing [Stern 1988] and microdroplet delivery [Mesquida 2001]. The AFM-CW and sample pretreatment or surface coatings were discussed in detail in section 3.1.2. The microdroplet delivery was performed by immersing the charged surface into a dispersion of water droplets in a non-conductive liquid (a water-in-oil emulsion) [Mesquida 2001]. The

droplets contained nanoparticles or any other water-soluble material and were driven electrostatically to the charge-pattern, where they delivered their contents on the surface [MesquidaDiss 2002].

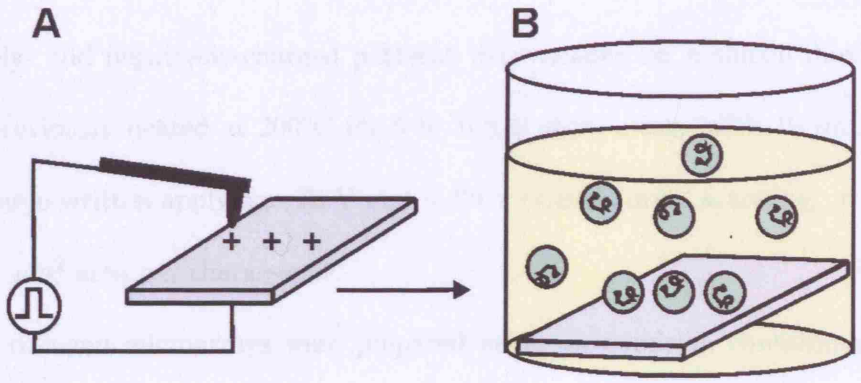

Figure 4.15: **Electric droplet lithography method.** A) Atomic force microscopy-based charge-writing. B) Microdroplet delivery.

The emulsions were prepared by dispersion of 20 μl aqueous protein solution in 2 ml perfluorocarbon oil FC-77 by 1 or 2 min ultrasonication in a Transonic T310 standard ultrasonic bath (Camlab Ltd., Cambridge, UK) followed by 5 s homogenisation at 9500 rpm using an Ultra-Turrax T25 homigeniser (Jankle & Kunkel, Ika-Labortechnik, Staufen, Germany) using the S25 N-8G dispersing tool and 20 s further ultrasonication. The homogeniser dispersing tool was cleaned by ultrasonication in 3 % Decon 90 (Decon Laboratories Ltd., Hove, UK) and in deionised water, and sterilised with ethanol after each emulsion. The charge-patterned sample was placed in a 5 ml beaker and the emulsion was poured over it. After 10 min immersion, the sample was removed from the emulsion. The resulting microdroplet attachment was imaged either using an optical light microscope (Olympus BX60, Middlesex, UK) operated in reflected light DIC (Differential Interference Contrast)

and recorded using a FireWire DFK 31AF03 colour camera (The Imaging Source, Bremen, Germany) or by AFM in tapping mode.

4.2.1.1 Collagen Microarray

Positively- and negatively-charged patterns were created on a silicon dioxide substrate previously heated at 200°C for 5 h. 6 x 6 spots arrays with 10 μm spacing were charge-written applying - 70 V and + 70 V pulses during scanning, in tapping mode, 1 μm^2 area per charge-spot.

The collagen microarrays were prepared using an emulsion containing, in the water phase, 1 mg/ml type-I-collagen from human placenta (Sigma-Aldrich Company Ltd., Poole, UK) in PBS diluted from a 2 mg/ml solution in acetic acid. The solution was dispersed in FC-77 after 2 min ultrasonication. No homogenization step was performed for this emulsion. After immersion for 10 min, the patterned collagen spots were imaged with an optical microscope.

The functionality of the collagen array was probed with mouse anti-collagen IgG, which was subsequently detected with fluorescently labelled anti-mouse IgG-FITC (Fig. 4.16). The collagen microarray was immersed in blocking buffer for 5 min and incubated for 30 min in monoclonal anti-collagen type I (60 μg/ml mouse IgG1 isotype in washing solution) (Sigma-Aldrich Company Ltd., Poole, UK). After washing the microarray, it was incubated for 30 min in GAM-FITC, rinsed with washing solution, mounted in antifade solution and imaged using a FireWire DFK 31AF03 colour camera (The Imaging Source, Bremen, Germany) installed in an Axioplan Universal Microscope for transmitted light and incident-light fluorescence

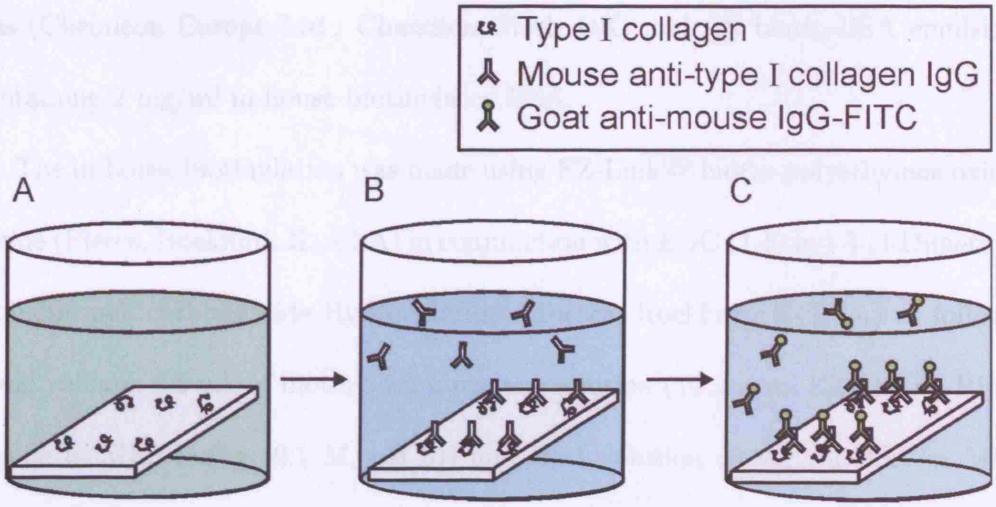

Figure 4.16: **Collagen microarray probing method.** A) Immersion in BSA blocking buffer for 5 min. B) Incubation in mouse anti-type I collagen IgG for 30 min followed by rinsing in washing solution. C) Incubation in goat anti-mouse IgG-FITC for 30 min followed by rinsing in washing solution.

(Zeiss, Gottingen, Germany) with the following filter setting: BP 450-490 nm for the excitation, FT 510 nm and LP 520 nm for the emission.

4.2.1.2 Multiprotein Array

To create a multiprotein array, each biomolecular species was delivered in a sequence of EDL cycles. Figure 4.17 shows a diagram depicting the method used for the creation of a microarray with three different proteins: inmunoglobulin G antibody raised in mouse (mouse IgG), inmunoglobulin G antibody raised in rabbit (rabbit IgG) and biotinylated bovine albumin serum (biotin-BSA).

A different emulsion was prepared for each of the three species, containing in the water phase: (1) mouse IgG emulsion, containing 2 mg/ml mouse anti-human Anexin II monoclonal immunoglobulin prepared in-house, (2) rabbit IgG emulsion containing 1 mg/ml rabbit anti-rat collagen type I polyclonal immunoglobu-

lins (Chemicon Europe Ltd., Chandlers Ford, UK) and (3) biotin-BSA emulsion, containing 2 mg/ml in-house biotinylated BSA.

The in-house biotinylation was made using EZ-Link® biotin-polyethylene oxide-amine (Pierce, Rockford, IL, USA) in conjunction with EDC (1-Ethyl-3-[3-Dimethyl-aminopropyl] carbodiimide Hydrochloride) (Pierce, Rockford, IL USA) as follows: equal volume, 0.5 ml, of biotinylating reagent solution (19 mg/ml EZ-Link®-PEO-Amine in MES buffer (0.1 M, pH 5)) and BSA solution (5 mg/ml BSA in MES buffer) were mixed. 50 μl EDC solution (10 mg/ml in MES buffer) was added and the mix was incubated for 2 h at room temperature. After incubation, any precipitate formed during the reaction was removed by centrifugation at 13000 rpm for 20 min in a Biofuge Fresco centrifuge (Heraeus, Hanau, Germany). The non-reacted biotinylation reagent and EDC by-products were removed from the biotin-BSA solution by dialysis using a Slide-A-Lyzer® dialysis cassette (10,000 MWCO, 0.5-3 ml capacity) (Pierce, Rockford, IL, USA). The buffer exchange was made in HEPES buffer (20 mM, pH 8). The resulting solution, 2 mg/ml BSA-biotin in HEPES buffer, was stored at 4°C.

Each EDL cycle consisted in, firstly, the creation of a row of 6 positively or negatively charged spots with 1 μm^2 area charge-written each and 10 μm spacing. Secondly, the first emulsion containing one of the species, rabbit IgG, was prepared and the charge-patterns were immersed in it for 10 min. After the immersion in the first emulsion, the sample was removed and the remaining charge neutralized with a Zerostat® anti-static gun (Aldrich, Gillingham, UK). Adjacent to the rabbit IgG spots, the same procedure was repeated in two more cycles using emulsions

containing biotin-BSA and mouse IgG, respectively.

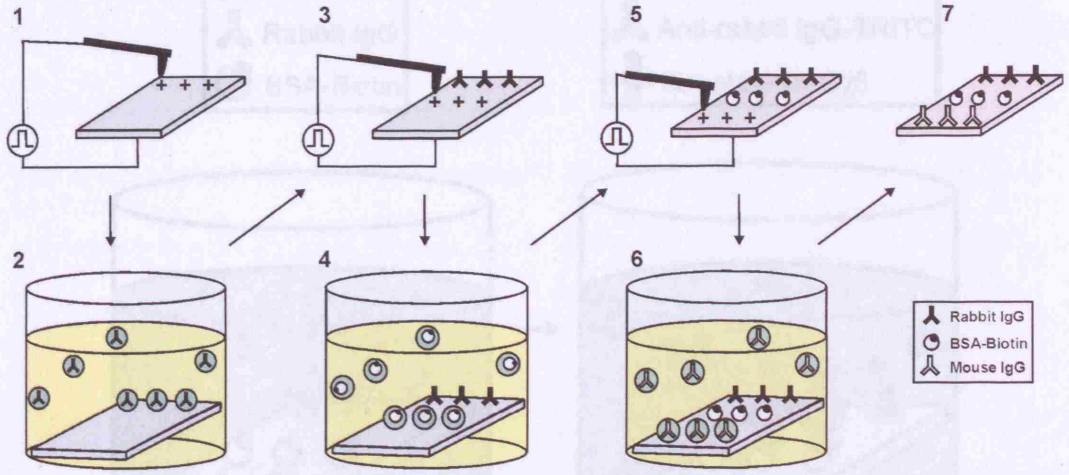

Figure 4.17: **Schematic diagram depicting the method used for multiple attachment.** (1) AFM-CW electrical pattern. (2) Immersion in emulsion containing rabbit IgG. (3) Neutralisation of previous charge-pattern and AFM-CW new charge-pattern. (4) Immersion in emulsion containing BSA-biotin. (5) Neutralisation of previous charge-pattern and AFM-CW new charge-pattern. (6) Immersion in emulsion containing mouse IgG. (7) Removal from emulsion.

In order to confirm the location and test the functionality of the attached (primary) proteins, the muliarray was probed with a mix of three fluorescently-labelled, secondary proteins: swine anti-rabbit IgG-TRITC (SAR IgG-TRITC), goat anti-mouse IgG-FITC (GAM IgG-FITC) and streptavidin-Cy5, each of them known to show a specific biomolecular interaction with the different primary proteins on the array: SAR IgG-TRITC with rabbit IgG, GAM IgG-FITC with mouse IgG and streptavidin-Cy5 with biotin-BSA. Non-specific attachment of the secondary proteins was prevented by blocking unspecific binding sites with BSA. After blocking, the sample was immersed with the fluorescent antibodies/streptavidin mixture (Fig. 4.18).

The detailed procedure for the interrogation of the multiprotein array was con-

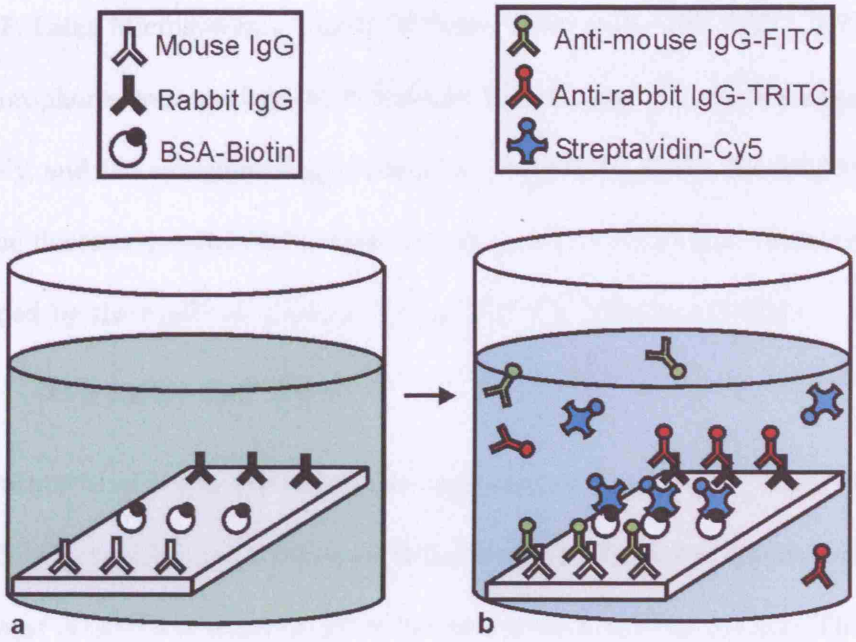

Figure 4.18: **Schematic diagram depicting the functionality assay.** Left: the sample in immersed in BSA blocking solution to reduce non specific binding. Right: the sample is incubated for 30 min in a PBS solution containing GAM IgG-FICT, SAR IgG-TRITC and streptavidin-Cy5.

ducted as follows: the microarray was immersed in blocking-buffer (1 % BSA/ PBS, 0.05 % sodium azide) for 5 min and incubated for 30 min, in darkness, with a mix (30 μl) containing equal volumes of GAM-FITC (fluorescein isothiocyanate-conjugated F(ab')2 fragment of goat anti-mouse immunoglobulins (Dako, Golstrup, Denmark), 25 μg/ml in washing solution (0.2 % BSA/PBS, 0.05 % sodium azide), SAR-TRITC (tetramethyl rhodamine isothiocyanate-conjugated swine anti-rabbit immunoglobulins (Dako, Golstrup, Denmark), 5 μg/ml in washing solution) and streptavidin-FlouroLinkTM Cy5TM (Amersham Life Science Inc., Arlington Heights, IL, USA), 10 μg/ml in washing solution. After the incubation the substrate was rinsed with washing-solution and mounted in antifade solution (Citifluor Ltd., London, UK). The fluorescence images were made using a confocal microscope (Leica

TCS NT, Leica Microsystems GmbH, Wetzlar, Germany). The FITC, TRITC and Cy5 fluorophores were excited with 488 nm, 568 nm and 647 nm wavelengths, respectively, and the emission imaged using the filters BP 550/30, BP 600/30 and LP 665. The fluorescence emitted is displayed in green, red and blue respectively and overlapped by the confocal software (Leica TCS NT, Version 1.6.587).

4.2.1.3 OTS layers and EDL

The attachment of microdroplets containing mouse IgG antibody to OTS-modified silicon dioxide surfaces was performed as follows. The SiO_2/Si samples were coated with a layer of OTS following the procedure described in section 3.1.1.2. The charge-patterns were written forming a cross-shaped geometry by scanning a 40 μm x 2 μm area, at 0° scanning angle, (scan size = 40 μm and aspect ratio = 20. 26 lines were scanned in contact mode in that area at 10 μm/s tip velocity) and a similar size area at 90° scanning angle to complete the cross applying either + 80 V or - 80 V voltage pulses during scanning for creating a positively and a negatively charged cross in each EDL cycle. The voltage was switched off during the change of scanning angle.

Charge-writing in contact mode over the OTS layer results in the formation of engraved topographical features (section 3.2.3.2). Therefore, control patterns were introduced in this experiment taking into account two factors: firstly, the microdroplets could show a preference to attach the patterns due to the topographical features instead of due to electrostatic attraction. Secondly, the fluorescently-labelled secondary antibody, typically used to detect the primary antibody (mouse IgG) delivered by EDL, could attach preferentially to the surface area modified by

scanning during AFM-CW, with or without the presence of the primary antibody. These factors could be a source of unwanted droplet mixing in the first case and false positive immunoassays in the second case. Thus, two EDL cycles were performed on the sample: the first one acting as a control, attaching microdroplets of PBS buffer and a second one attaching mouse IgG solved in PBS buffer having neutralised any remaining charge from the first cycle.

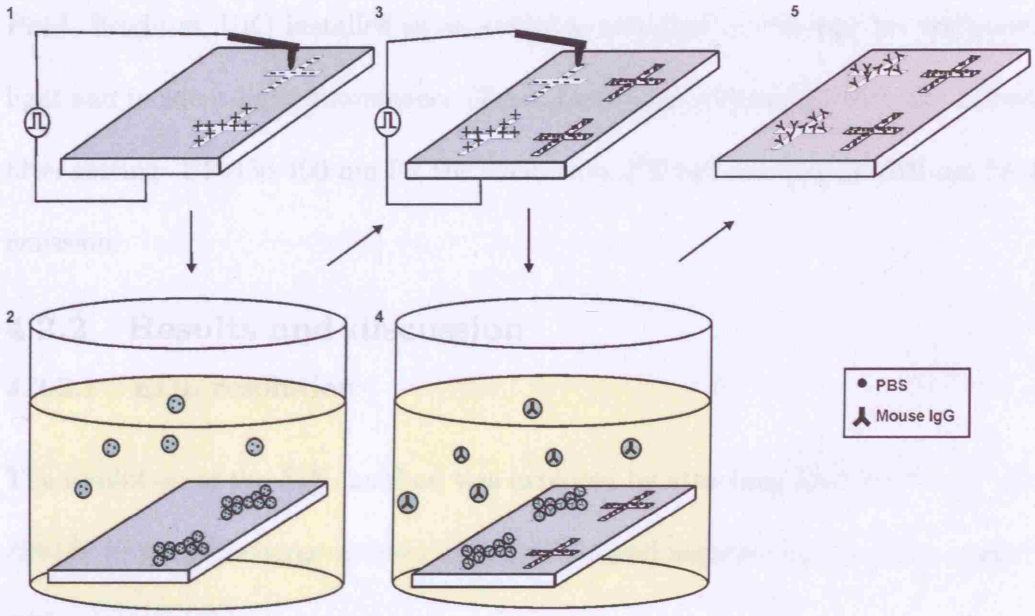

Figure 4.19: **Schematic diagram depicting the method for protein attachment on OTS/SiO_2.** (1) AFM-CW positive and negative electrical patterns. (2) Immersion in emulsion containing PBS. (3) Neutralisation of previous charge-pattern and AFM-CW new charge-patterns. (4) Immersion in emulsion containing Mouse IgG. (5) Removal from emulsion.

The emulsions were prepared by dispersing 40 μl of PBS buffer solution in 2 ml FC-77 by 2 min ultrasonication for the control emulsion and 40 μl of antibody solution (2 mg/ml mouse IgG in PBS buffer) for the antibody emulsion. The immersion time in the emulsion was 10 min for each EDL cycle. The attachment of microdroplets was imaged by AFM at the end of each cycle.

After the second EDL cycle, unspecific binding sites were blocked by immersion the sample in BSA blocking solution for 5 min. The sample was then probed with the labelled secondary antibody GAM IgG-FITC (25 μg/ml in washing solution (0.2 % BSA/PBS, 0.05 % sodium azide)) for 30 min in darkness. After the incubation time, the sample was rinsed with washing buffer, mounted in antifading reagent and imaged with a firewire, Qimaging 3.3 micropublisher, cooled digital camera (Digital Pixel, Brighton, UK) installed in an axioplan universal microscope for transmitted light and incident-light fluorescence (Zeiss, Gottingen, Germany) with the following filter setting: BP 450-490 nm for the excitation, FT 510 nm and LP 520 nm for the emission.

4.2.2 Results and discussion

4.2.2.1 EDL resolution

The resolution of the EDL method was explored by attaching BSA-biotin on silicon dioxide previously charge written with positive and negative arrays of charged-dots with approximately 1 μm spacing.

Each charge spot was written by applying a single voltage pulse of + 70 V or - 70 V. After charge-writing, a water-in-FC-77 emulsion was prepared using, for the aqueous phase, 2 mg/ml in-house biotinylated bovine serum albumin, fraction V (Roche, Penzberg, Germany). After immersing the charge-pattern in the biotin-BSA emulsion for 10 min, the sample was removed and the attachment was imaged in tapping mode.

Figure 4.20 shows that the protein attached equally well on positively and neg-

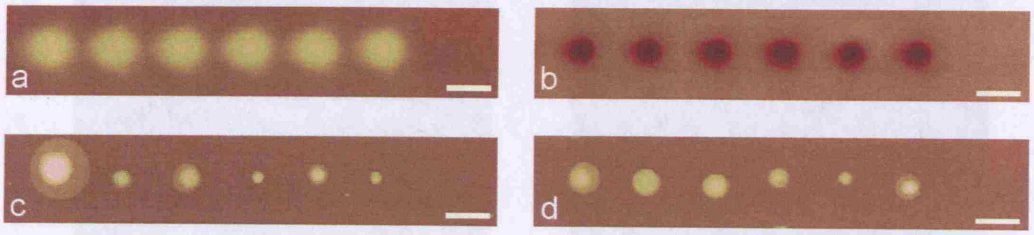

Figure 4.20: **EDL resolution.** Biotin-BSA microdroplets attached to positive and negative charge-pattern with approximately 1 μm spacing. a) KFM image of the positive charge-pattern, scale range = 5 V; b) KFM image of the negative charge-pattern, scale range = 5 V. c) AFM topography image of the microdroplets attached to the positive charge-pattern, scale range = 60 nm. d) AFM topography image of the microdroplets attached to the negative charge-pattern, scale range = 60 nm. Scale bars = 1 μm

atively charged-dot arrays with a resolution of approximately 1 μm. The protein spots attached to these charge-patterns had diameters in the range of a few hundred nanometres to 1.4 μm.

The resolution of EDL is limited by the diameter of the microdroplets. However, charge-patterns with a resolution in the 200 nm range can be written in SiO_2 [Jacobs 1999,a], [Uchihashi 1994]] and using $Si_3N_4/SiO_2/Si$ layered-electrets an even higher charge-pattern resolution, 30 nm, has been achieved [Tzeng 2006].

4.2.2.2 Single and multiple-protein microarrays

To demonstrate the EDL method with an extracellular matrix protein, arrays of type-I-collagen were patterned on silicon dioxide creating a single-protein microarray and their functionality was probed with mouse anti-collagen IgG, which was subsequently detected with fluorescently-labelled anti-mouse IgG-FITC. No significant differences were observed for the attachment to charge-patterns of different polarities (Fig. 4.21, (c), (d)). The different levels of fluorescence signal between

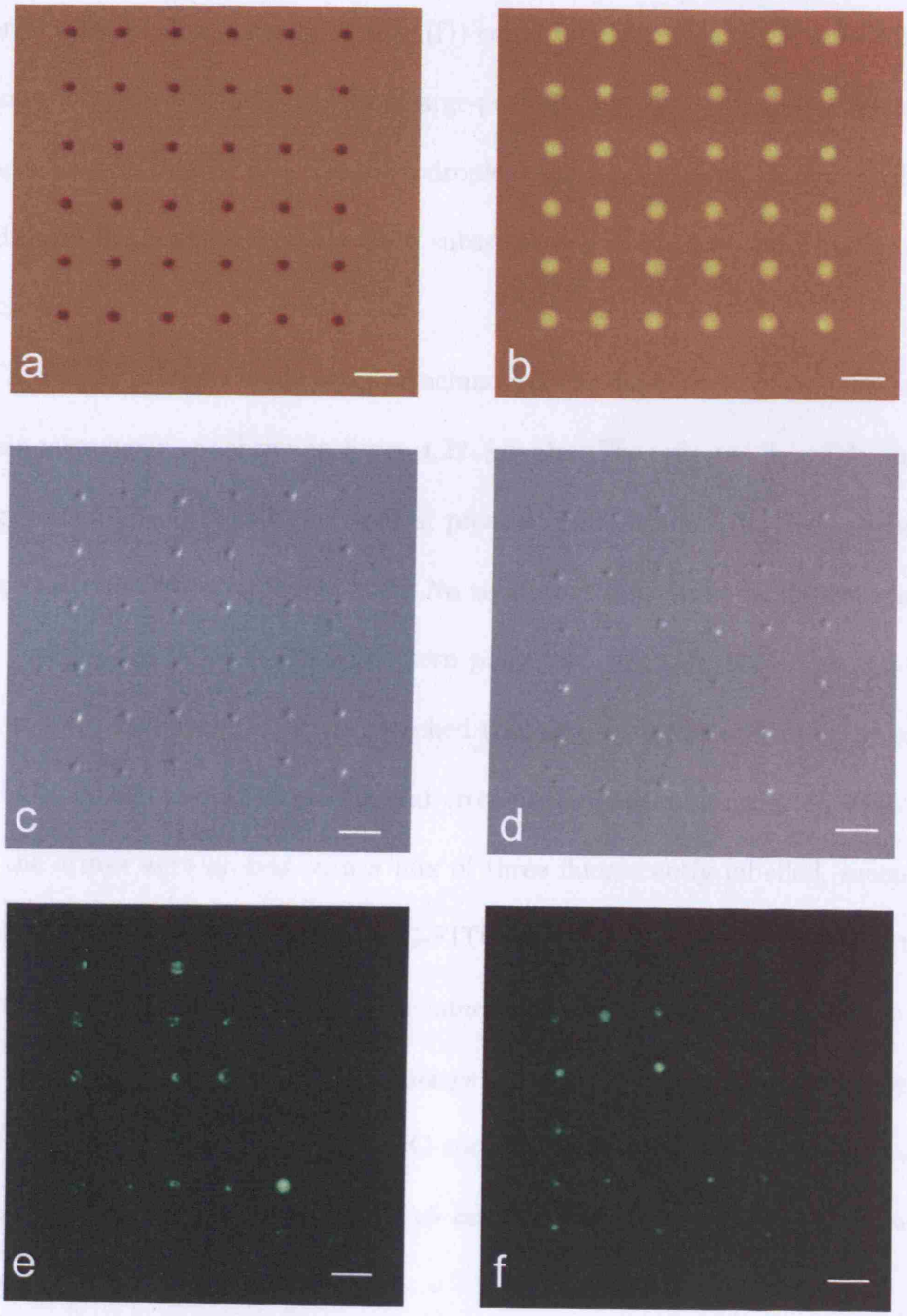

Figure 4.21: **Collagen microarrays.** a-b) KFM images of the negative (a) and positive (b) charge-patterns, scale range = 20 V. c-d) Reflected light DIC micrograph showing patterns of 6 x 6 spots of collagen attached to the negative (c) and positive (d) charge-patterns. e-f) Fluorescence images of the microarrays showing GAM IgG-FITC bound to the collagen-anti-collagen IgG complex. Scale bars = 10 μm

different protein spots (Fig. 4.21, (e), (f)) could be explained by differences in the amount of collagen attached to the charge-pattern (Fig. 4.21, (c), (d)). Part of the collagen content delivered by the microdroplets may have been washed away during the different washing steps as the SiO_2 substrate was not functionalised to promote attachment.

The charge-patterns used for the attachment of the different proteins in the multi-protein microarray are shown in figure 4.22, (a), (b). The reflected light DIC images in figures 4.22, (c-h), show the rows of protein spots attached to their respective charge-patterns after each EDL cycle. No significant differences in the attachment were observed for different charge-pattern polarities. In order to confirm the location, test the functionality of the attached (primary) proteins and investivage the possibility of any unwanted mixing and cross-contamination during the EDL process, the arrays were probed with a mix of three fluorescently labelled, secondary proteins: SAR IgG-TRITC, GAM IgG-FITC and streptavidin-Cy5, each of them known to show a specific biomolecular interaction with the different primary proteins on the array. The fluorescence images in figure 4.22, (i), (j), show, in green, GAM-FITC attached on the mouse IgG spots, in red, SAR-TRITC on the rabbit IgG spots and in blue, streptavidin-Cy5 on the biotin-BSA spots, with minimal cross-contamination.

Thus, the test showed that proteins delivered to the microarray by EDL retained their functionality to bind specifically to their corresponding fluorescent secondary proteins. Figure 4.22 shows all the primary proteins attached in the correct location in the positively charged array. In the case of the negatively charged multiarray, two

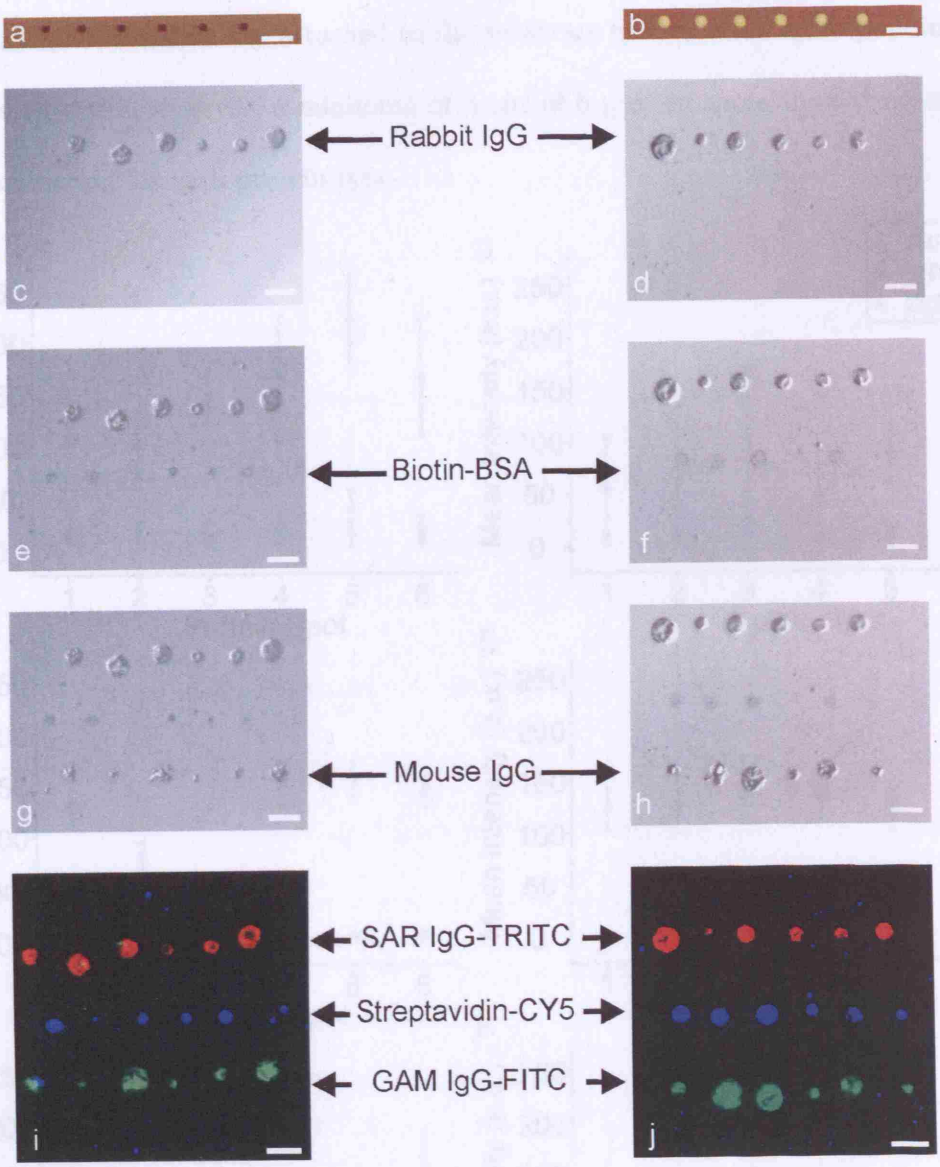

Figure 4.22: **Multiprotein microarray.** a-b) KFM images of the negative (a) and positive (b) charge-patterns used for the attachment, scale range = 20 V. c-h) Reflected light DIC micrograph showing patterns of 6 spots of rabbit IgG (c), biotin-BSA (e) and mouse IgG (g) attached sequentially to negative charge-patterns and 6 spots of rabbit IgG (d), biotin-BSA (f) and mouse IgG (h) attached sequentially to positive charge-patterns. i-j) Fluorescence image showing in green, the GAM IgG-FITC on the mouse IgG spots, in blue, the streptavidin-Cy5 on the BSA-biotin spots and in red, the SAR IgG-TRITC on the rabbit IgG spots in the multiprotein array made using negative charge-patterns (i) and in the one made using positive charge-patterns (j). Scale bars = 10 μm

microdroplets accidentally attached to the substrate in a location corresponding to another protein, however, a minimum of 5 out of 6 protein spots showed no cross-contamination for each protein type.

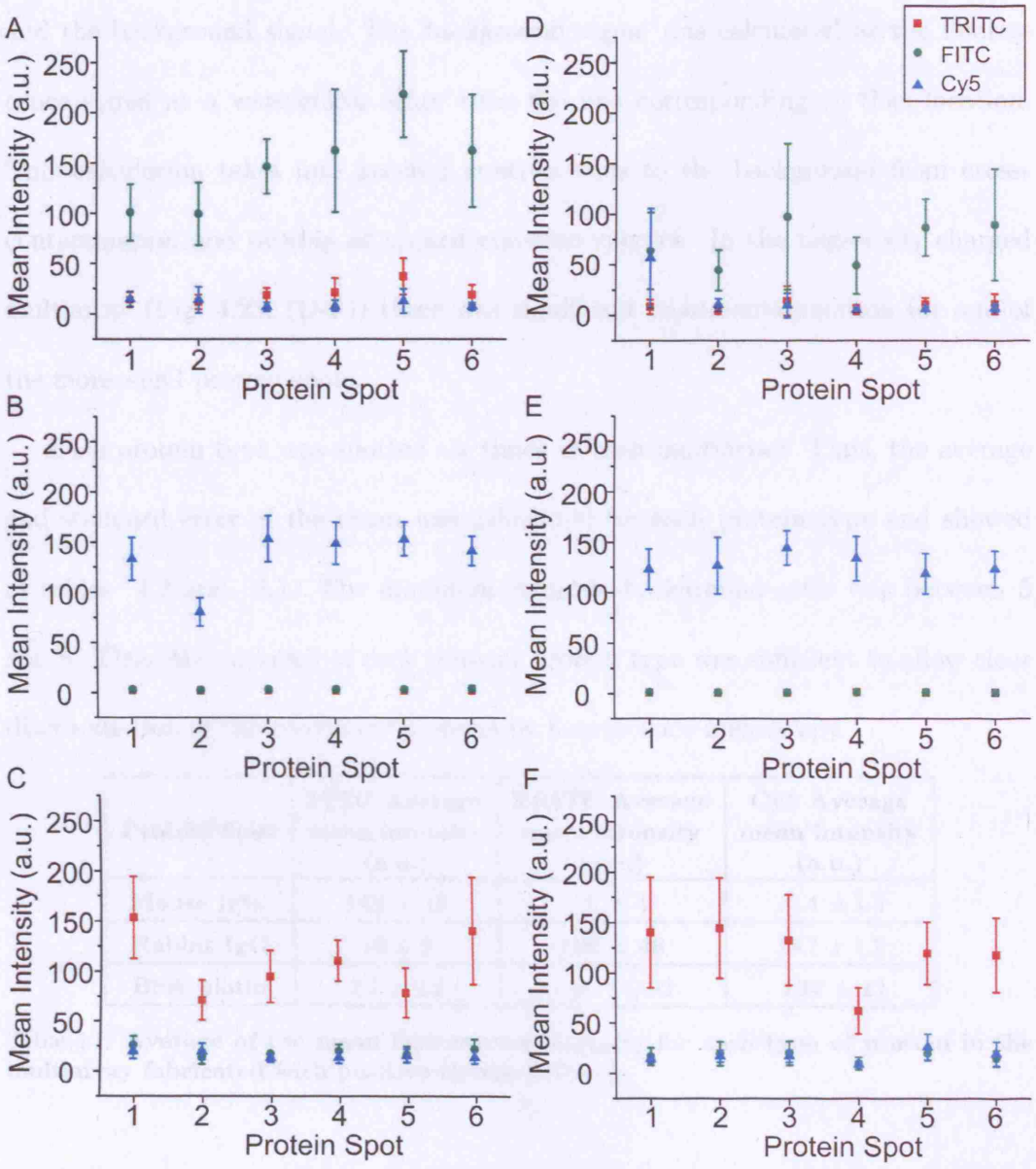

Figure 4.23: **Mean of the fluorescence intensity of the protein spots.** A-C) Spots from the multiarray fabricated positive charge-patterns: A)Mouse IgG spots, B) BSA-biotin spots, C) Rabbit IgG spots. D-F) Spots from the multiarray fabricated with negative charge-patterns: D) Mouse IgG spots, E)BSA-biotin spots, F) Rabbit IgG spots.

The mean intensity and standard deviation of the fluorescence signal of each protein spot are shown in figure 4.23. In the positively-charged multiarray (Fig. 4.23, (A-C)) there was no overlap between the expected fluorescence signal for each spot and the background signal. The background signal was calculated as the fluorescence signal at a wavelength other than the one corresponding to that location. This calculation takes into account contributions to the background from cross-contamination and overlap of optical emission spectra. In the negatively charged multiarray (Fig. 4.23, (D-F)) there was significant cross-contamination for one of the mouse-IgG protein spots.

Each protein type was spotted six times in each multiarray. Thus, the average and standard error of the mean was calculated for each protein type and showed in tables 4.2 and 4.1. The minimum signal-to-background-ratio was between 5 and 8. Thus, the coverage of each primary protein type was sufficient to allow clear discrimination of the secondary proteins by fluorescence microscopy.

Protein Spot	**FITC Average mean intensity (a.u.)**	**TRITC Average mean intensity (a.u.)**	**Cy5 Average mean intensity (a.u.)**
Mouse IgG	**148 ± 18**	20 ± 4	10.4 ± 1.5
Rabbit IgG	19 ± 2	**108 ± 48**	15.7 ± 1.2
BSA-biotin	2.1 ± 0.2	1.08 ± 0.02	**134 ± 11**

Table 4.1: **Average of the mean fluorescence intensity for each type of protein in the multiarray fabricated with positive charge-patterns.**

Protein Spot	FITC Average mean intensity (a.u.)	TRITC Average mean intensity (a.u.)	Cy5 Average mean intensity (a.u.)
Mouse IgG	**71 ± 9**	9.0 ± 1.3	16 ± 18
Rabbit IgG	16 ± 2	**119 ± 12**	17 ± 2
BSA-biotin	1.1 ± 0.1	1.1 ± 0.1	**128 ± 4**

Table 4.2: **Average of the mean intensity for each type of protein in the multiarray fabricated with negative charge-patterns.**

4.2.2.3 Attachment of mouse IgG to charge-patterns written on silicon dioxide coated with OTS

The surface potential patterns created for the attachment of mouse IgG microdroplets and control microdroplets are shown in figure 4.24. The absolute value of the peak surface potential differences achieved in both cases are $\geq$ 10 V. Thus, the KFM image appears truncated. The corresponding topography images show accumulation of aggregates on the edges of the scanned area as described in section 3.2.3.2. Inside the charged area, the topography image was distorted by the electrostatic forces experienced by the AFM tip due to the charge-pattern.

After performing each EDL cycle, one to attach the control microdroplets and a second one to attach the mouse IgG microdroplets, the attachment of the microdroplets to the patterns was imaged in tapping mode with an AFM. Figure 4.25 shows the attachment of the mouse IgG droplets to the negative (A) and positive (C) crosses and the attachment of control microdroplets to negative (B) and positive (D) crosses. The mouse IgG microdroplets are easily distinguishable in the AFM image. They attached to both polarities with preference to attach on the edges of the patterns. The agglomerates formed on the edges during AFM-CW could have

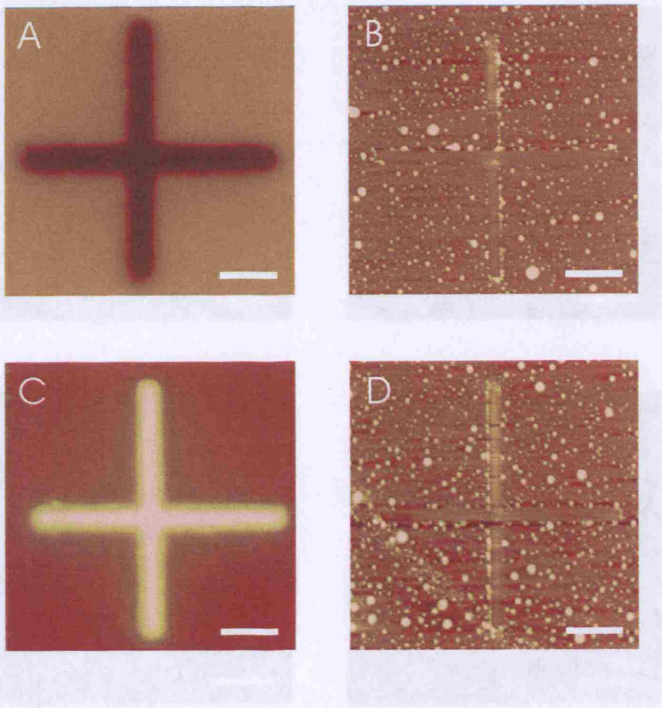

Figure 4.24: **Charge-patterns on OTS/SiO_2.** A) KFM image of a negatively-charged cross charge-written in contact mode. Scale range = 20 V. B) AFM topography image corresponding to the KFM image (A). Scale range = 200 nm. C) KFM image of a positively-charged cross charge-written in contact mode. Scale range = 20 V. D) AFM topography image corresponding to the KFM image (C). Scale range = 200 nm. Scale bars = 10 μm

clamped the microdroplets once they were attracted to the proximity of the pattern by the electrostatic charge. No mouse IgG droplets were observed in the control crosses as the charge was neutralised between EDL cycles.

The PBS control microdroplets were not easily distinguishable from the topography features of the OTS/SiO_2 samples. The microdroplets were smaller and left less residues than the protein ones. After blocking the sample with BSA, it was probed with GAM IgG-FITC. Figure 4.25, (E), shows a fluorescence image showing GAM IgG-FITC bound to the mouse IgG microdroplets only. There was no preferential attachment to the control patterns. The topography features did not influence the

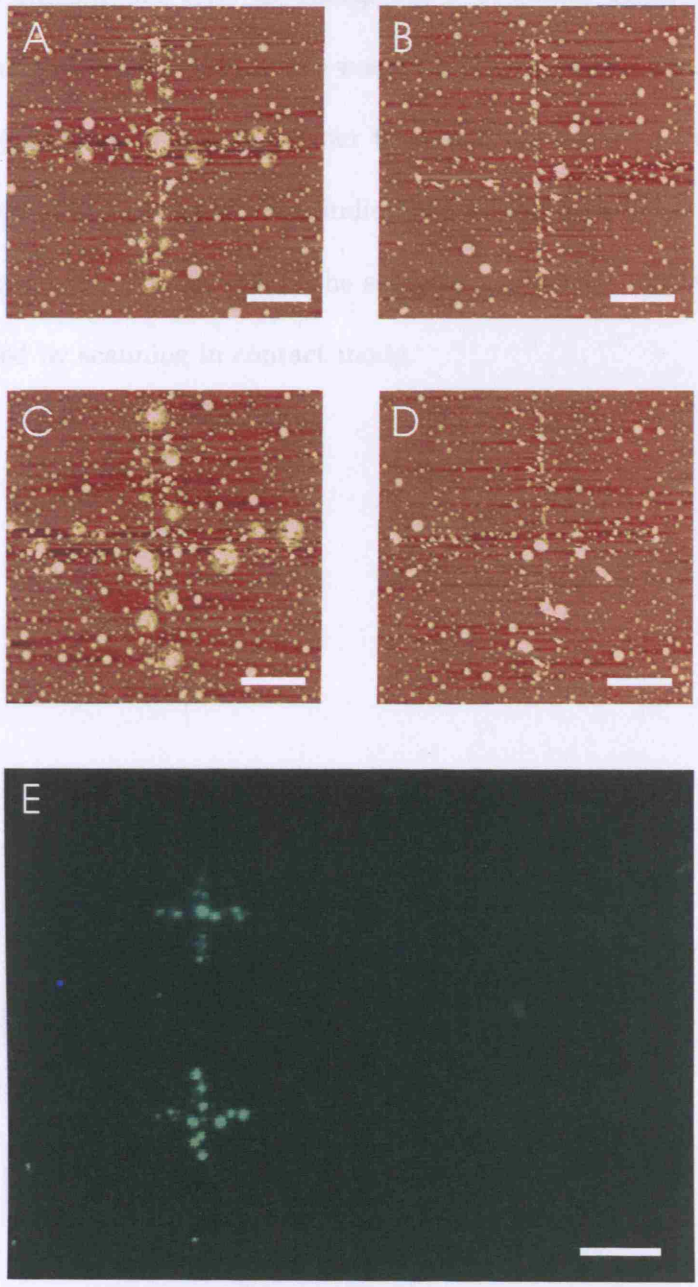

Figure 4.25: **Mouse IgG attachment to charge-patterns written on OTS/SiO_2.** A-D) Tapping mode, AFM topography images of: mouse IgG microdroplets attached to a negatively charged cross (A) and a positively charged cross (C) and control microdroplets attached to a negatively charged cross (B) and a positively charged cross (D). Scale range = 200 nm. Scale bars = 10 μm. E) Fluorescence image showing the GAM IgG-FITC bound to the mouse IgG microdroplets only. Scale bar = 40 μm.

attachment of microdroples after the charge was neutralised. Thus, neutralising any remaining charge after each EDL cycle was enough to prevent cross contamination between patterns. No fluorescence other than the one related to the mouse IgG microdroplets could be observed. This indicates that the BSA-block works well preventing any unspecific attachment of the secondary antibody to the topographical features created by scanning in contact mode.

Chapter 5

Conclusions and Outlook

The focus of this thesis was to explore the application of AFM-based charge-writing to the fabrication of functional biomolecular microarrays. Charge patterns written on PMMA, PS and SiO_2 with an AFM were used as electrostatic templates to promote the localised attachment of different proteins. Two approaches were investigated for the attachment: immersion in aqueous solutions which contained the protein of interest and immersion in water-in-oil emulsions with the protein confined in the water phase.

The stability of the charge-patterns during the attachment process was a key issue to be investigated for the electrets used, PMMA, PS and SiO_2, since different materials have different charge-trapping and charge decay mechanisms. The definition and stability of the charge-patterns was investigated using Kelvin-probe force microscopy.

Two main issues were found that could hinder the use of charge-patterns as electrostatic templates: lateral spread of the charge and rapid charge decay in water-based solutions. Lateral spread of the charge would limit the ultimate resolution of the pattern that could be achieved and distort its intended geometry. Charge-

patterns of both polarities showed poor lateral definition in PS. However, it was found that for PMMA and SiO_2, charge-patterns of only one polarity were distorted by lateral spread: the negative ones in PMMA and the positive ones in SiO_2. Using the EDL approach for the attachment step, the microdroplets dispersed in the dielectric oil FC-77 can attach to positively- as well as to negatively-charged patterns due to the contribution of dielectrophoretic forces [MesquidaDiss 2002]. Therefore it is not necessary to produce high resolution charge patterns in both polarities.

Nevertheless, in the case of SiO_2 substrates it was possible to improve the charge-pattern stability and definition. By subjecting the samples to a heat treatment in order to reduce the amount of water physisorpted in the oxide, the charge stability improved dramatically for both polarities. The use of OTS layers to minimise the influence of ambient humidity over the charge-patterns, reduced the lateral spread of the charge in the positive charge-patterns only. Positive charges were possibly located near the air/SiO_2 interface since lateral charge spread is associated with surface conductivity related to ambient humidity.

The stability in water of the charge-pattern written in SiO_2 was nevertheless very poor. After a few seconds of immersion, no charge-patterns could be detected. However, after 10 s immersion in water, 30 % of the initial charge could be measured in charge-patterns written in PMMA and after 20 s immersion, 80 % of the charge remained charge-patterns written in PS. Consequently, the electrostatic attachment of the protein avidin-fluorescein was attempted direcly from aqueous solution to charge-patterns written in PMMA and PS. To prevent charge decay, the attachment to charge-patterns in SiO_2 was performed using water-in-oil emulsions.

Preferential attachment of avidin-fluorescein could be achieved directly from aqueous solution to charge-patterned PS. However, there are indications that the attachment was not electrostatic. The protein did not attach to any of the areas charge-written in tapping mode. Nevertheless, it attached to all the areas charge-written in contact mode regardless of pattern polarity. Furthermore, it also attached to the areas scanned in contact mode without applying a bias voltage. It was thus concluded that topographical modifications created by contact mode scanning were the determining factor for the preferential attachment.

In the case of PMMA, charge-patterns were written in tapping mode to prevent any topography-related attachment. The positively-charged protein attached to the positively- as well as to the negatively-charged areas. If Coulombic forces were governing the attachment the biomolecule should have attached to the oppositely charged area only. The attachment to both polarities could be explained by the scanning-related effect observed in PMMA (section 3.2.1.3). The effect consisted in the formation of a surface potential contrast in the scanned areas after immersion in water. The scanned areas showed a negative surface potential with respect to the areas that had not been scanned. After immersing the sample in water for one minute and drying it, the surface potential difference between the scanned and non-scanned areas was observed to increase by a factor of up to 35. This difference also increased with the number of times that a particular area was scanned prior to immersion. Thus, this effect could be a dominant factor over the attachment of the positively-charged avidin-fluorescein. Charge-patterns are written by injecting charge-carriers during scanning. The scanning-related effect could thus also occur

during charge-writing. Since charge-patterns decay rapidly after immersion in water, the scanning-related surface potential contrast, which is enhanced by immersion in water, could thus become the factor governing the protein attachment. Nevertheless, the amount of surface potential contrast produced by scanning PMMA in tapping mode depended on the tip used and cleaning the AFM-tips with NH_4F prevented this effect from occurring.

The attachment of biomolecules to SiO_2 was achieved by EDL. Different proteins were confined in water microdroplets which where dispersed in the dielectric oil FC-77. Subsequently, the microdroplets attached electrostatically to charge-patterns written in SiO_2 delivering their contents on the surface. A resolution of approximately 1 μm was achieved using this method. The resolution was limited by the diameter of the microdroplets as charge-patterns of less than 100 nm feature size can be created in SiO_2 layers. The microdroplets were dispersed by ultrasonication but the emulsions obtained by this method were not monodisperse. Water-in-FC-77 emulsions are unstable and there are no commercially available, suitable surfactants. On the other hand, the use of surfactants may promote protein denaturation. An advantage of using SiO_2 substrates over polymeric substrates is that they do not dissolve in non-polar liquids such as heptane or hexane. A wide range of dielectric solvents would thus be compatible with SiO_2 and could be employed in the future for the creation of improved emulsions.

The microdroplets attached to charge-patterns of both polarities. This result was expected as the charge-patterns consisted of sharp surface potential peaks that favoured the contribution of dielectrophoretic forces to the attachment. Charge-

patterns of either polarity could thus be used for driving the microdroplet attachment. Microarrays containing collagen protein, IgG proteins and BSA-biotin were created on SiO_2 and their functionality was confirmed by standard immunoassay techniques. Surface coatings were also explored in the case of OTS/SiO_2 samples and proved compatible with charge-writing, protein attachment and functionality.

Furthermore, a multiprotein array containing mouse IgG, rabbit IgG and BSA-biotin was created. The correct location of the proteins was confirmed by immunoassay techniques. The fluorescence images showed minimal cross-contamination. The attached proteins kept their ability to capture biomolecules from solution via species-specific interactions or biotin-avidin interactions and were able to function in parallel without significant cross-talk. The minimum signal-to-background-ratio was between 5 and 8. The protein coverage was thus sufficient to allow clear discrimination of the secondary proteins by fluorescence microscopy.

The creation of a multiprotein array was possible because the driving force governing the attachment was a local electrostatic force that could be switched on and off arbitrarily since charge-patterns could be written and subsequently be neutralised. However, this was not the case for the attachment performed by immersion in aqueous solutions. The force governing the attachment was related to the permanent physical changes generated in the surface of the polymers during charge-writing rather than to the electrostatic charges injected. Thus, the sequential immersion of the sample in solutions containing different biomolecules would lead to cross-contamination.

In conclusion, the EDL approach permitted the sequential delivery of micro-

droplets containing different biomolecules to the same substrate. The immobilised biomolecules maintained their functionality and a resolution of approximately 1 μm between protein spots was achieved. The fundamental requirements for the fabrication of high-throughput protein arrays, with applications in high-speed biomedical diagnostics and drug screening, were thus met. Moreover, the ability to pattern protein arrays on SiO_2 substrates could also facilitate the integration of biomolecules with microelectronics devices.

In order to fabricate protein arrays at industrial scale, a complete automation of the processes involved in the EDL technique would be necessary. Since AFM-CW is a serial technique, it can be relatively slow. However several approaches could be used in the future to increase speed. Charge-writing could clearly benefit from the development of high-speed scanning probe systems and multiple-tip scanning [Humphris 2005], [Vettiger 2000]. Charge-patterns can also be produced in parallel biasing patterned electrodes [Jacobs 2001]. However, the key issue to automate the technique is to engineer the delivery step to take place without moving the sample from the instrument used for charge-patterning. One could envisage each emulsion containing the encapsulated biomolecules being flushed over the sample after each charge-patterning step. During the delivery step, the charge-patterning tool (a single probe or a patterned electrode) could be retracted to prevent any contamination and repositioned for the next location using a high precision robot. The integration of charge-patterning and biomolecule delivery in the same instrument would maximise speed and the alignment between patterns containing different biomolecules.

Finally, since EDL is a technique based in electrostatic attraction, no chemical

reactions or specific interactions between the substrates and the species to be attached are needed. Thus, it can be used in a wide variety of substrates, including polymers, oxide layers key for microfabrication or multilayers of dielectrics. Surface coatings may also be employed and virtually any molecule or particle in aqueous solution could, in principle, be confined in microdroplets dispersed in a dielectric oil. Thus, the greatest advantage of the EDL technique is indeed its versatility.

Appendix A

Charge-Writing on Silicon Scanning-Probe Oxide

Local oxidation of metals and semiconductors is a simple and flexible technique for the fabrication of nanostructures [Dagata 1995]. Silicon oxide features of a few nm thickness have been created on hydrogen-passivated Si substrates applying voltages below 10 V to a metallic coated scanning probe operated in air [Dagata 1990]. Expanding the applications of this method, the possibility of creating charge-patterns on SPM-oxide structures was explored to selectively build up on such oxide structures using electrostatic forces.

The substrates used were pieces of a p-type Si $< 100 >$ wafer with $\rho = 14.0\ \Omega\cdot$cm - 20.0 $\Omega\cdot$cm (Scottish Microelectronics Centre, Edinburgh University, Edinburgh, UK). The surface was cleaned by 120 s plasma cleaning and hydrogen-passivated by 4 min immersion in a 40 % aqueous solution of NH_4F (Fluka, Buchs, Switzerland) to prevent spontaneous oxidation [Higashi 1991]. Polypropylene containers were used since NH_4F etches glass. The substrates were then removed from the etching solution and rinsed with UHQ-water using a pipette and dried under a stream of N_2 and fixed to specimen discs with silver paint. The etching solution used was diluted with water

and neutralised with a 1 M Na_2CO_3 solution before disposal.

The magnitude of the oxide features is strongly dependent on humidity [Fang 2004]. Low humidity results in lower and narrower features. The ambient humidity during anodic oxidation was 55 ± 5 % measured with a thermo-hygrometer (Scientific laboratory supplies) placed close to the AFM head.

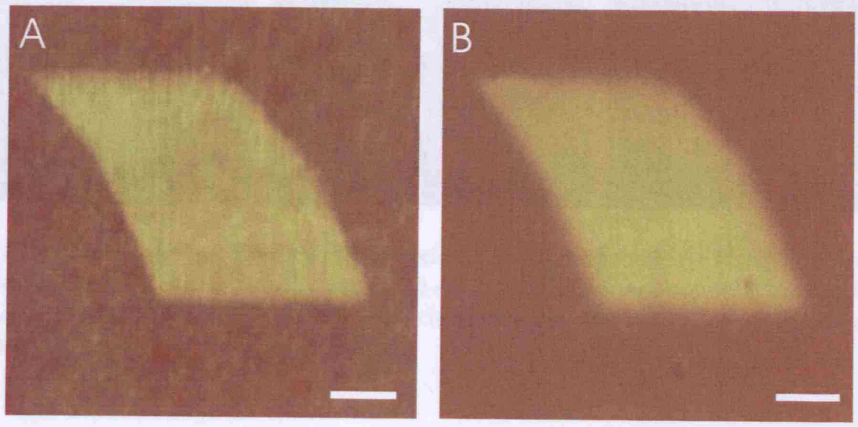

Figure A.1: **SPM-oxide pattern written on hydrogen passivated p-type < 100 > Si.** A) Contact mode AFM topography image of the oxidised area. The oxide height was 4.7 ± 1.4 nm, z-scale range = 30 nm. B) KFM surface potential image of the oxidised area. There was a surface potential difference of up to 200 mV between the bare Si surface and the oxidised area, scale range = 1 V. Scale bars = 1 μm.

An oxide feature was created on the Si substrate by scanning a 3 x 3 μm^2 area in contact mode at 0.6 μm/s tip velocity applying -15 V DC between the substrate and the AFM cantilever tip (W_2C-coated Si cantilever B. Table 3.3). The total number of lines scanned during the anodic oxidation was 512. Figure A.1 shows the topography and the surface potential of the oxidised area after thermally annealing the sample at 200°C for 3 h. The oxide height was 4.7 ± 1.4 nm. It was calculated by fitting the distributions of height values to two Gaussian curves, one for the distribution of height values of the bare Si and the other for the values on the oxide

region. The distance between the mean values of each distribution is the height of the oxide respect to the Si surface. The error of such distance was calculated by propagating the standard deviation of the distributions.

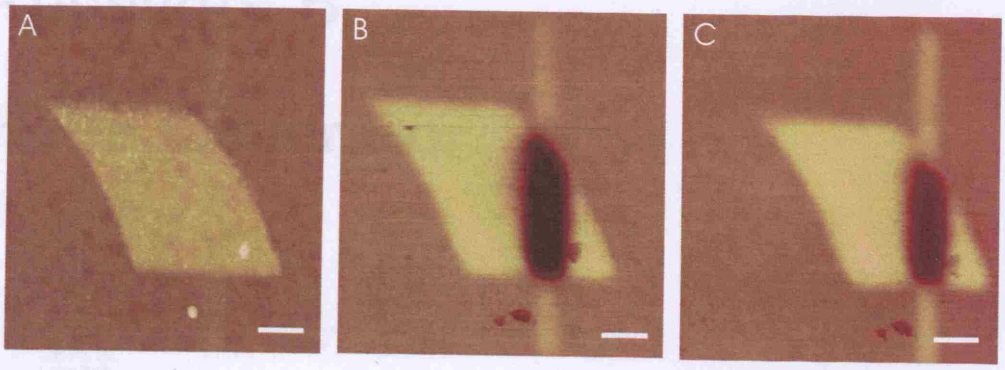

Figure A.2: **AFM charge-writing on SPM-oxide.** A) Contact mode AFM topography image of the SPM-oxide charge-written, z-scale range = 30 nm. B) KFM surface potential image after AFM-CW. Scale range = 0.5 V. C) KFM surface potential image 2 h after AFM-CW, scale range = 0.5 V. Scale bars = 1 μm.

A 7 μm-long line was scanned in contact mode across the SPM-oxide feature applying a - 15 V DC voltage between the tip and the sample. The relative humidity of the room was 37 %, lower than during the creation of the oxide feature. Thus, only minor oxidation occurred on the scanned Si surface (Fig. A.2, (A)). The area of the SPM-oxide where the negative voltage was applied was, as expected, charged negatively (Fig. A.2, (B)). The surface potential difference between the negatively-charged area in the oxide and the Si surface was 0.4 V. This surface potential feature could still be imaged 2 h after charge-writing after decaying to 50 % of its initial value (Fig. A.2, (C)). This preliminary experiment shows that charge-patterns could be created on thin SPM-oxides with a good degree of pattern stability and could open up new routes for device nanofabrication.

Appendix B

Pulse Generator

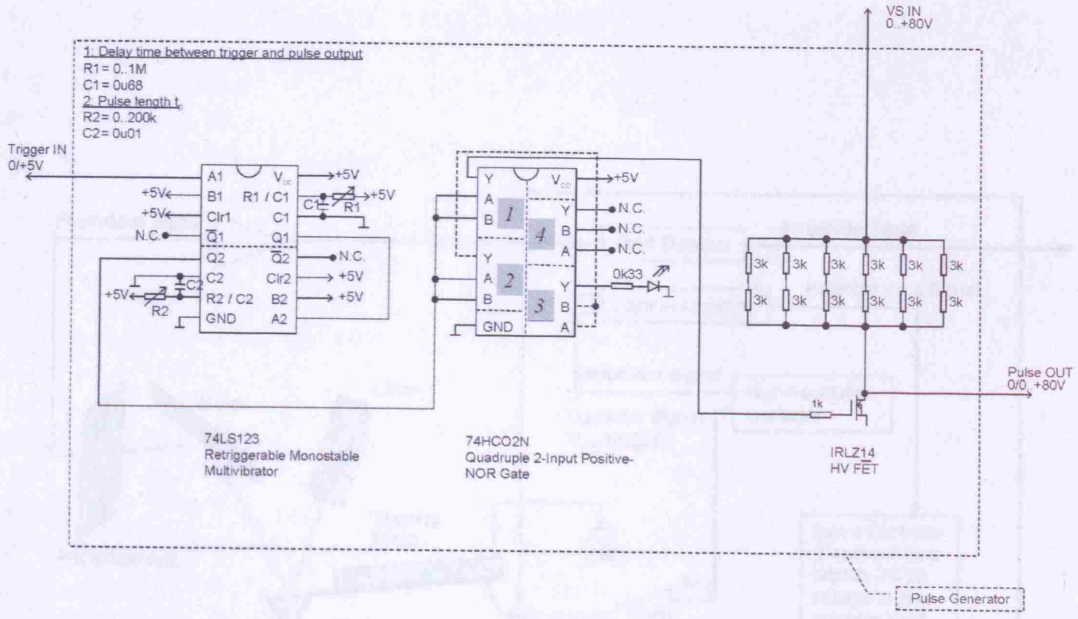

Figure B.1: **Pulse generator.** The trigger signal is fed in at A1. The delay between the falling edge of Trigger IN and the rising edge of the voltage pulse on Pulse OUT is adjusted via R1 and C1. The pulse length, t_p, is set by R2 and C2. The pulse signal passes an inverter (NOR Gate) before switching the HV FET at Pulse OUT. The dashed circuit line at the NOR Gate is not necessary for operation but the LED can be used additionally for checking the device's operation. Custom-built by Patrick Mesquida [MesquidaDiss 2002]. Extra resistors were added by Macarena Blanco to minimise overheating.

Appendix C

Surface Potential Detection System

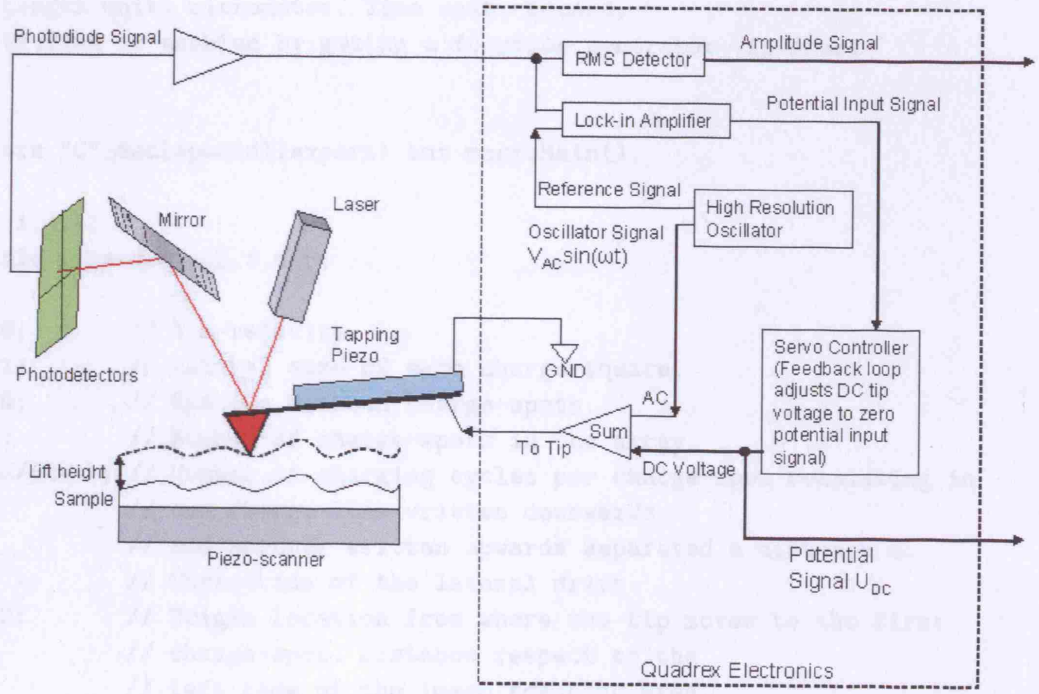

Figure C.1: **Simplified block diagram of KFM surface potential detection.** .

Appendix D

Source Codes

D.1 One-dimensional array of charge-spots

```
#include <litho.h>
#include <gui.h>
// Generates line of charge-spots.
// Length unit: micrometer. Time unit: second.
// Writing is enabled by gating a function generator via Ana3.


extern "C"_declspec(dllexport) int macroMain()
{
int i,j,k;
double v,ss,d,o,p,h,f,s,b;

v=10;       // Tip velocity.
ss=1;       // Lateral size of each charge-square.
d=10;       // Spacing between charge-spots.
p=6;        // Number of charge-spots in the array.
o=ss/(2*h); // Number of charging cycles per charge-spot consisting in
            // one charge-line written downwards
            // and another written upwards separated a distance h.
s=0.1;      // Correction of the lateral drift.
b=10;       // Origin location from where the tip moves to the first
            // charge-spot. Distance respect to the
            // left side of the image scanning area.

LITHO_BEGIN

LithoDisplayStatusBox();      // Display litho status box.
LithoScan(false);             // Turn off scanning.

AskOk("1-D array of charge-spots","Select a tip voltage, Up.");
```

```
f=0;                        // Drift correction.
h=0.1;                      // Charge-lines separation in a charge-spot.
for (k=1;k<=100;k++)        // Tip moves to the left.
    {
    LithoTranslate(-1,0,v);
    }

LithoTranslate(b,0,v);      // Tip moves to the origin location.

for (j=1;j<=p;j++)
    {
    LithoTranslate(d+ss-f,0,v);  // Tip moves to the next charge-spot.
    for (i=1;i<=9;i++)
        {                        // Charge-writing charge-spot:
        LithoSet(lsAna3,5);      // Sets Ana3 to 5 V.
        LithoTranslate(0,-ss,v); // Writes charge-line downwards.
        LithoTranslate(-h,0,v);  // Tip moves to the next line.
        LithoTranslate(0,ss, v); // Writes charge-line upwards.
        LithoTranslate(-h,0,v);  // Tip moves to the next line.
        LithoSet(lsAna3,0);      // Sets Ana3 to 0 V.
        }
    f=f+s;                       // Drift correction.
    h=h+0.005;                   // Drift correction.
    }

AskOk("1-D array of charge-spots","Disconnect Ana2.");

LITHO_END

return 0;                        // 0 makes macro unload

}
```

D.2 Two-dimensional array of charge-spots

```
#include <litho.h>
#include <gui.h>
// Generates p lines with p charge-spots each.
// Length unit: micrometer. Time unit: second.
// Writing is enabled by gating a function generator via Ana3.

extern "C"_declspec(dllexport) int macroMain()
{
int i,j,k,r,g;
double v,ss,d,o,p,h,f,s,b,m;

v=10;       // Tip velocity.
ss=1;       // Lateral size of each charge-spot.
d=10;       // Spacing between charge-spots.
p=6;        // Number of charge-squares per line and number of lines.
o=ss/(2*h); // Number of charging cycles per charge-spot consisting in
            // one charge-line written downwards and another written
            // upwards separated a distance h.
s=0.1;      // Drift correction.
b=10;       // Distance respect to the left side of the image scanning
            // area. Charge-writing starting point.
m=0;        // Drift correction.

LITHO_BEGIN

LithoDisplayStatusBox();    // Display litho status box.
LithoScan(false);           // Turn off scanning.

for (g=1;g<=100;g++)
    {
    LithoTranslate(0,1,v);  // Tip moves to the top side of the image.
    }

AskOk("2-D array of charge-spots","Select a tip voltage, Up.");

for (r=1;r<=p;r++)
    {
    f=0;
    h=0.1;
    for (k=1;k<=100;k++)
        {
        LithoTranslate(-1,0,v);     // Tip moves to the left.
        }
    LithoTranslate(b,0,v);          // Tip moves to the origin location.
```

```
    for (j=1;j<=p;j++)
        {
        LithoTranslate(d+ss-f,0,v); // Tip moves to the next charge-spot.
        for (i=1;i<=9;i++)
            {                       // Charge-writing charge-spot:
            LithoSet(lsAna3,5);     // Sets Ana3 to 5 V
            LithoTranslate(0,-ss,v);// Writes charge-line downwards.
            LithoTranslate(-h,0,v); // Tip moves to the next line.
            LithoTranslate(0,ss,v); // Writes charge-line upwards.
            LithoTranslate(-h,0,v); // Tip moves to the next line.
            LithoSet(lsAna3,0);     // Sets Ana3 to 0 V.
            }
        f=f+s;                      // Drift correction.
        h=h+0.005;                  // Drift correction.
        }
        LithoTranslate(0,-(d-m),v); // Tip moves to the next line.
        m=m+0.8;                    // Drift correction.
    }

    AskOk("2-D array of charge-spots","Disconnect Ana2.");

    LITHO_END

    return 0;                      // 0 makes macro unload
}
```

D.3 Array of vertical lines

```
#include <litho.h>
#include <gui.h>

// Generates o vertical lines of ss/2 length.
// The voltage Up can be selected for each line.
// Length unit: micrometer. Time unit: second.
// Writing enabled by gating a function generator via Ana3.

extern "C"_declspec(dllexport) int macroMain()
{
int j,o;
double v,ss,s;
v=4;                    // Tip velocity.
ss=20;                  // Image frame size.
s=4;                    // Line spacing.
o=6;                    // Number of lines.

LITHO_BEGIN

LithoDisplayStatusBox();          // Display litho status box.
LithoScan(false);                 // Turn off scanning.
LithoCenterXY();                  // Move tip to center of field.
LithoTranslate(-0.3*ss,0.5*ss,v); // Move tip to starting point.
for (j=1;j<=o;j++)
    {
    AskOk("Array of lines","Select a tip voltage, Up.");
    LithoSet(lsAna3,5);       // Sets Ana3 at 5 V.
    LithoTranslate(0,-ss,v);  // Writes one line.
    LithoSet(lsAna3,0);       // Sets Ana3 at 0 V.
    LithoTranslate(s,ss,v);   // Moves to start point of next line.
    }

AskOk("Array of lines","Disconnect Ana2.");

LITHO_END

return 0;                     // 0 makes macro unload
}
```

D.4 Letters IRC

```
// Generates the letters I R C written with single voltage pulses.
// Length unit: micrometer. Time unit: second.
// Writing is enabled by gating a function generator via Ana3.

#include<litho.h>
#include <gui.h>

extern "C"_declspec(dllexport) int macroMain()
{
double size = 2.5;          // Size of the total pattern.
double rate = 60;           // Tip velocity.
double step = 0.1;          // Distance between applied pulses.
double height = 2*size/5; // Height of the letter.
double width = size/5;      // Width of the letter.
double t = 0.002;           // Voltage pulse length.
int i;
int o = height/step;
int p = width/step;
int q = p/2;

LITHO_BEGIN

LithoDisplayStatusBox();                  // Display litho status box.
LithoScan(false);                         // Turn off scanning.
LithoCenterXY();                          // Move tip to center of field.
LithoTranslate(-size/3, size/5, rate);  // Move tip to first letter.

AskOk("Letters IRC","Select a tip voltage, Up (press OK).");

//Letter I starting from the top.

for (i=1;i<=o;i++)
    {
    LithoTranslate(0,-step,rate);
    LithoPulse(lsAna3,5,t);
    LithoPause(0.002);
    }
for (i=1;i<=o;i++)
    {
    LithoTranslate(0,step,rate);
    LithoPulse(lsAna3,5,t);
    LithoPause(0.002);
    }
for (i=1;i<=o;i++)
```

```
    {
    LithoTranslate(0,-step,rate);
    LithoPulse(lsAna3,5,t);
    LithoPause(0.002);
    }

LithoTranslate(width,0,rate);

//Letter R starting from the bottom left.

for (i=1;i<=o;i++)
    {
    LithoPulse(lsAna3,5,t);
    LithoPause(0.002);
    LithoPulse(lsAna3,5,t);
    LithoPause(0.002);
    LithoTranslate(0,step,rate);
    }
for (i=1;i<=p;i++)
    {
    LithoPulse(lsAna3,5,t);
    LithoPause(0.002);
    LithoPulse(lsAna3,5,t);
    LithoPause(0.002);
    LithoTranslate(step,0,rate);
    }
for (i=1;i<=p;i++)
    {
    LithoPulse(lsAna3,5,t);
    LithoPause(0.002);
    LithoPulse(lsAna3,5,t);
    LithoPause(0.002);
    LithoTranslate(0,-step,rate);
    }
for (i=1;i<=p;i++)
    {
    LithoPulse(lsAna3,5,t);
    LithoPause(0.002);
    LithoPulse(lsAna3,5,t);
    LithoPause(0.002);
    LithoTranslate(-step,0,rate);
    }

LithoTranslate(width/2,0,rate);
```

```
for (i=1;i<=p;i++)
    {
    LithoTranslate(step/2,-step,rate);
    LithoPulse(lsAna3,5,t);
    LithoPause(0.002);
    LithoPulse(lsAna3,5,t);
    LithoPause(0.002);
    }
LithoPulse(lsAna3,5,t);
LithoPause(0.002);
LithoPulse(lsAna3,5,t);
LithoPause(0.002);

LithoTranslate(width, 0, rate);

//C starting from the bottom right

LithoTranslate(width, 0, rate);

for (i=1;i<=p;i++)
    {
    LithoPulse(lsAna3,5,t);
    LithoPause(0.002);
    LithoPulse(lsAna3,5,t);
    LithoPause(0.002);
    LithoTranslate(-step,0,rate);
    }
for (i=1;i<=o;i++)
    {
    LithoPulse(lsAna3,5,t);
    LithoPause(0.002);
    LithoPulse(lsAna3,5,t);
    LithoPause(0.002);
    LithoTranslate(0,step,rate);
    }
for (i=1;i<=p;i++)
    {
    LithoPulse(lsAna3,5,t);
    LithoPause(0.002);
    LithoPulse(lsAna3,5,t);
    LithoPause(0.002);
    LithoTranslate(step,0,rate);
    }
LithoPulse(lsAna3,5,t);
LithoPause(0.002);
```

```
LithoPulse(lsAna3,5,t);
LithoPause(0.002);

LithoTranslate(width, -height, rate);

AskOk("Letras IRC","Disconnect Ana2.");

LITHO_END

return 0;          //0 makes macro unload

}
```

D.5 One-dimensional array of single-pulsed charge-dots

```
#include <litho.h>
#include <gui.h>

// Generates a line of dots applying a single voltage pulse per dot.
// Length unit: micrometer. Time unit: second.
// Single pulses triggered via Ana3.

extern "C"_declspec(dllexport) int macroMain()
{
int i,o;
double v,s,ss;

v=10;               // Tip velocity.
ss=20;              // Scan size.
o=6;                // Number of dots.
s=1.5;              // Dots spacing.

LITHO_BEGIN

LithoDisplayStatusBox();     // Display litho status box.
LithoScan(false);            // Turn off scanning.
LithoCenterXY();             // Move tip to center of field.
LithoTranslate(-ss/2,0,v);   // Move tip to starting point.
AskOk("1-D array of charge-dots","Select a tip voltage, Up.");
LithoTranslate(0.12*ss,0,v);
LithoPause(0.002);
for (i=1;i<o;i++)
    {
    LithoPulse(lsAna3,5,0.001);   // Sets Ana3 to 5 V.
    LithoPause(0.002);
    LithoTranslate(s,0,v);        // Moves tip to next dot
    }

AskOk("1-D array of charge-dots","Disconnect Ana2.");

LITHO_END
return 0;                         // 0 makes macro unload
}
```

Definition of Terms

List of symbols

ϵ	Dielectric permittivity
ϕ_s	Surface potential
ρ	Electrical resistivity
M_w	Molecular weight
q	Electrical charge
U_{DC}	DC offset voltage applied in the KFM measurement
Up	Magnitude of the voltage pulse applied during AFM-CW

Acronyms

AFM	Atomic Force Microscope/-y
AFM-CW	Atomic Force Microscope Charge-Writing
BSA	Bovine Serum Albumin
DIC	Differential Interference Contrast
DPN	Dip-Pen Nanolithography
EDC	(1-Ethyl-3-[3-Dimethylaminopropyl]carbodiimide Hydrochloride)
EDL	Electric Droplet Lithography
FIB	Focused Ion Beam
FITC	fluorescein isothiocyanate
FWHM	Full Width at Half Maximum
GAM	Goat Anti-Mouse
IgG	Immunoglobulins G
KFM	Kelvin-probe Force Microscopy
LbL	Layer-by-Layer
MEMS	Micro-Electrical Mechanical System
MES	[(2-N-morpholino)ethanesulfonic acid]
OTS	n-octadecyltrichlorosilane
PBS	phosphate-buffered saline
PDMS	poly-(dimethylsiloxane)
PG	Pulse Generator
PLL	Poly-L-Lysine
PMMA	Poly(methyl methacrylate)
PS	Polystyrene
PTFE	Polytetrafluoroethylene
SAM	Signal Access Module
SAMs	Self Assembled Monolayers

SAR	Swine Anti-Rabbit
SNOM	Scanning Near-field Optical Microscopy
SPM	Scanning Probe Microscopy
STM	Scanning Tunnelling Microscopy
TRITC	Tetramethyl rhodamine isothiocyanate
UHQ	Ultra-High Quality (Water)

List of Figures

List of Tables

List of Publications and Presentations

List of Publications and Presentations

Publications

- E.M. Blanco, S.A. Nesbitt, M.A. Horton and P. Mesquida. A multiprotein microarray on silicon dioxide fabricated by electric droplet lithography. *Adv. Mater.* **19,** 2469-2473.
- P. Mesquida, E.M. Blanco, R. McKendry. Patterning amyloid peptide fibrils by AFM charge writing. *Langmuir* **22,** 9089-9091 (2006).

Presentations

- E.M. Blanco, P. Mesquida and M. Horton. Localised electrostatic attachment of functional biomolecules on silicon dioxide. UKSPM, UK Annual Scanning Probe Microscopy Meeting, London, UK, 2006. Oral presentation.
- E.M. Blanco, P. Mesquida, M. Horton. Localised electrostatic attachment of functional biomolecules in silicon dioxide. FRONTIERS Workshop, Understanding Processes at the Molecular Level, Lenzerheide, Switzerland, 2006. Oral presentation.
- E.M. Blanco, P. Mesquida and M. Horton. Spatially selective attachment of biomolecules using AFM-based charge writing. Second IRC-NIMS Summer School, Cambridge, UK, 2005. Oral presentation.
- E.M. Blanco, P. Mesquida. Directed deposition of biomolecules using AFM charge writing. UKSPM, UK Annual Scanning Probe Microscopy Meeting, Nottingham, UK, 2004. Oral presentation.
- E.M. Blanco, P. Mesquida and M. Horton. Directed deposition of biomolecules using AFM charge writing. First Japan-UK Nanotechnology Students' Summer School, Tsukuba, Japan, 2004. Oral presentation.
- E.M. Blanco, P. Mesquida. Directed deposition of charged nano-objects using AFM charge writing. Special Reception at the House of Commons for Britain's Younger Scientists, Engineers and Technologists in UK Science Week, London, UK, 2004. Poster.

- P. Mesquida, E.M. Blanco, D.J. Kang, M. Horton, M. Stoneham, D. Klenerman, A. Round. Self-assembly of smart materials using charges as glues. IRC Science Meeting at the Institute of Physics, London, 2003. Poster.
- E.M. Blanco and P. Mesquida. Novel methods for creating biologically patterned surfaces. iNANOschool, Nanoscience and Photonics PhD Graduate School, Ebeltoft, Denmark, 2003. Poster.

References

[Amato 1997] I. Amato. Candid cameras for the nanoworld. *Science* **276,** 1982 (1997).

[Amjadi 1999] H. Amjadi. Charge storage in double layers of thermally grown silicon dioxide and APCVD silicon nitride. *IEEE T. Dielect. El. In.* **6,** 852-857 (1999).

[Anderson 2004] D.G. Anderson, S. Levenberg and R. Langer. Nanoliter-scale synthesis of arrayed biomaterials and application to human embryonic stem cells. *Nat. Biotechnol.* **22,** 863-866 (2004).

[Barry 2003] C.R. Barry, M.G. Steward, N.Z. Lwin and H.O. Jacobs. Printing nanoparticles from the liquid and gas phases using nanoxerography. *Nanotechnology* **14,** 1057-1067 (2003).

[Becker 2006] K.F. Becker, V. Metzger, S. Hipp and H. Hofler. Clinical proteomics: new trends for protein microarrays. *Curr. Med. Chem.* **13,** 1831-1837 (2006).

[Betzig 1991] E. Betzig, J.K. Trautman, T.D. Harris, J.S. Weiner and R.L. Kostelak. Breaking the diffraction barrier-Optical microscopy on a nanometric scale. *Science* **251,** 1468-1470 (1991).

[Betzig 1992] E. Betzig and J.K. Trautman. Near-field optics: microscopy, spectroscopy and surface modification beyond the diffraction limit. *Science* **251,** 189-195 (1992).

[Binnig 1983] G. Binnig, H. Rohrer, C. Gerber and E. Weibel. (111) facets as the origin of reconstructed Au(110) surfaces. *Surf. Sci.* **131,** L379-L384 (1983).

[Binnig 1986] G. Binnig, C.F. Quate and C. Gerber. Atomic Force Microscope. *Phys. Rev. Lett.* **56,** 930-933 (1986).

[Binnig 1987] G. Binnig and H. Rohrer. Scanning tunnelling microscopy-form birth to adolescence. *Rev. Mod. Phys.* **59,** 615-625 (1987).

[Brayshaw 2004] D.J. Brayshaw, M. Berry and T.J. McMaster. Molecular adsorption: early stage surface exploration. *Ultramicroscopy* **100,** 145-151 (2004).

[Bruckbauer 2004] A. Bruckbauer, D. Zhou, D-J. Kang, Y. E. Korchev, *et al.*. An addressable antibody nanoarray produced on a nanostructured surface. *J. Am. Chem. Soc.* **126,** 6508-6509 (2004).

[Burnham 1990] N.A. Burnham, D.D. Dominguez, R.L. Mowery and R.J. Colton. Probing the surface forces of monolayer films with an atomic-force microscope. *Phys. Rev. Lett.* **64,** 1931-1934 (1990).

[Colton 2004] R.J. Colton. Nanoscale measurements and manipulation. *J. Vac. Sci. Technol. B* **22,** 1609-1635 (2004).

[Csucs 2003] G. Csucs, *et al.* Microcontact printing of macromolecules with submicrometer resolution by means of polyolefin stamps. *Langmuir* **19,** 6104 (2003).

[Craighead 2003] H.G. Craighead. Nanostructure science and technology: impact and prospects for biology. *J. Vac. Sci. Technol. A* **21,** S216-S221 (2003).

[Cui 1998] L.L. Cui, J. Jiang, Z.G. Xia, G.J. Chen and Z.Z. Wang. Charge storage and transport in polymethylmethacrylate (PMMA) film. *J. Electrostatics* **44,** 61-65 (1998).

[Dagata 1990] J.A. Dagata, *et al.* Modification of hydrogen-passivated silicon by a scanning tunneling microscope operated in air. *Appl. Phys. Lett.* **56,** 2001-2003 (1990).

[Dagata 1995] J.A. Dagata, *et al.* Device fabrication by scanned probe oxidation. *Science* **270,** 1625-1626 (1995).

[Decher 1997] G. Decher. Fuzzy nanoassemblies: toward layered polymeric multicomposites. *Science* **277,** 1232-1237 (1997).

[Demers 2002] L.M. Demers, *et al.* Direct patterning of modified oligonucleotides on metals and insulators by dip-pen nanolithography. *Science* **296,** 1836-1838 (2002).

[Dupont-Gillain 2000] C.C. Dupont-Gillain, *et al.* Plasma-oxidised polysterene: wetting properties ans surface reconstruction. *Langmuir* **16,** 8194-8200 (2000).

[Enikov 2004] E.T. Enikov and A. Palaria. charge-writing in silicon-silicon dioxide for nano-assembly. *Nanotechnology* **15,** 1211-1216 (2004).

[Fan 2004] F.Q. Fan and K.J. Stebe. Assembly of colloidal particles by evaporation on surfaces with patterned hydrophobicity. *Langmuir* **20,** 3062-3067 (2004).

[Fang 2004] T.-H. Fang. Mechanisms of nanooxidation of Si(100)from atomic force microscopy *Microelectron. J.* **35,** 701707 (2004)

[FC77] Fluorinert FC77 product information, 3M Company, St.Paul MN, USA (available under "electronic materials" from http://www.3m.com/).

[Feder 1976] J. Feder. Storage and examination of high-resolution charge images in Teflon foils. *J. Appl. Phys.* **47,** 1741-1745 (1976).

[Forster 1998] S. Forster and M. Antonietti. Amphiphilic block copolymers in structure-controlled nanomaterial hybrids. *Adv. Mater.* **10,** 195-217 (1998).

[Fritz 2002] J. Fritz, E.B. Cooper, S. Gaudet, P.K. Sorger and S.R. Manalis. Electronic detection of DNA by its intrinsic molecular charge. *PNAS* **99,** 14142-14146 (2002).

[Frost 2003] F. Frost and B. Rauschenbach. Nanostructuring of solid surfaces by ion-beam erosion. *Appl. Phys. A-Mater.* **77,** 1-9 (2003).

[Fudouzi 2002] H. Fudouzi, M. Kobayashi and N. Shinya. Site-controlled deposition of microsized particles using an electrostatic assembly. *Adv. Mater.* **14,** 1649-1652 (2002).

[Fujihira 1999] M. Fujihira. Kelvin-probe force microscopy of molecular surfaces. *Annu. Rev. Mater. Sci.* **29,** 353-380 (1999).

[Fukano 1994] Y. Fukano, *et al.* Parameter dependence of stable state of densely contact-electrified electrons on thin silicon oxide. *Jpn. J. Appl. Phys.* **33,** 6739-6745 (1994).

[Geissler 2004] M. Geissler and Y. Xia. Patterning: principles and some new developments. *Adv. Mater.* **16,** 1252-1269 (2004).

[Goel 2003] M. Goel. Electret sensors, filters and MEMS devices: new challenges in materials research. *Curr. Sci.* **85,** 443-453 (2003).

[Haghiri-Gosnet 1995] A.M. Haghiri-Gosnet, *et al.* Fabrication of sub-30 nm masks for x-ray nanolithography. *J. Vac. Sci. Technol. B* **13,** 3066-3069 (1995).

[Hanley 2002] L. Hanley and S.B. Sinnott. The growth and modification of materials via ion-surface processing. *Surf. Sci.* **500,** 500-522 (2002).

[Hall 2006] D.J. Hall and S. Seaton. Flexible Protein Microarray Inkjet Printing. *Genet. Eng. News* **26,** 14 (2006).

[Heidelberger 1929] M. Heidelberger and F.E. Kendall. A quantitative study of the precipitation reaction between type III pneumococcus polysaccaride and purified homologous antibody. *J. Exp. Med.* **50,** 809-823 (1929).

[Higashi 1991] G. S. Higashi, *et al.* Comparison of Si(111) surfaces prepared using aqueous solutions of NH_4F versus HF. *Appl. Phys. Lett.* **58,** (1991).

[Hori 2000] Y. Hori, The lateral migration of surface charges on poly(methyl-methacrylate) graft-copolymerized onto polypropylene film. and its dependency on relative humidity. *J. Electrostatics* **48,** 127-143 (2000).

[Humphris 2005] A.D.L. Humphris, M.J. Miles and J.K. Hobbs. A mechanical microscope: High-speed atomic force microscopy. *Appl. Phys. Lett.* **86,** 034106 (2005).

[Ijiro 2002] K. Ijiro, *et al.* Base-pair mapping by chemical force microscopy on nucleobase self-assembled monolayers. *Colloid. Surface. A* **198,** 677-682 (2002).

[Isaacs 1999] L. Isaacs, D.N. Chin, N. Bowden, Y. Xia and G.M. Whitesides. *Supermolecular materials and technologies,* (John Wiley & Sons, New York, 1999).

[Ito 1984] H. Ito and C.G. Willson. Applications of photoinitiators to the design of resists for semiconductor manufacturing. *ACS Symposium Series* **242,** 11-23 (1984).

[Iwata 2002] F. Iwata, *et al.* Nanometre-scale modification of a urethaneurea copolymer film using local field enhancement at an apex of a metal coated probe. *Nanotechnology* **13,** 138-142 (2002).

[Jacobs 1997] H.O. Jacobs, H.F. Knapp, S. Müller and A. Stemmer, Surface potential mapping: A qualitative material contrast in SPM, *Ultramicroscopy* **69,** 39-49 (1997).

[Jacobs 1998] H.O. Jacobs, *et al.* Resolution and contrast in Kelvin-probe force microscopy. *J. Appl. Phys.* **84,** 1168-1176 (1998).

[Jacobs 1999,a] H.O. Jacobs and A. Stemmer. Measuring and modifying the electric surface potential distribution on a nanometre scale: a powerful tool in science and technology. *Surf. Interface. Anal.* **27,** 361-367 (1999).

[Jacobs 1999,b] H.O. Jacobs, H.F. Knapp and A. Stemmer. Practical aspects of Kelvin-probe force microscopy. *Rev. Sci. Instrum.* **70,** 1756-1760 (1999).

[Jacobs 2001] H.O. Jacobs and G.M. Whitesides. Submicrometer patterning of charge in thin-film electrets. *Science* **291,** 1763-1766 (2001).

[Jones 1995] T.B. Jones. *Electromechanics of Particles,* (Cambridge University Press, Cambridge, England, 1995).

[Junno 1995] T. Junno, K. Deppert, L. Montelius, and L. Samuelson. Controlled manipulation of nanoparticles with an atomic force microscope. *Appl. Phys. Lett.* **66,** 3627-3629 (1995).

[Kelvin 1898] Kelvin Lord, Phil. Mag. 46 82-120

[Kikukawa 1995] A. Kikukawa, S. Hosaka and R. Imura. Silicon pn junction imaging and characterizations using sensitivity enhanced Kelvin-probe force microscopy. *Appl. Phys. Lett.* **66,** 3510-3512 (1995).

[Kim 2001] B.M. Kim, *et al.* In-situ electrical study of a reversible surface modification and a nanomachining of gold microstrips by the voltage-biased atomic force microscope tip in air. *Jpn. J. Appl. Phys.* **40,** 4340-4343 (2001).

[Klehn 1999] B. Klehn and U. Kunzea. Nanolithography with an atomic force microscope by means of vector-scan controlled dynamic plowing. *J. Appl. Phys.* **85,** 3897-3903 (1999).

[Knapp 1999] H.F. Knapp and A. Stemmer. Preparation, comparison and performance of hydrophobic AFM tips. *Surf. Interface. Anal.* **27,** 324-331 (1999).

[Kohler 1976] G. Kohler and C. Milstein. Derivation of specific antibody-producing tissue culture and tumor lines by cell-fusion. *Eur. J. Immunol.* **6,** 511-519 (1976).

[Kohler 2004] M. Kohler, W. Fritzsche, *Nanotechnology. An introduction to Nanostructuring Techniques*,(Wiley-VCH,2004).

[Kotov 1995] N.A. Kotov, I. Dékány and J.H. Fendler. Layer-by layer self-assembly of polyelectrolyte-semiconductor nanoparticle composite films. *J. Phys. Chem.* **99,** 13065-13069 (1995).

[Kratschmer 1987] E. Kratschmer and M. Issacson. Progress in self-developing metal fluoride resists. *J. Vac. Sci. Technol. B* **5,** 369-373 (1987).

[Krausch 1995] G. Krausch, *et al.* Near field microscopy and lithography with uncoated fiber tips: a comparison. *Opt. Commun.* **119,** 283-288 (1995).

[Kreiner 2004] T. Kreiner. Gene Expression Microarrays: A Revolutionary Evolution. *Am. Biotechnol. Lab.* **22,** 8-9 (2004).

[Kressmann 1996] R. Kressmann, G.M. Sessler and P. Günther. Space-charge electrets. *IEEE Trans. Dielectrics El.* **3,** 607-622 (1996).

[Kuramochi 2004] H. Kuramochi, *et al.* Nano-oxidation and in-situ faradaic current detection using dynamic carbon nanotube probes. *Nanotechnology* **15,** 1126-1130 (2004).

[Kuschel 2004] C. Kuschel, *et al.* Cell adhesion profiling using extracellular matrix protein arrays. *Biotechniques* **40,** 523-531 (2004).

[Leach 2003] R.N. Leach, F. Stevens, C. Seiler, S.C. Langford, and J.T. Dickinson. Nanometer-scale solvent-assisted modification of polymer surfaces using the atomic force microscope. *Langmuir* **19,** 10225-10232 (2003).

[Lee 1994] G.U. Lee, D.A. Kidwell and R.J. Colton. Sensing discrete streptavidin biotin interactions with atomic-force microscopy. *Langmuir* **10,** 354-357.

[Lee 2006] S.W. Lee, B-K Oh, R.G. Sanedrin, K. Salaita, T. Fujigaya and C.A. Mirkin. Biologically active protein nanoarrays generated using parallel dip-pen nanolithography. *Adv. Mater.* **18,** 1133-1136 (2006).

[Lercel 1993] M. Lercel, *et al.* Self assembled monolayer e-beam resists on GaAs and SiO2. *J. Vac. Sci. Technol. B* **11,** 2823-2828 (1993).

[Lin 2004] X. Lin, X. Jiang and L. Lu. DNA deposition on carbon electrodes under controlled dc potentials. *Biosens. Bioelectron.* **20,** 1709-1717 (2005).

[Liotta 2003] L.A. Liotta *et al.* Protein microarrays: meeting analytical challenges for clinical applications. *Cancer Cell* **3,** 317-325 (2003).

[Lopes 2001] W.A. Lopes and H.M. Jaeger. Hierarchical self-assembly of metal nanostructures on diblock copolymer scaffolds. *Nature* **414,** 735-738 (2001).

[Lyuksyutov 2003] S.F. Lyuksyutov, P.B. Paramonov, S. Juhl and R.A. Vaia. Amplitude-modulated electrostatic nanolithography in polymers based on atomic force microscopy. *Appl. Phys. Lett.* **83,** 4405-4407 (2003).

[Lyuksyutov 2004] S. Juhl, D. Phillips, R.A. Vaia, S.F. Lyuksyutov, P.B. Paramonov. Precise formation of nanoscopic dots on polystyrene film using z-lift electrostatic lithography. *Appl. Phys. Lett.* **85,** 3836-3838 (2004).

[MacBeath 2000] G. MacBeath and S.L. Schreiber. Printing proteins as microarrays for high-throughput function determination. *Science* **289,** 1760-1763 (2000).

[MacBeath 2002] G. MacBeath. Protein microarrays and proteomics. *Nat. Genet.* **32,** 526-532 Suppl. (2002).

[Malecki 1999] J.A. Malecki. Linear Decay of Charge in Electrets. *Phys. Rev. B* **59,** 9954-9960 (1999).

[Maoz 2000] R. Maoz, E. Frydman, S.R. Cohen and J. Sagiv 'Constructive nanolithography': inert monolayers as patternable templates for in-situ nanofabrication of metal-semiconductor-organic surface structures. A generic approach, *Adv. Mater.* **12,** 725-731 (2000).

[Martin 1986] Y. Martin and H.K. Wickramasinghe. Magnetic imaging by 'force microscopy' with 1000 Å resolution. *Appl. Phys. Lett.* **50,** 1455-1457 (1987).

[Mazia 1975] D. Mazia, G. Schatten and W. Sale. Adhesion of cells to surfaces coated with polylysine. Applications to electron microscopy. *J. Cell Biol.* **66**, 198-200 (1975).

[Mate 1987] C.M. Mate, G.M. McClelland, R. Erlandsson and S. Chiang. Atomic-scale friction of a tungsten tip on a graphite surface. *Phys. Rev. Lett.* **59,** 1942-1945 (1987).

[Maoz 1999] R. Maoz, S.R. Cohen and J. Sagiv, Nanoelectrochemical patterning of monolayer surfaces: toward spatially defined self-assembly of nanostructures. A*dv. Mater.* **11,** 55-61 (1999).

[MesquidaDiss 2002] P. Mesquida. *charge-writing with an Atomic Force Microscope Tip and Electrostatic Attachment of Colloidal Particles to the Charge-Patterns.* Ph.D. thesis, ETH Zurich, (2002), (http://e-collection.ethbib.ethz.ch/show?type=diss&nr=14854).

[Mesquida 2001] P. Mesquida and A. Stemmer. Attaching silica nanoparticles from suspension onto surface charge-patterns generated by a conductive atomic force microscope tip. *Adv. Mater.* **13,** 1395-1398 (2001).

[Mesquida 2002] P. Mesquida, H.F. Knapp and A. Stemmer. charge-writing on the nanometre scale in a fluorocarbon film. *Surf. Interface Anal.* **33,** 159-162 (2002).

[Mesquida 2005] P. Mesquida, Ammann, C.E. MacPhee and R.A. McKendry. Microarrays of peptide fibrils created by electrostatically controlled deposition. *Adv. Mater.* **17,** 893-897 (2005).

[Meyer 1998] G. Meyer, L. Bartels and K. Rieder. Atom manipulation with the scanning tunnelling microscope: nanostructuring and femtochemistry. *Jpn. J. Appl. Phys.* **37,** 7143-7147 (1998).

[Morris 1999] V.J. Morris, A.R. Kirby and A.P. Gunning. *Atomic Force Microscopy for Biologists.*(Imperial College Press, London, 1999).

[Mort 1989] J. Mort. *The Anatomy of Xerography: its Invention and Evolution.* (Mc-Farland, London, 1989).

[Mukerjee 1981] P. Mukerjee and T. Handa. Adsorption of fluorocarbon and hydrocarbon surfactants to air-water, hexane-water and perfluorohexane-water interfaces. Relative affinities and fluorocarbon-hydrocarbon nonideality effect. *J.Phys. Chem.* **85,** 2298-2303 (1981).

[Naujoks 2003] N. Naujoks and A. Stemmer. Localised functionalisation of surfaces with molecules from solution using electrostatic attraction. *Microelectron. Eng.* **67-68,** 736-741 (2003).

[Naujoks 2004] N. Naujoks, and A. Stemmer. Using local surface charges for the fabrication of protein patterns. *Coll. Surf. A* **249,** 69-72 (2004).

[Naujoks 2005] N. Naujoks and A. Stemmer. Micro and nanoxerography in liquids-controlling pattern definition. *Microelectron. Eng.* **78-79,** 331-337 (2005).

[Nonnenmacher 1991] M. Nonnenmacher, M.P. O'Boyle and H.K. Wickramasinghe. Kelvin-probe force microscopy. *Appl.Phys. Lett.* **58,** 2921-2923 (1991).

[Okamoto 2000] T. Okamoto, *et al.* Microarray fabrication with covalent attachment of DNA using bubble jet technology. *Nat. Biotechnol.* **18,** 438-441 (2000).

[Olthuis 1992] W. Olthuis and P. Bergveld. Charge storage and decay in silicon dioxide electrets. *IEEE T. Electr. Insul.* **27,** 691-697 (1992).

[Oshima 1998] H. Oshima and K. Furusawa. *Electrical Phenomena at Interfaces. Fundamentals, Measurements and Applications.* Surfactant Science Series, vol. 76, (M. Dekker, 2nd ed., New York, 1998).

[Overney 2002] R.M. Overney, *et al.* Friction measurements on phase-separated thin films with a modified atomic force microscope. *Nature* **359,** 133-135 (1992).

[Park 1997] M. Park, *et al.* Block copolymer lithography: periodic arrays of $\approx 10^11$ holes in 1 square centimeter. *Science* **276,** 1401-1404 (1997).

[Reiner 2006] J.E. Reiner, *et al.* Optically trapped aqueous droplets for single molecule studies. *Appl. Phys. Lett.* **89,** 013904 (2006).

[Renault 2003] J.P. Renault, *et al.* Fabricating arrays of single protein molecules on glass using microcontact printing *J. Phys. Chem. B* **107,** 703-711 (2003).

[Rozkiewicz 2006] D.I. Rozkiewicz, *et al.* Covalent microcontact printing of proteins for cell patterning. *Chem. Eur. J.* **12,** 6290-6297 (2006).

[Sadtler 1996] V.M. Sadtler, M.P. Krafft and J.G. Riess. Achieving stable, reverse water-in fluorocarbon emulsions. *Angew. Chem. Int. Ed. Engl.* **35,** 1976-1978 (1996).

[Salaita 2006] K. Salaita, Y.H. Wang, C.A. Mirkin *et al.* Massively parallel dip-pen nanolithography with 55000-pen two dimensional arrays. *Angew. Chem. Int. Ed.* **45,** 7220-7223 (2006).

[Santinacci 2001] L. Santinacci, T. Djenizian, and P. Schmuki. Nanoscale patterning of Si(100) surfaces by scratching through the native oxide layer using atomic force microscope. *Appl. Phys. Lett.* **79,** 1882-1884 (2001).

[Saurenbach 1992] F. Saurenbach and B.D. Terris. Electrostatic writing and imaging using a force microscope. *IEEE T. Ind. Appl.* **28,** 256-260 (1992).

[Schitter 2001] G. Schitter, P. Menold, H.F. Knapp, F. Allgower and A. Stemmer. High performance feedback for fast scanning atomic force microscopes. *Rev. Sci. Instr.* **72,** 3320-327 (2001).

[Sessler 1987] G.M. Sessler. *Electrets,* Springer topics in applied physics Vol. 33, (Springer Verlag, 2nd ed., Berlin, Germany, 1987).

[Sessler 1999] G.M. Sessler and G.M. Yang. Charge dynamics in electron-irradiated polymers. *Braz. J. Phys.* **29,** 233-240 (1999).

[Schonenberger 1992] C. Schönenberger. Charge flow during metal-insulator contact. *Phys. Rev. B* **45,** 6831-6834 (1992).

[Shonenberger 1996] C. Shönenberger and N. Kramer. Nanolithography on hydrogen terminated silicon by scanning probe microscopy. *Microelectron. Eng.* **32,** 206-213 (1996).

[Silzel 1998] J.W. Silzel, *et al.* Mass-sensing, multianalyte microarray immunoassay with imaging detection. *Clin. Chem.* **44,** 2036-2043 (1998).

[Stern 1988] J.E. Stern, B.D. Terris, H.J. Mamin and D. Rugar. Deposition and imaging of localized charge on insulator surfaces using a force microscope. *Appl. Phys. Lett.* **53,** 2717-2719 (1988).

[Sugawara 1994] Y. Sugawara, *et al.* Atomic force microscopy studies of contact-electrified charges on silicon oxide film. *J. Vac. Sci. Technol. B* **12,** 1627-1630 (1994).

[Takahashi 2004] T. Takahashi and S. Ono. Tip-to-sample distance dependence of an electrostatic force in KFM measurements. *Ultramicroscopy* **100,** 287-292 (2004).

[Tersoff 1985] J. Tersoff and D.R. Hamann. Theory of the scanning tunneling microscope. *Phys. Rev. B* **31,** 805-813 (1985).

[Tzeng 2006] S.D. Tzeng, K.J. Lin, J.C. Hu, L.J. Chen and S. Gwo. Templated self-assembly of colloidal nanoparticles controlled by electrostatic nanopatterning on a $Si_3N_4/SiO_2/Si$ electret. *Adv. Mater.* **18,** 1147-1151 (2006).

[Tomizaki 2005] K. Tomizaki, K. Usui and H. Mihara. Protein-detecting microarrays: current accomplishments and requirements. *ChemBioChem* **6,** 782-799 (2005).

[Uchihashi 1994] T. Uchihashi, *et al.* Heat treatment and steaming effects of silicon oxide upon electron dissipation on silicon oxide surface. *Jpn. J. Appl. Phys.* **33,** L1128-L1130 (1994).

[Veeco 2002] Digital Instruments Veeco Metrology Group. Nanoscope IV Controller Manual. (2002).

[Venkatasubbarao 2004] S. Venkatasubbarao. Microarrays-status and prospects. *Trends in Biotechnology* **22,** 630-637 (2004).

[Vettiger 2000] P. Vettiger, *et al.* The Millipede more than one thousand tips for future AFM data storage. *IBM J. Res. Dev.* **44,** 323-340 (2000).

[Voet 1995] D. Voet and J.G. Voet. *Biochemistry*, (John Willey & Sons Inc., 2nd ed., New York, 1995).

[Wadu-Mesthrige 1999] K. Wadu-Mesthrige, S. Xu, N.A. Amro, and G.Y. Liu. Fabrication and Imaging of Nanometer-Sized Protein Patterns. *Langmuir* **15,** 8580-8583 (1999).

[Wadu-Mesthrige 2000] K. Wado-Mesthrige, N.A. Amro and G.Y. Liu. Immobilization of proteins on self-assembled monolayers. *Scanning* **20,** 380-388 (2000).

[Wadu-Mesthrige 2001] K. Wado-Mesthrige, *et al.* Fabrication of nanometer-sized protein patterns using atomic force microscopy and selective immobilization. *Biophys. J.* **80,** 1891-1899 (2001).

[Wang 2004] J.Z. Wang, Z.H. Zheng, H.W. Li, W.T.S. Huck and H. Sirringhaus. Dewetting of conducting polymer inkjet droplets on patterned surfaces. *Nat. Mater.* **3,** 171-176 (2004).

[Weiser 1933] H.B. Weiser. *Inorganic Colloidal Chemistry, Vol 1,* (Wiley, New York, 1933).

[Wickramasinghe 1994] F. Zenhausern, M.P. OBoyle, and H.K. Wickramasinghe. Apertureless near-field optical microscope. *Appl. Phys. Lett.* **65,** 1623-625 (1994).

[Wouters 2003] D. Wouters, B. Kösters and U.S. Schubert. Constructive nanolithography: arranging gold nanoparticles and proteins on surfaces. *Polym. Prepr. (Am. Chem. Soc., Div. Polym. Sci.)* **44,** 169-170 (2003).

[Wright 1998] W.M.D. Wright and D.G. Chetwynd. Can charge-writing aid nanotechnological manipulation? *Nanotechnology* **9,** 133-142 (1998).

[Wybourne 1996] M.N. Wybourne, M. Yan, J.F.W. Keana and J.C. Wu. Creation of biomolecule arrays by electrostatic immobilization on electron-beam-irradiated polystyrene thin films. *Nanotechnology* **7,** 302-305 (1996).

[Xia 1995] Y.N. Xia and G.M. Whitesides. Reduction in the size of features of patterned SAMs generated by microcontact printing with mechanical compression of the stamp. *Adv. Mater.* **7,** 471-473 (1995)

[Yan 2006] M. Yan and G.H. Bernstein. Apparent height in tapping mode of electrostatic force microscopy. *Ultramicroscopy* **106,** 582-586 (2006).

[Yin 2001] Y. Yin, Y. Lu, B. Gates and Y. Xia. Template-assisted self-assembly: a practical route to complex aggregates of monodispersed colloids with well-defined sizes, shapes and structures. *J. Am. Chem. Soc.* **123,** 8718-8729 (2001).

[Lyuksyutov 2004] S. Juhl, D. Phillips, R.A. Vaia, S.F. Lyuksyutov, P.B. Paramonov. Precise formation of nanoscopic dots on polystyrene film using z-lift electrostatic lithography. *Appl. Phys. Lett.* **85,** 3836-3838 (2004).

[MacBeath 2000] G. MacBeath and S.L. Schreiber. Printing proteins as microarrays for high-throughput function determination. *Science* **289,** 1760-1763 (2000).

[MacBeath 2002] G. MacBeath. Protein microarrays and proteomics. *Nat. Genet.* **32,** 526-532 Suppl. (2002).

[Malecki 1999] J.A. Malecki. Linear Decay of Charge in Electrets. *Phys. Rev. B* **59,** 9954-9960 (1999).

[Maoz 2000] R. Maoz, E. Frydman, S.R. Cohen and J. Sagiv 'Constructive nanolithography': inert monolayers as patternable templates for in-situ nanofabrication of metal-semiconductor-organic surface structures. A generic approach, *Adv. Mater.* **12,** 725-731 (2000).

[Martin 1986] Y. Martin and H.K. Wickramasinghe. Magnetic imaging by 'force microscopy' with 1000 Å resolution. *Appl. Phys. Lett.* **50,** 1455-1457 (1987).

[Mazia 1975] D. Mazia, G. Schatten and W. Sale. Adhesion of cells to surfaces coated with polylysine. Applications to electron microscopy. *J. Cell Biol.* **66**, 198-200 (1975).

[Mate 1987] C.M. Mate, G.M. McClelland, R. Erlandsson and S. Chiang. Atomic-scale friction of a tungsten tip on a graphite surface. *Phys. Rev. Lett.* **59,** 1942-1945 (1987).

[Maoz 1999] R. Maoz, S.R. Cohen and J. Sagiv, Nanoelectrochemical patterning of monolayer surfaces: toward spatially defined self-assembly of nanostructures. A*dv. Mater.* **11,** 55-61 (1999).

[MesquidaDiss 2002] P. Mesquida. *charge-writing with an Atomic Force Microscope Tip and Electrostatic Attachment of Colloidal Particles to the Charge-Patterns.* Ph.D. thesis, ETH Zurich, (2002), (http://e-collection.ethbib.ethz.ch/show?type=diss&nr=14854).

[Mesquida 2001] P. Mesquida and A. Stemmer. Attaching silica nanoparticles from suspension onto surface charge-patterns generated by a conductive atomic force microscope tip. *Adv. Mater.* **13,** 1395-1398 (2001).

[Mesquida 2002] P. Mesquida, H.F. Knapp and A. Stemmer. charge-writing on the nanometre scale in a fluorocarbon film. *Surf. Interface Anal.* **33,** 159-162 (2002).

[Mesquida 2005] P. Mesquida, Ammann, C.E. MacPhee and R.A. McKendry. Microarrays of peptide fibrils created by electrostatically controlled deposition. *Adv. Mater.* **17,** 893-897 (2005).

[Meyer 1998] G. Meyer, L. Bartels and K. Rieder. Atom manipulation with the scanning tunnelling microscope: nanostructuring and femtochemistry. *Jpn. J. Appl. Phys.* **37,** 7143-7147 (1998).

[Morris 1999] V.J. Morris, A.R. Kirby and A.P. Gunning. *Atomic Force Microscopy for Biologists.*(Imperial College Press, London, 1999).

[Mort 1989] J. Mort. *The Anatomy of Xerography: its Invention and Evolution.* (Mc-Farland, London, 1989).

[Mukerjee 1981] P. Mukerjee and T. Handa. Adsorption of fluorocarbon and hydrocarbon surfactants to air-water, hexane-water and perfluorohexane-water interfaces. Relative affinities and fluorocarbon-hydrocarbon nonideality effect. *J.Phys. Chem.* **85,** 2298-2303 (1981).

[Naujoks 2003] N. Naujoks and A. Stemmer. Localised functionalisation of surfaces with molecules from solution using electrostatic attraction. *Microelectron. Eng.* **67-68,** 736-741 (2003).

[Naujoks 2004] N. Naujoks, and A. Stemmer. Using local surface charges for the fabrication of protein patterns. *Coll. Surf. A* **249,** 69-72 (2004).

[Naujoks 2005] N. Naujoks and A. Stemmer. Micro and nanoxerography in liquids-controlling pattern definition. *Microelectron. Eng.* **78-79,** 331-337 (2005).

[Nonnenmacher 1991] M. Nonnenmacher, M.P. O'Boyle and H.K. Wickramasinghe. Kelvin-probe force microscopy. *Appl.Phys. Lett.* **58,** 2921-2923 (1991).

[Okamoto 2000] T. Okamoto, *et al.* Microarray fabrication with covalent attachment of DNA using bubble jet technology. *Nat. Biotechnol.* **18,** 438-441 (2000).

[Olthuis 1992] W. Olthuis and P. Bergveld. Charge storage and decay in silicon dioxide electrets. *IEEE T. Electr. Insul.* **27,** 691-697 (1992).

[Oshima 1998] H. Oshima and K. Furusawa. *Electrical Phenomena at Interfaces. Fundamentals, Measurements and Applications.* Surfactant Science Series, vol. 76, (M. Dekker, 2nd ed., New York, 1998).

[Overney 2002] R.M. Overney, *et al.* Friction measurements on phase-separated thin films with a modified atomic force microscope. *Nature* **359,** 133-135 (1992).

[Park 1997] M. Park, *et al.* Block copolymer lithography: periodic arrays of $\approx 10^11$ holes in 1 square centimeter. *Science* **276,** 1401-1404 (1997).

[Reiner 2006] J.E. Reiner, *et al.* Optically trapped aqueous droplets for single molecule studies. *Appl. Phys. Lett.* **89,** 013904 (2006).

[Renault 2003] J.P. Renault, *et al.* Fabricating arrays of single protein molecules on glass using microcontact printing *J. Phys. Chem. B* **107,** 703-711 (2003).

[Rozkiewicz 2006] D.I. Rozkiewicz, *et al.* Covalent microcontact printing of proteins for cell patterning. *Chem. Eur. J.* **12,** 6290-6297 (2006).

[Sadtler 1996] V.M. Sadtler, M.P. Krafft and J.G. Riess. Achieving stable, reverse water-in fluorocarbon emulsions. *Angew. Chem. Int. Ed. Engl.* **35,** 1976-1978 (1996).

[Salaita 2006] K. Salaita, Y.H. Wang, C.A. Mirkin *et al.* Massively parallel dip-pen nanolithography with 55000-pen two dimensional arrays. *Angew. Chem. Int. Ed.* **45,** 7220-7223 (2006).

[Santinacci 2001] L. Santinacci, T. Djenizian, and P. Schmuki. Nanoscale patterning of Si(100) surfaces by scratching through the native oxide layer using atomic force microscope. *Appl. Phys. Lett.* **79,** 1882-1884 (2001).

[Saurenbach 1992] F. Saurenbach and B.D. Terris. Electrostatic writing and imaging using a force microscope. *IEEE T. Ind. Appl.* **28,** 256-260 (1992).

[Schitter 2001] G. Schitter, P. Menold, H.F. Knapp, F. Allgower and A. Stemmer. High performance feedback for fast scanning atomic force microscopes. *Rev. Sci. Instr.* **72,** 3320-327 (2001).

[Sessler 1987] G.M. Sessler. *Electrets,* Springer topics in applied physics Vol. 33, (Springer Verlag, 2nd ed., Berlin, Germany, 1987).

[Sessler 1999] G.M. Sessler and G.M. Yang. Charge dynamics in electron-irradiated polymers. *Braz. J. Phys.* **29,** 233-240 (1999).

[Schonenberger 1992] C. Schönenberger. Charge flow during metal-insulator contact. *Phys. Rev. B* **45,** 6831-6834 (1992).

[Shonenberger 1996] C. Shönenberger and N. Kramer. Nanolithography on hydrogen terminated silicon by scanning probe microscopy. *Microelectron. Eng.* **32,** 206-213 (1996).

[Silzel 1998] J.W. Silzel, *et al.* Mass-sensing, multianalyte microarray immunoassay with imaging detection. *Clin. Chem.* **44,** 2036-2043 (1998).

[Stern 1988] J.E. Stern, B.D. Terris, H.J. Mamin and D. Rugar. Deposition and imaging of localized charge on insulator surfaces using a force microscope. *Appl. Phys. Lett.* **53,** 2717-2719 (1988).

[Sugawara 1994] Y. Sugawara, *et al.* Atomic force microscopy studies of contact-electrified charges on silicon oxide film. *J. Vac. Sci. Technol. B* **12,** 1627-1630 (1994).

[Takahashi 2004] T. Takahashi and S. Ono. Tip-to-sample distance dependence of an electrostatic force in KFM measurements. *Ultramicroscopy* **100,** 287-292 (2004).

[Tersoff 1985] J. Tersoff and D.R. Hamann. Theory of the scanning tunneling microscope. *Phys. Rev. B* **31,** 805-813 (1985).

[Tzeng 2006] S.D. Tzeng, K.J. Lin, J.C. Hu, L.J. Chen and S. Gwo. Templated self-assembly of colloidal nanoparticles controlled by electrostatic nanopatterning on a $Si_3N_4/SiO_2/Si$ electret. *Adv. Mater.* **18,** 1147-1151 (2006).

[Tomizaki 2005] K. Tomizaki, K. Usui and H. Mihara. Protein-detecting microarrays: current accomplishments and requirements. *ChemBioChem* **6,** 782-799 (2005).

[Uchihashi 1994] T. Uchihashi, *et al.* Heat treatment and steaming effects of silicon oxide upon electron dissipation on silicon oxide surface. *Jpn. J. Appl. Phys.* **33,** L1128-L1130 (1994).

[Veeco 2002] Digital Instruments Veeco Metrology Group. Nanoscope IV Controller Manual. (2002).

[Venkatasubbarao 2004] S. Venkatasubbarao. Microarrays-status and prospects. *Trends in Biotechnology* **22,** 630-637 (2004).

[Vettiger 2000] P. Vettiger, *et al.* The Millipede more than one thousand tips for future AFM data storage. *IBM J. Res. Dev.* **44,** 323-340 (2000).

[Voet 1995] D. Voet and J.G. Voet. *Biochemistry*, (John Willey & Sons Inc., 2nd ed., New York, 1995).

[Wadu-Mesthrige 1999] K. Wadu-Mesthrige, S. Xu, N.A. Amro, and G.Y. Liu. Fabrication and Imaging of Nanometer-Sized Protein Patterns. *Langmuir* **15,** 8580-8583 (1999).

[Wadu-Mesthrige 2000] K. Wado-Mesthrige, N.A. Amro and G.Y. Liu. Immobilization of proteins on self-assembled monolayers. *Scanning* **20,** 380-388 (2000).

[Wadu-Mesthrige 2001] K. Wado-Mesthrige, *et al.* Fabrication of nanometer-sized protein patterns using atomic force microscopy and selective immobilization. *Biophys. J.* **80,** 1891-1899 (2001).

[Wang 2004] J.Z. Wang, Z.H. Zheng, H.W. Li, W.T.S. Huck and H. Sirringhaus. Dewetting of conducting polymer inkjet droplets on patterned surfaces. *Nat. Mater.* **3,** 171-176 (2004).

[Weiser 1933] H.B. Weiser. *Inorganic Colloidal Chemistry, Vol 1,* (Wiley, New York, 1933).

[Wickramasinghe 1994] F. Zenhausern, M.P. OBoyle, and H.K. Wickramasinghe. Apertureless near-field optical microscope. *Appl. Phys. Lett.* **65,** 1623-625 (1994).

[Wouters 2003] D. Wouters, B. Kösters and U.S. Schubert. Constructive nanolithography: arranging gold nanoparticles and proteins on surfaces. *Polym. Prepr. (Am. Chem. Soc., Div. Polym. Sci.)* **44,** 169-170 (2003).

[Wright 1998] W.M.D. Wright and D.G. Chetwynd. Can charge-writing aid nanotechnological manipulation? *Nanotechnology* **9,** 133-142 (1998).

[Wybourne 1996] M.N. Wybourne, M. Yan, J.F.W. Keana and J.C. Wu. Creation of biomolecule arrays by electrostatic immobilization on electron-beam-irradiated polystyrene thin films. *Nanotechnology* **7,** 302-305 (1996).

[Xia 1995] Y.N. Xia and G.M. Whitesides. Reduction in the size of features of patterned SAMs generated by microcontact printing with mechanical compression of the stamp. *Adv. Mater.* **7,** 471-473 (1995).

[Yan 2006] M. Yan and G.H. Bernstein. Apparent height in tapping mode of electrostatic force microscopy. *Ultramicroscopy* **106,** 582-586 (2006).

[Yin 2001] Y. Yin, Y. Lu, B. Gates and Y. Xia. Template-assisted self-assembly: a practical route to complex aggregates of monodispersed colloids with well-defined sizes, shapes and structures. *J. Am. Chem. Soc.* **123,** 8718-8729 (2001).